Université de Neuchâtel

Institut de Microtechnique

EFFICIENT PHASE GRATINGS FOR BEAM SPLITTING AND BEAM SHAPING

Thèse

Peter Ehbets

Ce document représente une forme réduite
de la thèse pour l'obtention du grade de docteur ès sciences
de l'Université de Neuchâtel

Neuchâtel, mai 1995

IMPRIMATUR POUR LA THÈSE

Efficient phase gratings for beam splitting and beam shaping

de M. Peter Ehbets

UNIVERSITÉ DE NEUCHÂTEL

FACULTÉ DES SCIENCES

La Faculté des sciences de l'Université de Neuchâtel sur le rapport des membres du jury,

Messieurs N.F. de Rooij, R. Dändliker, J. Jahns (Hagen), J.P. Turunen (Joensuu) et J. Leger (Minnesota)

autorise l'impression de la présente thèse.

Neuchâtel, le 8 juin 1995

Le doyen:

H.-H. Nägeli

Liste de Publications

Cette thèse est une collection des publications scientifiques de l'auteur dans le domaine de l'optique diffractive:

I P. Ehbets, H. P. Herzig, D. Prongué, and M. T. Gale, "High efficiency continuous surface-relief gratings for two-dimensional array generation," Opt. Lett. **17**, 908-910 (1992).

II M. T. Gale, M. Rossi, H. Schütz, P. Ehbets, H. P. Herzig, and D. Prongué, "Continuous-relief diffractive optical elements for two-dimensional array generation," Appl. Opt. **32**, 2526-2533 (1993).

III P. Ehbets, M. Rossi, and H. P. Herzig, "Continuous-relief fan-out elements with optimized fabrication tolerances," Opt. Eng. **34**, December issue(1995).

IV P. Ehbets, H. P. Herzig, R. Dändliker, P. Regnault, and I. Kjelberg, "Beam shaping of high-power laser diode arrays by continuous surface-relief elements," J. of Mod. Opt. **40**, 637-645 (1993).

V M. Stalder and P. Ehbets, "An electrically switchable diffractive optical element for image processing," Opt. Lett. **19**, 1-3 (1994).

VI H. P. Herzig, P. Ehbets, D. Prongué, and R. Dändliker, "Fan-out elements recorded as volume holograms: optimized recording conditions," Appl. Opt. **31**, 5716-5723 (1992).

VII P. Ehbets, H. P. Herzig, Ph. Nussbaum, P. Blattner, and R. Dändliker, "Interferometric fabrication of modulated submicron gratings in photoresist," Appl. Opt. **34**, 2540-2547 (1995).

VIII P. Ehbets, H. P. Herzig, and R. Dändliker, "TIR holography analyzed by coupled wave theory," Opt. Commun. **89**, 5-11 (1992).

IX P. Ehbets, H. P. Herzig, M. Kuittinen, F. S. M. Clube, and Y. Darbellay, "High-carrier-frequency fan-out gratings fabricated by TIR holographic lithography," Opt. Eng. **34**, 2377-2383 (1995).

Une version complète de la thèse est déposée à la Bilbiothèque de l'Université, Université de Neuchâtel, Ave. du 1er - Mars 26, CH-2000 Neuchâtel, Suisse.

High-efficiency continuous surface-relief gratings for two-dimensional array generation

P. Ehbets, H. P. Herzig, and D. Prongué

Institute of Microtechnology, University of Neuchâtel, Rue A.-L. Breguet 2, CH-2000 Neuchâtel, Switzerland

M. T. Gale

Paul Scherrer Institute, Badenerstrosse 569, CH-8048 Zürich, Switzerland

Received March 3, 1992

Continuous surface-relief phase gratings for two-dimensional (2-D) array generation have been realized by laser-beam writing lithography. For a 9 × 9 fan-out element, a diffraction efficiency of 94% and a uniformity of better than ±8% have been achieved. These are, to our knowledge, the best published results for 2-D surface-relief fan-out elements. Separable and nonseparable solutions for the design of 2-D fan-out elements are discussed.

Space-invariant fan-out elements split a single laser beam into quasi plane waves, which are focused by a lens as shown in Fig. 1. Such phase gratings that generate arrays of light spots are widely used in parallel processing systems.

In order to realize highly efficient fan-out elements, recent efforts have concentrated on multilevel phase structures[1] and continuous phase profiles.[2] The fabrication of multilevel phase structures involves microlithographic technologies that are well mastered and widely available. The drawback of this approach is that the number of masks increases with the number of phase levels. Thus precise alignment has to be performed at each process. Continuous phase profiles are recognized as providing the highest diffraction efficiency. On the other hand, their fabrication is considerably more challenging.[3]

In this Letter we report on a successful implementation of the optimized continuous phase function for a two-dimensional (2-D) fan-out element as a continuous surface-relief grating in photoresist. The fabrication was possible by using the laser-beam writing system developed at the Paul Scherrer Institute in Zürich[4] (PSIZ). The advantage of this technology is that the structure is written in one single step, thus errors due to successive alignments are avoided.

The optimization used for the design of one-dimensional (1-D) fan-out elements is described in detail in Ref. 5. In this Letter the theory is generalized for 2-D design. The optimization process consists of two basic steps: the first leads to high efficiency, and the second yields perfect uniformity of the generated array of light spots with only a slight decrease in efficiency. One of the basic questions of optimizing continuous phase profiles is the relevant parameter set to describe the continuous surface relief. Contrary to the optimization of multilevel phase gratings,[1] we describe the fan-out elements by the array of spots that appear in the Fourier plane. This approach defines a minimum set of parameters for the exact representation of the continuous surface relief. The parameters to be optimized are the amplitudes and phases of an array of point sources. The desired field distribution in the back focal plane of the lens (Fig. 1) can be written as

$$U(x,y) = \sum_{m=1}^{M}\sum_{n=1}^{N} A_{mn}\exp(i\phi_{mn})\delta(x - x_m, y - y_n), \tag{1}$$

where A_{mn} is the amplitude, ϕ_{mn} is the phase, and (x_m, y_n) is the position of the m,nth spot of a 2-D array. As we are only interested in the intensity distribution of the object, the phases ϕ_{mn} are free parameters.

The field distribution $\hat{U}(u,v)$ in the grating plane is related to the field $U(x,y)$ by a Fourier transform (FT):

$$\hat{U}(u,v) = |\hat{U}(u,v)|\exp[i\Psi(u,v)] = \mathrm{FT}\{U(x,y)\}, \tag{2}$$

where $|\hat{U}(u,v)|$ is the magnitude and $\Psi(u,v)$ is the phase of the field distribution in the grating plane. The irradiance distribution $I(u,v)$ in the grating

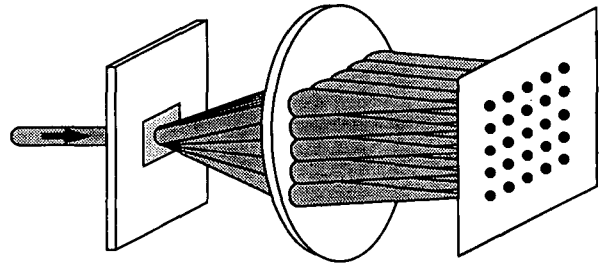

Fig. 1. Readout of the fan-out element.

0146-9592/92/130908-03$5.00/0

plane can then be written as

$$I(u,v) = |\hat{U}(u,v)|^2$$
$$= \sum_{mn} A_{mn}^2 + 2 \sum_{m<m'} \sum_{n<n'} A_{mn} A_{m'n'} \times \cos\{2\pi[u(x_m - x_{m'}) + v(y_n - y_{n'})] + \phi_{mn} - \phi_{m'n'}\}, \quad (3)$$

where the first term on the right-hand side of Eq. (3) is constant and equal to the mean object irradiance. The second term describes the variations of the irradiance. These intermodulations are due to interference between the object waves in the grating plane.

To reproduce the desired object $U(x,y)$ perfectly, the hologram must have a transfer function proportional to $\hat{U}(u,v)$, which means an intensity transfer function proportional to $I(u,v)$ and a phase transfer function equal to $\exp[i\Psi(u,v)]$. With a single element, the intensity transfer function can be realized only by absorption. In order to minimize the losses due to the required intensity transfer function, the variations of the object irradiance in the hologram plane have to be minimized. Therefore the optimization criterion can be formulated as

$$\iint [I(u,v) - \langle I \rangle]^2 \, du\,dv \rightarrow \min. \quad (4)$$

The variables of the optimization are the phases ϕ_{mn} of the point sources, given in Eq. (1), while the amplitudes of the point sources for a uniform fan-out are all equal ($A_{mn} = 1$). The optimization problem is solved by applying a downhill simplex algorithm. The optimization criterion (4) reduces the intermodulation terms of Eq. (3) to a minimum. The residual intermodulation still causes some absorption. In order to reach the highest diffraction efficiency, we opt for a pure phase element and clip the residual intensity transfer function to $I(u,v) = 1$. Clipping the residual intermodulation terms hardly alters the high efficiency but reduces the uniformity of the fan-out. In order to improve the uniformity of the fan-out, we use an additional optimization process. By iteratively changing the amplitudes of the initial point sources A_{mn} slightly to $A_{mn}^{(i)}$, where i counts the number of iteration loops, the resulting amplitudes of the output can be perfectly balanced. This second optimization decreases only slightly the optimized diffraction efficiency from step one. The substitution of the optimum set of phases ϕ_{mn} and the new amplitudes $A_{mn}^{(i)}$ into Eqs. (1) and (2) defines the optimized phase function $\Psi(u,v)$ of the fan-out element, which generates a perfectly uniform array of spots. This phase function is implemented as a continuous surface-relief element without quantization.

In order to reduce the computing time, separable solutions are attractive for generating large $M \times N$ arrays. In this case the object is described by $U(x,y) = F_1(x)F_2(y)$. Thus only the 1-D problem, as described in Ref. 5, has to be solved. On the other hand, if the 1-D solution of an $N \times 1$ array yields a diffraction efficiency of η, the corresponding 2-D solution of the $N \times N$ array will be less efficient, namely, η^2. Since 2-D nonseparable solutions have more free parameters for the optimization, the minimum intermodulations of the irradiance distribution will be smaller than for the separable solution. We have found for a 3×3 array a theoretical efficiency of 85.7% for the separable solution and 93.9% for the nonseparable solution. For a 5×5 array the efficiency was calculated to be 84.8% for the separable solution and 93.0% for the nonseparable solution.

The 9×9 fan-out element has the best performance. In this case, we have found for the separable solution as well as for the nonseparable solution the same diffraction efficiency. Theoretically this element has an efficiency of 98.6% and perfect uniformity. We have realized the separable solution, which is symmetric for all axes of the array. The 2-D solution is obtained by crossing two 1-D solutions. The phase distribution of the 1-D optimum phase profile is then described by nine point sources with amplitudes A_i and phases ϕ_i. The numerical values are given in Table 1. The amplitudes and phases of the optimum point sources for the 2-D solution are then determined by $A_{mn} = A_m A_n$ and $\phi_{mn} = \phi_m + \phi_n$, where $m,n = 1 \ldots 9$. One unit cell of the optimized phase profile for the 9×9 fan-out element is shown in Fig. 2.

The optimized phase function for the 9×9 fan-out element was realized in photoresist with the laser-beam writing system at the PSIZ, which results in a continuous surface-relief element. A complete description of the laser writing system at the PSIZ can be found in Ref. 4. This system uses x–y scanning and is therefore well suited for the fabrication of periodic 1-D and 2-D diffractive optical elements, such as kinoforms. The resist-coated substrate is mounted on a precision air-bearing x–y translation table and scanned under a modulated focused laser beam. The writing light source is a HeCd laser operating at a wavelength of 442 nm. The beam intensity is computer controlled by an accousto-optic modulator, which is synchronous with the raster scan movement. The exposure data are computed from the desired microrelief and the measured (nonlinear) resist development characteristics. Development of the resist then results in a microrelief of the desired structure. We have used Shipley AZ 1400 resist and AZ 303 developer, diluted 1:7, to obtain a

Table 1. Optimum Amplitudes A_i and Phases ϕ_i for the Nine-Beam Fan-out ($i = 1 \ldots 9$)

	A_i								
	1.059	0.957	0.987	0.998	1.022	0.998	0.987	0.957	1.059
ϕ_i (rad)	1.772	0.135	3.887	2.455	3.142	2.455	3.887	0.135	1.772

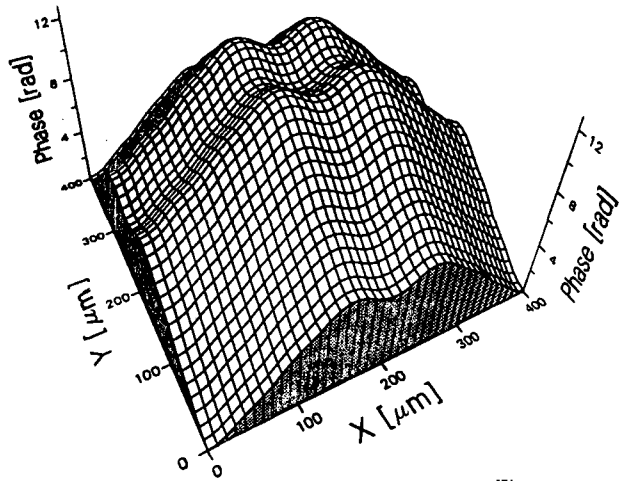

Fig. 2. One period of the optimized phase profile for a 9 × 9 fan-out element.

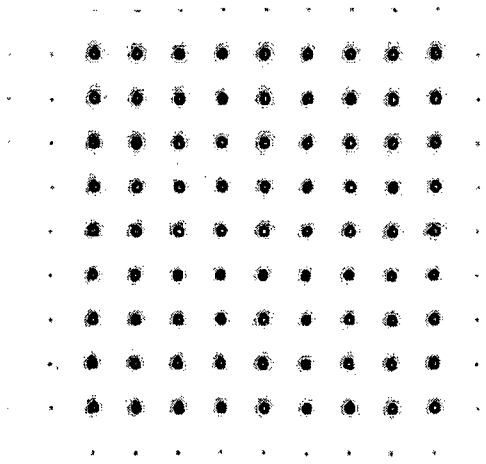

Fig. 3. 9 × 9 array of generated spots.

relatively linear dependence of the developed microrelief on the local exposure.

The spot size of the writing beam and the spacing of the raster lines are chosen according to the structure size of the microrelief. As our fan-out element has a slowly varying phase function (Fig. 2), a relatively large spot size can be used. This, together with a sufficient overlap of the raster scan,[6] reduces the sensitivity of the laser writing system to vibrations and therefore improves the quality of the relief surface. A spot size of 8 μm (1/e intensity points) and a raster line space of 2 μm have been used for the fabrication. The periodicity of the 9 × 9 fan-out element was chosen to be 400 μm. One unit cell of the optimized phase function was represented by 200 × 200 pixels. The phase data were then converted into resist thickness values, with a reconstruction wavelength of $\lambda = 488$ nm and a refractive index of the resist at this wavelength of $n = 1.64$. These parameters determine the maximum modulation depth of the surface-relief grating to be 1.55 μm.

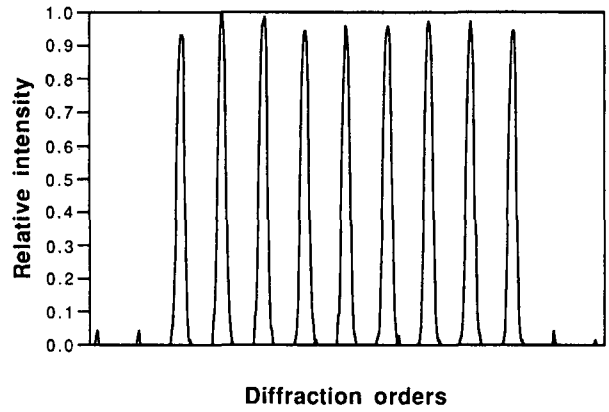

Fig. 4. Measured intensity profile of the central row.

For the reconstruction, the 9 × 9 fan-out element was illuminated by a collimated argon-ion laser beam. The generated spot array was evaluated by using a CCD camera. The experimenal results show an efficiency of 94% (relative to the total transmitted light) and a uniformity error within ±8% of the average diffracted beam power for the whole 9 × 9 arrray. Within one line or one row the uniformity is better than ±5%. Figure 3 shows the generated 9 × 9 pattern of light spots in the back focal plane of the lens (see Fig. 1), and Fig. 4 shows the intensity profile of the central row, which also contains the zero order. Once a master microrelief has been fabricated in photoresist, it can be reproduced by modern replication technology. Casting or embossing from a metal shim enables the fabrication of a large number of high-quality replicas. Such replicas are currently being fabricated.

We have shown that high-quality fan-out elements can be realized as continuous surface-relief gratings. The laser-beam writing system permits the fabrication of accurate master microreliefs in a photoresist that are suitable for further replication. The diffraction efficiency of 94% and uniformity of better than ±8% over the whole 9 × 9 array are, to our knowledge, the best results so far published for 2-D surface-relief fan-out elements.

References

1. J. Turunen, J. Fagerholm, A. Vasara, and M. R. Taghizadeh, J. Opt. Soc. Am. A **7,** 1202 (1990).
2. H. P. Herzig, D. Prongué, and R. Dändliker, Jpn. J. Appl. Phys. **29,** L1307 (1990).
3. D. Daly, S. M. Hodson, and M. C. Hutley, Opt. Commun. **82,** 183 (1991).
4. M. T. Gale, G. K. Lang, J. M. Raynor, H. Schütz, and D. Prongué, "Fabrication of kinoform structures for optical computing," Appl. Opt. (to be published).
5. D. Prongué, H. P. Herzig, R. Dändliker, and M. T. Gale, "Optimized kinoform structures for highly efficient fan-out elements,"Appl. Opt. (to be published).
6. M. T. Gale and K. Knop, Proc. Soc. Photo-Opt. Instrum. Eng. **308,** 347 (1983).

a reprint from Applied Optics

Continuous-relief diffractive optical elements for two-dimensional array generation

Michael T. Gale, Markus Rossi, Helmut Schütz, Peter Ehbets, Hans Peter Herzig, and Damien Prongué

Continuous surface-relief diffractive optical elements for two-dimensional array generation (fan-out) are designed and fabricated. Separable and nonseparable solutions for the two-dimensional element design are compared. The phase-grating microstructures are generated by laser-beam writing lithography in a single exposure step and converted to nickel shims by electroplating, enabling low-cost replicas to be produced by using laboratory and commercial replication processes. Results are presented for a 9 × 9 fan-out diffractive optical element with a measured efficiency of 94% and an overall uniformity within ±8%; replicas in epoxy have the same efficiency and a uniformity of ±15%.

Key words: Diffractive optical elements, fan-out, laser-beam writing lithography, replication.

Introduction

Space-invariant fan-out optical elements split a single laser beam into an array of quasi plane waves that can be focused by a lens to generate an array of equally intense light spots. Such diffractive optical elements (DOE's) have applications in optical-computing and parallel-processing systems.[1] The performance requirements include high efficiency and good uniformity of the array. Recent research has concentrated on the realization of multilevel elements[2] and continuous surface-relief elements.[3]

Continuous surface-relief microstructures represent an attractive alternative to multilevel structures and are, in general, capable of offering higher efficiency.[4] They can be fabricated by laser-beam writing in photoresist by using a high-precision scanning system with tight control of the resist processing.[5] Once this technology has been established, it can be effectively used for the fabrication of a wide variety of phase DOE's and other micro-optical components; the writing procedure is a single-step process, so the main effort in fabricating new microstructures would be in the design and programming. The fabrication of replicas by embossing or casting from a metal shim enables large numbers of elements to be generated from a single recording.

A laser-beam writing system for the fabrication of continuous-microrelief structures with programmable complex phase profiles has been built at the Paul Scherrer Institute in Zurich (PSIZ). The basic system has been described in an earlier study, together with results for one-dimensional (1-D) fan-out DOE's.[5] The theory for the design of the optimized continuous phase-transfer function of such 1-D fan-out elements is described in Ref. 6 and is generalized for two-dimensional (2-D) design in Ref. 7. Here, nonseparable solutions for a range of 2-D fan-out elements are proposed and compared with separable solutions that are obtained by crossing two 1-D solutions. Detailed experimental results are presented for an original photoresist recording and a replica of a 9 × 9 fan-out element, both of which have high efficiency and good uniformity.

Design of Two-Dimensional Fan-Out Elements

Theory

The design process for fan-out elements consists of two basic steps: the first leads to high efficiency, and the second optimizes the uniformity of the generated array of light spots with only a minimal decrease in efficiency. In contrast to the optimization of multilevel phase gratings described in Ref. 2, the transfer function of the fan-out element is defined here not in the grating plane but by the array of light spots in the Fourier plane. This approach results in a minimum set of parameters for the exact representation of the

M. T. Gale, M. Rossi, and H. Schütz are with the Paul Scherrer Institute, Badenerstrasse 569, 8048 Zurich, Switzerland. P. Ehbets, H. P. Herzig, and D. Prongué are with the Institute of Microtechnology, University of Neuchâtel, Rue A.-L. Breguet 2, 2000 Neuchâtel, Switzerland.

Received 29 June 1992.
0003-6935/93/142526-08$05.00/0.

continuous phase function in the grating plane. The parameters to be optimized are the amplitudes and the phases of an array of point sources.

The desired field distribution in the back focal plane of the lens (Fig. 1) can be written as

$$U(x,y) = \sum_{m=1}^{M}\sum_{n=1}^{N} A_{mn}\exp(i\phi_{mn})\delta(x - x_m, y - y_n), \quad (1)$$

where A_{mn} is the amplitude, ϕ_{mn} is the phase, and (x_m, y_n) is the position of the (mth, nth) spot of a 2-D array.

The field distribution $\hat{U}(u, v)$ in the grating plane is related to the field $U(x, y)$ by a Fourier transform:

$$\hat{U}(u, v) = \int_{-\infty}^{\infty}\int_{-\infty}^{\infty} U(x, y)\exp[2\pi i(xu + yv)]dxdy$$
$$= \sum_{m=1}^{M}\sum_{n=1}^{N} A_{mn}\exp(i\phi_{mn})\exp[2\pi i(x_m u + y_n v)]. \quad (2)$$

The field $\hat{U}(u, v)$ can be written in terms of magnitude $|\hat{U}(u, v)|$ and phase $\Psi(u, v)$:

$$\hat{U}(u, v) = |\hat{U}(u, v)|\exp[i\Psi(u, v)], \quad (3)$$

where $\Psi(u, v) = \arg(\hat{U})$.

The irradiance distribution $I(u, v)$ in the grating plane can then be expressed as

$$I(u, v) = |\hat{U}(u, v)|^2 = \sum_{m=1}^{M}\sum_{n=1}^{N} A_{mn}{}^2 + \sum_{mn}\sum_{m'n'} A_{mn}A_{m'n'}$$
$$\times \cos[2\pi[u(x_m - x_{m'}) + v(y_n - y_{n'})]$$
$$+ \phi_{mn} - \phi_{m'n'}], \quad (4)$$

where $m \neq m'$, $n \neq n'$, and $m + n \leq m' + n'$.

The first term on the right side of Eq. (4) is constant and equal to the mean object irradiance $\langle I \rangle$. The second term in Eq. (4) describes the variations of the irradiance in the grating plane. These irradiance variations are intermodulation effects and are caused by interference between the waves associated with the $M \times N$ point sources in the focal plane. In the case of regular arrays the expression for the intermodulation terms can be further simplified if the interference terms of equal spatial frequency are collected. We then obtain

$$I(u, v) - \langle I \rangle$$
$$= 2\sum_{mn}\sum_{m'n'} A_{mn}A_{m'n'}$$
$$\times \cos\{2\pi s[u(m - m') + v(n - n')] + \phi_{mn} - \phi_{m'n'}\}$$
$$= 2\sum_{i=1}^{M-1}\sum_{j=1}^{N-1} B_{ij}\cos[2\pi s(ui + vj) + \Phi_{ij}], \quad (5)$$

where $i = m - m'$, $j = n - n'$, s is the distance between two neighboring point sources, and B_{ij} and Φ_{ij} are the amplitudes and the phases, respectively, for one spatial frequency component of the intermodulation terms.

To perfectly reproduce the desired object $U(x, y)$, the fan-out element must have a transfer function proportional to $\hat{U}(u, v)$, which means an intensity transfer function proportional to $I(u, v)$ and a phase transfer function equal to $\exp[i\psi(u, v)]$. In order to reach the highest efficiency a pure phase element is chosen and the intensity transfer function is clipped to $I(u, v) = \text{const}$. Clipping the intensity variations changes the transfer function of the fan-out element and introduces errors at readout. In order to minimize these errors the intermodulation effects in the grating plane have to be reduced as much as possible. The optimization criterion can be formulated as

$$\iint\left\{\sum_{i=1}^{M-1}\sum_{j=1}^{N-1} B_{ij}\cos[2\pi s(ui + vj) + \Phi_{ij}]\right\}^2 dudv \rightarrow \min. \quad (6)$$

Since the intermodulation terms in Eq. (6) have different spatial frequencies, they are orthogonal, and the merit function of the efficiency optimization becomes

$$\sum_{i=1}^{M-1}\sum_{j=1}^{N-1} B_{ij}{}^2 \rightarrow \min. \quad (7)$$

The variables of the efficiency optimization are the phases ϕ_{mn} of the point sources, given in Eq. (1), while the amplitudes of the point sources for a uniform fan-out are all equal ($A_{mn} = 1$). The optimization problem is solved by applying a downhill simplex algorithm.[8] As a result of the first optimization step, a set of optimum phases $\phi_{mn}{}^{opt}$ is obtained. The transfer function of the fan-out element, defined in Eq. (3), is characterized by the phase-transfer function $\exp[i\psi(u, v)]$, calculated for uniform amplitudes and the optimum set of phases. It was found that clipping the minimized intermodulation terms hardly alters the high efficiency, but it reduces the uniformity of the generated array.

In order to improve the uniformity of the fan-out an additional optimization process is used. By iteratively changing the amplitudes of the initial point

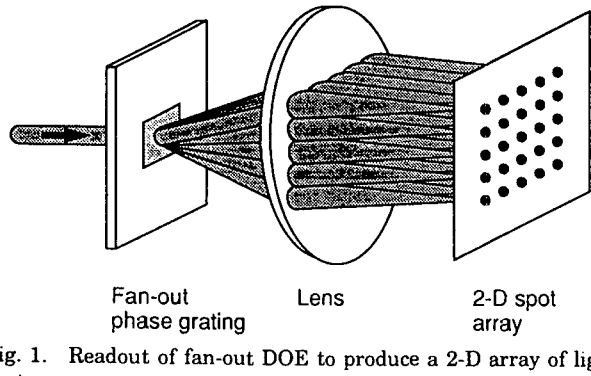

Fig. 1. Readout of fan-out DOE to produce a 2-D array of light spots.

sources A_{mn} slightly to $A_{mn}^{(i)}$, where i is the number of iteration loops, the resulting amplitudes of the generated array can be perfectly balanced. The second optimization process is equivalent to the 1-D case, which is presented in Ref. 6; it results in only a slight decrease in the optimized diffraction efficiency from step one. The insertion of both the optimum set of phases ϕ_{mn}^{opt} and the new amplitudes $A_{mn}^{(i)}$ in Eqs. (1) and (2) defines the optimized phase function $\psi(u, v)$ of the fan-out element, which generates a highly uniform array of spots.

Separable and Nonseparable Solutions

The above theory is used to design nonseparable solutions for different $N \times N$ arrays. In order to treat the most general case, no symmetries of the $N \times N$ arrays are considered. This means that $(N \times N - 1)$ variables ϕ_{mn} have to be admitted for the efficiency optimization. The phase of one light spot can be kept constant. The number of variables can be a limiting factor for the optimization of large fan-outs. Separable solutions are attractive for generating large $N \times N$ arrays in order to reduce the computing time. In this case the object is described by $U(x, y) = F(x)F(y)$, and thus only the 1-D problem has to be solved. On the other hand, if the 1-D solution of a $N \times 1$ array yields a diffraction efficiency η, the corresponding 2-D solution of the $N \times N$ array is less efficient, namely η^2. The results for the separable and nonseparable solutions are summarized in Table 1. The efficiencies of the $N \times N$ fan-out are shown after the first and second optimization steps. After the second optimization the uniformity error of the generated array is smaller than 0.1% for all calculated solutions.

As expected, the efficiencies of the nonseparable solutions after the uniformity optimization are always higher than the corresponding separable solutions. The only exception is the 9×9 fan-out. It provides the highest diffraction efficiency, and in this special case a better solution for a nonseparable design has not been found to our knowledge. The results from Table 1 show that nonseparable solutions are mainly of interest for $N \times N$ fan-outs with $N < 9$. For larger 2-D fan-outs the separable solution already provides an efficiency higher than 90%. It can be observed that the efficiencies of the nonseparable solutions decrease less during the second optimization step than those of the separable solutions. The reason is that the intermodulation effects can be better eliminated for the 2-D design.

Symmetries for the phases ϕ_{mn} of the 2-D array reduce the number of optimization variables for 2-D nonseparable solutions. The obtained efficiencies lie between the two limit values given by the separable and nonseparable asymmetric solutions presented in Table 1.

Table 1. Optimized Efficiencies for 2-D Fan-Out Elements

$N \times N$ Array	Efficiency after First Optimization (%)[a]	Efficiency after Second Optimization (%)[b]	Type of Solution
2 × 2	64.1	64.1	Separable
2 × 2	91.8	91.8	Nonseparable
3 × 3	88.4	85.7	Separable
3 × 3	94.1	93.9	Nonseparable
4 × 4	84.6	84.4	Separable
4 × 4	95.6	95.5	Nonseparable
5 × 5	96.0	84.8	Separable
5 × 5	93.6	92.6	Nonseparable
6 × 6	86.7	78.7	Separable
6 × 6	94.0	93.0	Nonseparable
7 × 7	96.0	93.7	Separable
7 × 7	96.1	94.2	Nonseparable
8 × 8	92.5	92.1	Separable
8 × 8	95.1	93.6	Nonseparable
9 × 9	98.8	98.6	Separable
9 × 9	98.8	98.6	Nonseparable
10 × 10	96.4	91.0	Separable
10 × 10	96.5	94.1	Nonseparable
11 × 11	97.6	95.5	Separable
11 × 11	97.6	95.5	Nonseparable

[a]First optimization is the efficiency optimization.
[b]Second optimization is the uniformity optimization.

Fabrication Tolerances

The realization of these efficient 2-D fan-out elements with the predicted small uniformity error requires accurate fabrication of the surface-relief profile. Figure 2 shows the computed tolerances for the relief profile of the 9×9 (separable design) array of Table 1. Errors in the relief profile are represented by an overall linear scale factor in the profile modulation of the microrelief. Whereas a scaling error of 1% in the amplitude of the microrelief leads to a reduction in efficiency of less than 0.1%, it results in a uniformity error of almost 10%. Achieving good uniformity thus requires accurate control over the microrelief amplitude and profile.

Fabrication by Laser Writing

A 9×9 fan-out element of separable design was fabricated by laser-beam writing. The 2-D solution was obtained by crossing two symmetric 1-D solutions, which created an element with a theoretical efficiency of 98.6% and an almost perfect uniformity.

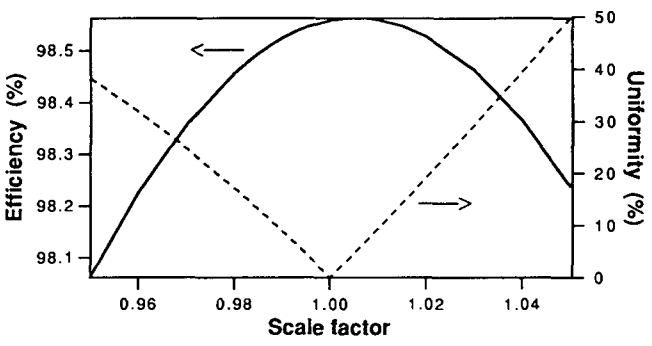

Fig. 2. Computed dependence of the efficiency (solid curve) and the uniformity (dashed curve) upon linear scaling errors in the profile modulation for the 9×9 fan-out element.

The numerical values of the optimized 1-D array are given in Table 2. The amplitiudes and phases of the optimum point sources for the 2-D solution are then determined by $A_{mn} = A_m A_n$ and $\phi_{mn} = \phi_m + \phi_n$, where $(m, n) = 1 \ldots 9$. The unit cell of the optimized phase profile for the 9 × 9 fan-out element is shown in Fig. 3.

The optimized phase function for the 9 × 9 fan-out element was obtained in photoresist by using the laser-beam writing system at PSIZ, resulting in a continuous surface-relief DOE. The basic writing system and data processing are shown in Fig. 4, and they are described in more detail elsewhere.[5,9] A resist-coated substrate is mounted on a precision air-bearing xy translation table and is scanned under a focused laser spot with a typical raster line spacing of 1 or 2 μm and a dynamic rms positioning accuracy of ~150 nm. Exposure data are computed from the desired final microrelief and from the (measured) resist development characteristic. Shipley AZ 1400 resist is used for film thicknesses up to 5 μm and is developed in AZ 303 developer to obtain a relatively linear dependence of the developed microrelief as a function of the local exposure.[6] The resist exposure is controlled by an acousto-optic modulator driven by custom-developed hardware that enables a complete line of 8-bit intensity data to be synchronously clocked out by interferometer pulses that are derived from the table-positioning controller. The xy table scanning speed is ~1 cm/s, which, combined with the deceleration and acceleration ramping overhead at the end of each line, leads to an exposure time of ~6 h for a 10 mm × 10 mm DOE. Development of the exposed resist film results in the required microrelief structure, which can be then further processed to produce a replication shim.

The periodicity of the 9 × 9 fan-out element was chosen to be 400 μm. As the 9 × 9 fan-out element has a slowly varying phase function (see Fig. 3), a relatively large writing spot size and considerable overlap of the raster scan lines can be used. This improves the quality of the relief surface by minimizing modulation at the scan-line periodicity[10] as well as by reducing the sensitivity of the laser writing system to vibrations. A spot size of 8 μm ($1/e$ intensity points) and a raster line spacing of 2 μm were used for this fabrication work. One unit cell of the optimized phase function was represented by 200 × 200 pixels, and the DOE phase data was converted into microrelief profile by taking into account the refractive index n of the final microstructure material and the readout wavelength λ.

DOE's were fabricated and evaluated as original resist recordings ($n = 1.64$ for $\lambda = 488$ nm) and as replicas in Epo-tek 301-2 epoxy[11] ($n = 1.56$ for $\lambda = 633$ nm) and polyvinyl chloride (PVC) ($n = 1.54$ for $\lambda = 633$ nm). The modulation depth of the resulting microstructures varied between ~1.5 and ~2.4 μm. A reproducibility of approximately ±3% in the profile depth was achieved with careful control of the resist film preparation and the development procedure. Because of the tight fabrication tolerances (see Fig. 2), DOE's were typically fabricated in groups of nine with programmed 1% or 2% steps of the modulation amplitude around the design value. The DOE with the best uniformity was then selected from the developed or replicated microstructures.

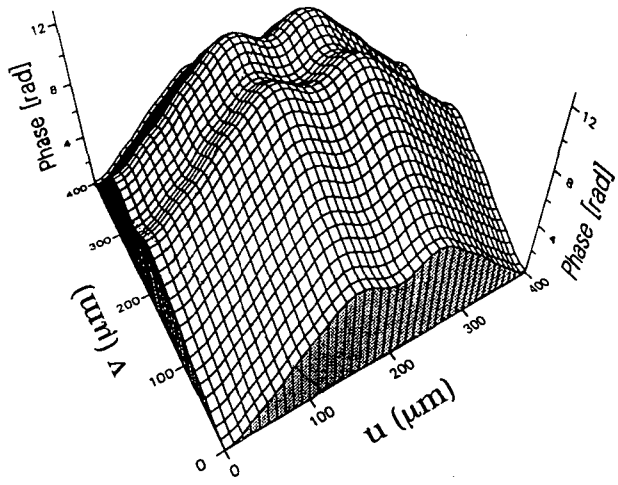

Fig. 3. One period (unit cell) of the optimized phase profile for a 9 × 9 fan-out element.

Replication

An important feature of DOE's recorded as surface-relief microstructures is the ability to reproduce the structures by replication techniques such as embossing and casting. For small quantities this can be carried out in the laboratory with relatively simple apparatus; low-cost mass production can benefit from commercial replication processes for holograms and other surface-relief structures.

All replication technologies require the fabrication of a metal shim (a copy of the surface-relief microstructure). Figure 5 illustrates the route from the original recording in photoresist via nickel shims to replicas (further details can be found in Ref. 12). The first step is to fabricate the master (first-generation) shim by evaporating a thin silver film (~100-nm thick) to form a conductive coating on the photoresist surface. A nickel shim is then produced

Table 2. Optimum Amplitudes A_i and Phases ϕ_i for the Nine-Beam Fan-Out ($i = 1 \ldots 9$)

Point-Source Parameter	i								
	1	2	3	4	5	6	7	8	9
A_i	1.059	0.957	0.987	0.998	1.022	0.998	0.987	0.957	1.059
ϕ_i (rad)	1.772	0.135	3.887	2.455	3.142	2.455	3.887	0.135	1.772

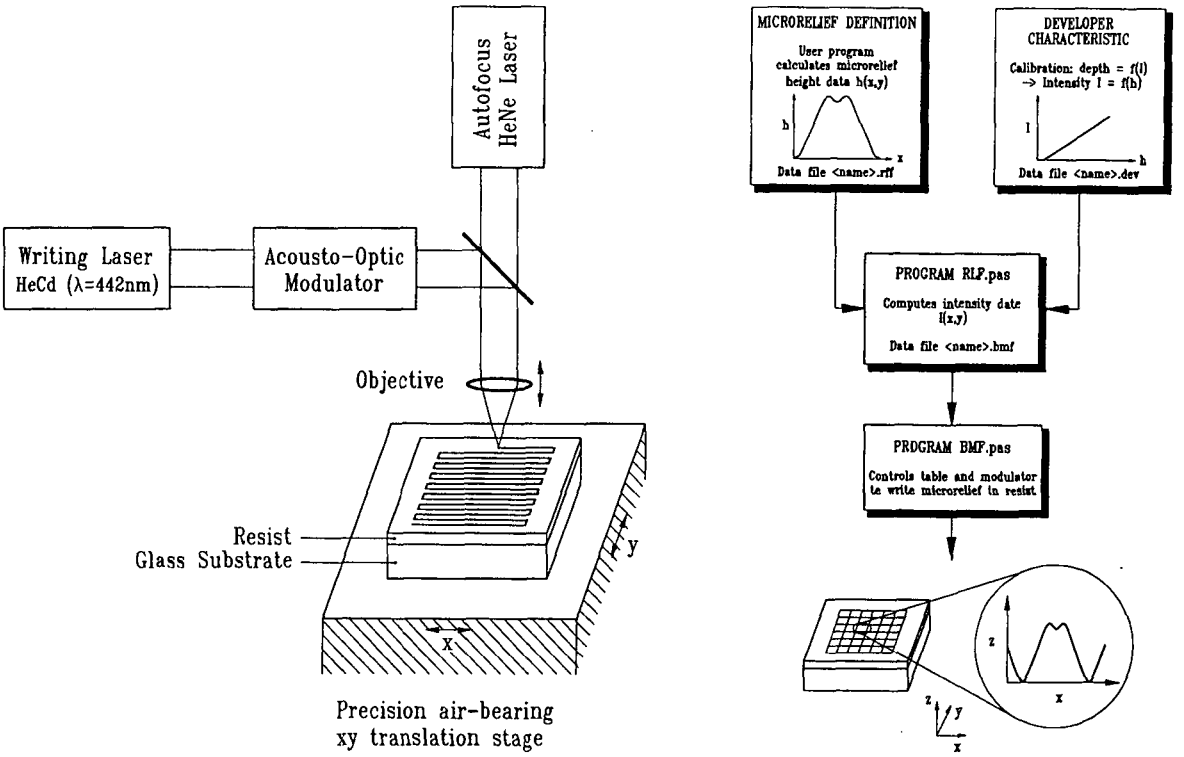

Fig. 4. Schematic of the software and hardware in the laser-beam writing system.

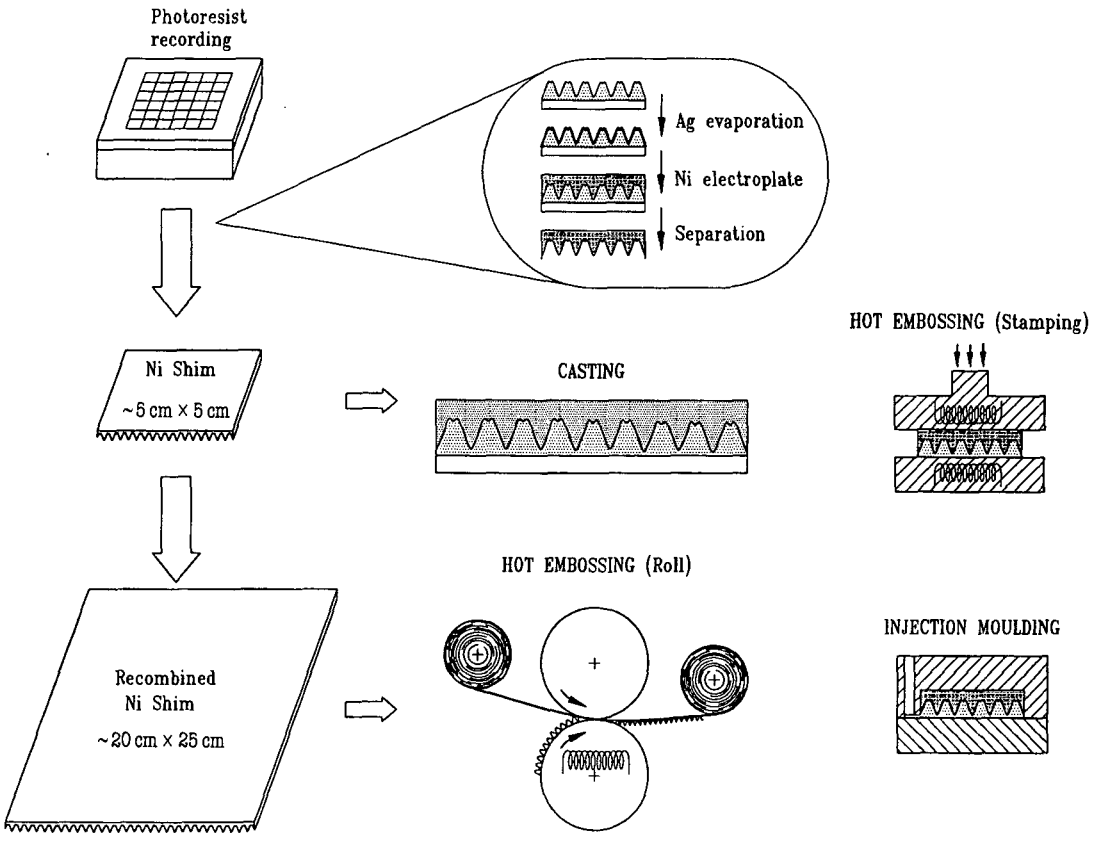

Fig. 5. Fabrication of replicas from an initial photoresist DOE recording. Casting and hot stamping are relatively simple processes suitable for replication in the laboratory. Roll embossing and injection moulding are industrial replication technologies suited to low-cost mass production.

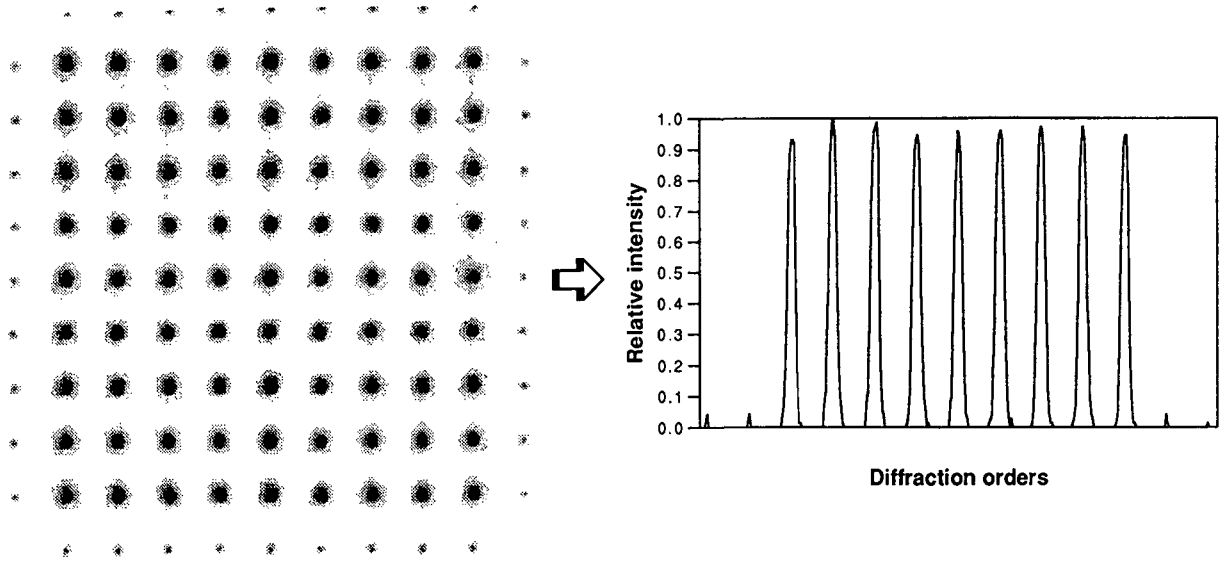

Fig. 6. Fan-out DOE in photoresist: measured spot pattern and intensities along the central line.

by electroplating Ni to a typical thickness of 60–100 μm (the photoresist microstructure is destroyed on separation from this metal copy). Subsequent generations of shims are obtained by passivating the shim surface in dichromate and electroplating a further copy. In general, third-generation shims are most suitable for the replication process, since the profile polarity is correct for producing a replica identical to the original photoresist recording, and multiple copies can be generated from a single second-generation shim without risking the first-generation master.

The main approaches for replication (see Fig. 5) are the following:

Casting. High-quality replicas can be fabricated in the laboratory by casting into a thin film of curable epoxy (e.g., Epo-tek 301-2) coated onto a glass substrate. Curing is typically thermal, although UV-curable materials can also be used.

Embossing. Both flat-bed (stamping) and continuous-roll embossing are currently used for the commercial replication of surface-relief microstructures such as security holograms and diffractive packaging film.[12,13] Roll embossing into thermoplastic film (such as PVC) is capable of achieving fast replication (up to 1 m^2/s) at low cost (down to $\$1/m^2$). Current hot-embossing technology has been developed for microstructures up to ~1 μm in amplitude; successful replication of deeper microstructures requires careful optimization of the materials and process conditions.

Injection moulding. Replication using injection-moulding processes such as those used for the production of compact disks have been shown to produce high-quality replicas of microrelief structures in poly(methyl methacrylate).[14] Although this technology probably has the higher costs per unit area, the basic process is well established for compact disk production and is capable of producing excellent replicas.

The current PSIZ laser writing system produces recordings and shims of typically 5 cm × 5 cm in size. These are used for laboratory replication tests and

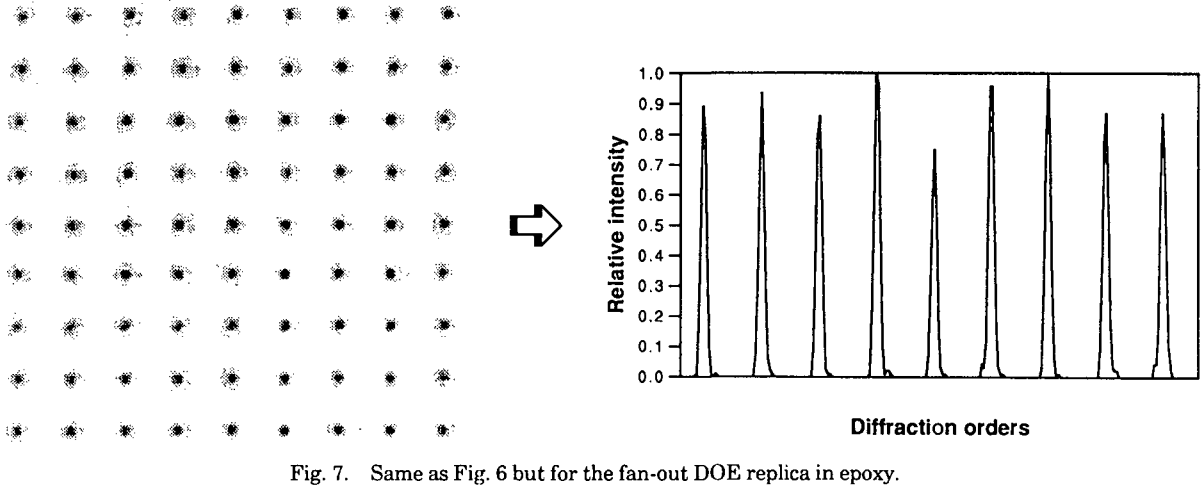

Fig. 7. Same as Fig. 6 but for the fan-out DOE replica in epoxy.

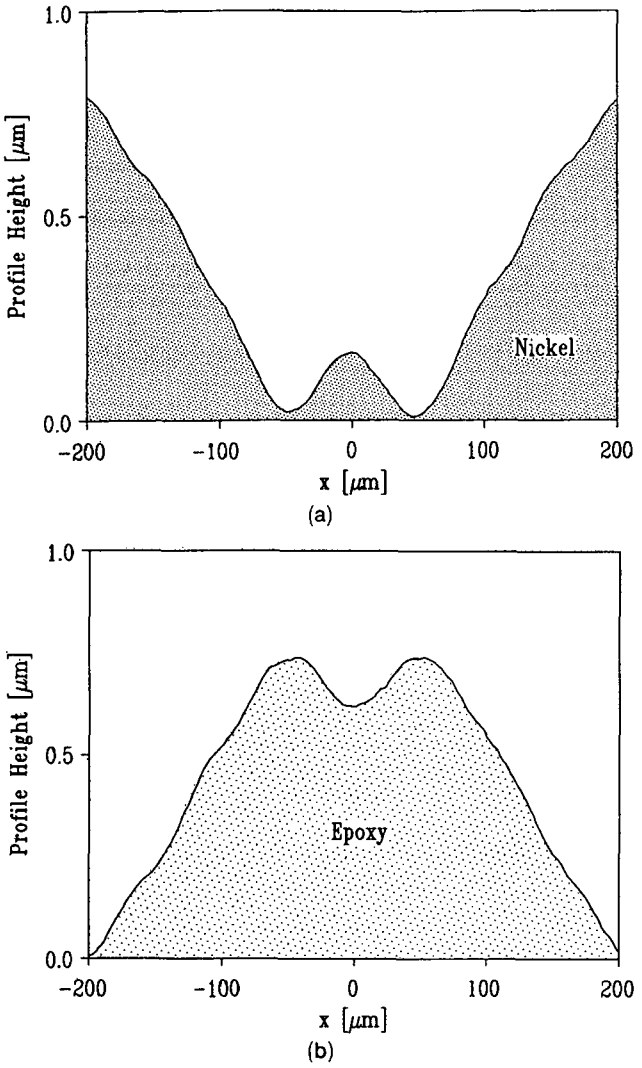

Fig. 8. Profile measurements of (a) a nickle shim and (b) the replica in epoxy. The slight difference in the profiles and modulation amplitudes are due to different measurement line positions.

small volume production by casting or flat-bed embossing. Commercial equipment for flat-bed and roll embossing of holographic microstructures requires shims of typically 20 cm × 25 cm in size. For test embossings in PVC, such production shims were generated by recombination from the smaller shims produced from the laser-written microstructure.[15]

Results

DOE's with 9 × 9 fan-out (separable design) were fabricated in photoresist by laser-beam writing and converted to nickel shims by electroplating. Replicas were then produced by casting into epoxy on glass and by embossing into PVC sheet. Large, recombined shims are currently being used for test replication in PVC on a commercial embossing system.

Figure 6 shows the image recorded by the CCD camera at the back focal plane of the lens (cf. Fig. 1) for the reconstruction from a 9 × 9 fan-out DOE in photoresist illuminated by a collimated argon laser beam (λ = 448 nm). The figure shows the image of the reconstructed spots and the intensities in the central row (which includes the zero order). The spot intensities were measured by using a detector with an aperture diameter equal to one fifth the spot spacing. Uniformity is defined as $(I_{max} - I_{min})/(I_{max} + I_{min})$, where I_{max} and I_{min} are the maximum and minimum spot intensities. The efficiency values given are the sum of the spot intensities as a fraction of the total light transmitted through the DOE. The measurements for this DOE obtained an efficiency of 94% and a uniformity of ±8% over the whole 9 × 9 array. Within one line or one row the uniformity was better than ±5%.

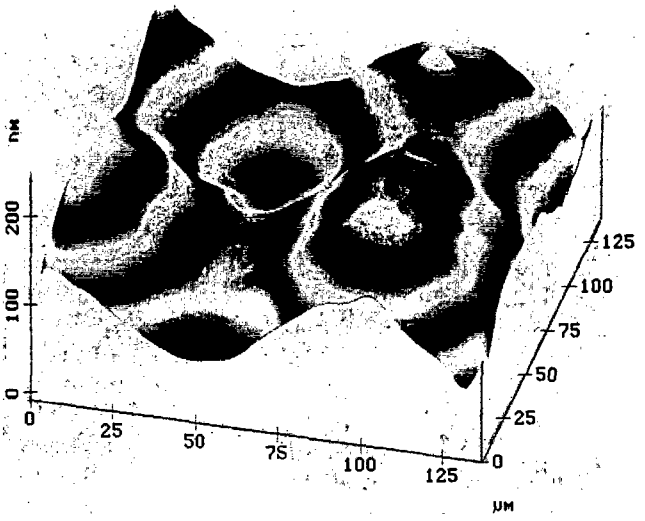

Fig. 9. Atomic force microscope image showing a 2-D profile at the center of a fan-out DOE unit cell.

Corresponding results for a replicated fan-out DOE in epoxy are shown in Fig. 7. The structure was designed for a refractive index n = 1.56 (Epo-tek 301-2) and a readout at λ = 633 nm. The efficiency is also ~94%, but the uniformity is somewhat lower, ~±15%, which can be traced to errors in the recording process leading to a relief amplitude that is deeper than the design value (cf. Fig. 2). Line surface profile measurements for a nickel shim and the replicated DOE in epoxy are shown in Fig. 8 (the slightly different modulation amplitudes are due to different measurement line positions). An atomic force microscope profile measurement of the central 140 μm × 140 μm of the 400 μm × 400 μm unit cell is shown in Fig. 9.

Conclusions

The design of continuous-relief DOE microstructures for 2-D array generation has been investigated, and the performance of separable and nonseparable solutions has been compared. Nonseparable solutions are of interest mainly for $N \times N$ format with $N < 9$. For larger 2-D fan-out structures the separable solution already provides a satisfactory efficiency of >90%.

Fan-out DOE's have been fabricated by laser-beam writing in photoresist. Replicas were produced from the photoresist recording by electroplating a nickel shim and hot embossing into thermoplastic film or by

casting in optical epoxy. Replicated 9 × 9 fan-out DOE's fabricated with the latter approach showed an excellent efficiency of 94% and a uniformity of ±15%. The technology enables a wide variety of DOE microstructures to be fabricated by using a single-step writing process and reproduced in large or small volume at reasonable cost.

The authors are grateful to C. Appassito, G. K. Lang, and J. M. Raynor for their contributions in developing the control hardware and software for the laser writing system and to J. S. Pedersen for electroplating the replication shims. We also thank R. Dändliker, K. Knop, and R. E. Kunz for numerous fruitful discussions and ideas. This work was supported in part by the Board of the Swiss Federal Institutes of Technology.

References and Notes

1. N. Streibl, "Beam shaping with optical array generators," J. Mod. Opt. **36,** 1559–1573 (1989).
2. J. Turunen, J. Fagerholm, A. Vasara, and M. R. Tagizadeh, "Detour-phase kinoform interconnects: the concept and fabrications considerations," J. Opt. Soc. Am. **7,** 1202–1208 (1990).
3. H. P. Herzig, D. Prongué, and R. Dändliker, "Design and fabrication of highly efficient fan-out elements," Jpn. J. Appl. Phys. **29,** L1307–L1309 (1990).
4. D. Daley, S. M. Hodson, and M. C. Hutley, "Fan-out gratings with a continuous profile," Opt. Commun. **82,** 183–187 (1991).
5. M. T. Gale, G. K. Lang, J. M. Raynor, H. Schütz, and D. Prongué, "Fabrication of kinoform structures for optical computing," Appl. Opt. **31,** 5712–5715 (1992).
6. D. Prongué, H. P. Herzig, R. Dändliker, and M. T. Gale, "Optimized kinoform structures for highly efficient fan-out elements," Appl. Opt. **31,** 5706–5711 (1992).
7. P. Ehbets, H. P. Herzig, D. Prongué, and M. T. Gale, "High-efficiency continuous surface-relief gratings for two-dimensional array generation," Opt. Lett. **17,** 908–910 (1992).
8. W. H. Press, B. P. Flannery, S. A. Teukolsky, and W. T. Vetterling, *Numerical Recipes in Pascal* (Cambridge U. Press, Cambridge, 1989).
9. M. T. Gale, G. K. Lang, J. M. Raynor, and H. Schütz, "Fabrication of micro-optical components by laser beam writing in photoresist," in *Micro-Optics II,* A. M. Scheggi, ed., Proc. Soc. Photo-Opt. Instrum. Eng. **1506,** 65–70 (1991).
10. M. T. Gale and K. Knop, "The fabrication of fine lens arrays by laser beam writing," in *Industrial Applications of Laser Technology,* W. F. Fagan, ed., Proc. Soc. Photo-Opt. Instrum. Eng. **398,** 347–353 (1983).
11. Product of Epoxy Technology, Inc., Billerica, Mass.
12. B. Kluepfel and F. Ross, eds., *Holography Market Place* (Ross, Berkeley, Calif., 1991).
13. M. T. Gale, "Diffractive microstructures for security applications," IEE Conf. Publ. London **342,** 205–209 (1991).
14. A. Neyer, T. Knoche, P. Dannberg, and L. Müller, "New fabrication technology for polymer optical waveguides," in *Integrated Photonics Research,* Vol. 10 of 1992 OSA Technical Digest Series (Optical Society of America, Washington, D.C., 1992), paper WB2-1.
15. The recombination and PVC embossings were carried out by 3D Ltd., Unterägeri, CH-6314, Switzerland.

Continuous-relief fan-out elements with optimized fabrication tolerances

Peter Ehbets, Markus Rossi*, and Hans Peter Herzig

Institute of Microtechnology

University of Neuchâtel

Rue A.-L. Breguet 2

CH-2000 Neuchâtel, Switzerland

*Paul Scherrer Institute Zurich

Badenerstrasse 569

CH-8048 Zurich, Switzerland

to be published in

Optical Engineering

December issue, 1995

Abstract

The design of kinoform fan-out elements with high efficiency and reduced sensitivity to vertical profile scaling errors is presented. We start from a high-efficient continuous-phase fan-out solution and optimize the position of the 0-2π transitions in the phase function, in order to achieve a high fabrication error tolerance. The sensitivity of Fourier-transform and focusing fan-out elements to vertical etch depth errors is analyzed. The limitations for the fabrication of such structures by laser beam writing are discussed. In particular, the influence of the finite writing spot diameter on the fan-out performance is investigated. Design rules for fan-out elements, which consider fabrication constraints, are derived. Experimental results are presented for cylindrical focusing fan-out elements with small uniformity error (2%) and weak profile scaling dependence.

Subject terms: kinoform, fan-out, diffractive optics, laser beam writing.

1. Introduction

Space-invariant fan-out elements are key components for optical interconnections and find also applications in optical senors and in material processing. They split an incoming laser beam into an array of diffraction orders of equal power, which are focused by a Fourier-transform lens. The requirements on fan-out elements are a high efficiency and, in general, an uniformity error in the generated spot array below 10%.

On-axis diffractive optical elements (DOEs) with high diffraction efficiency require the fabrication of a kinoform which can be realized by either a continuous[1] or a multi-level[2] surface-relief grating structure. Unfortunately, low uniformity errors need a very accurate fabrication of the surface-relief profile, which is with both techniques difficult to achieve .[1,3] As a consequence, fabrication error tolerances are an important parameter and have to be included in the design process of kinoform elements.

In this paper, we concentrate on the design of continuous-relief fan-out elements which can be fabricated by laser beam writing. Alternative fabrication approaches for such structures are direct electron-beam writing[4] or gray-tone mask lithography[5]. These technologies produce the desired surface relief in a single lithographic step. Therefore, they can achieve a high lateral positioning accuracy. However, vertical profile depth errors are more difficult to control and are mainly responsible for poor fan-out performance. The goal of this paper is to present a design approach for continuous-relief fan-out elements which have high diffraction efficiency and a reduced sensitivity of the fan-out reconstruction quality to vertical profile depth errors.

In the second section, we review the design of highly efficient fan-out gratings. In addition, we consider the inclusion of focusing power to the fan-out element. The combination of multiple beam splitting and focusing in a single planar DOE enables the realization of compact micro-optical systems. In the third section, we analyze the sensitivity of Fourier-transform and focusing fan-out elements to profile depth scaling errors. In the fourth section, the fabrication by laser beam writing is discussed and the influence of the finite writing spot diameter on the fan-out performance is

analyzed. Finally, in section five, experimental results for cylindrical focusing fan-out elements with small profile scaling dependence are presented.

2. Design of fan-out elements

We restrict the discussion for the following to a one-dimensional geometry. The extension to the two-dimensional case is straight forward. The goal of the fan-out design process is to determine a phase function $\phi_f(x)$ which equalizes and maximizes the power in the N fan-out diffraction orders, which are defined by the Fourier coefficients

$$A_p = \frac{1}{d} \int_0^d \exp\{ i\phi_f(x) \} \exp\{ -i2\pi px/d \} \, dx \, , \tag{1}$$

where d is the grating period. In order to achieve the highest diffraction efficiency, we use the phases of the complex amplitudes of the diffraction orders A_p as free optimization parameters and calculate, as described in Refs. [1,6,7], an analog phase function $\phi_f(x)$. For the optimization process, we describe the quality of a Nx1 fan-out function $\phi_f(x)$ by the diffraction efficiency

$$\eta = \sum_{p=1}^{N} I_p \Big/ \sum_{p=-\infty}^{\infty} I_p \, , \tag{2}$$

and by the uniformity error

$$\sigma = \frac{I_{max} - I_{min}}{I_{max} + I_{min}} \, , \tag{3}$$

where I_{max}, I_{min} represent the maximum and minimum intensities of the N fan-out diffraction orders $I_p = |A_p|^2$. For regular fan-out elements (no suppressed diffraction orders in the fan-out pattern), high diffraction efficiencies over 90% are achieved. The dashed curve in Fig. 1 shows one period of the continuous phase function $\phi_f(x)$ for a 9x1 fan-out element which produces the fan-out pattern with a diffraction efficiency of $\eta = 99.3\%$ and perfect uniformity.

Focusing fan-out elements

A focusing fan-out element performs simultaneously the multiple beam splitting and the focusing operation. We assume illumination with a monochromatic plane wave and consider the read-out

geometry for a transmissive focusing fan-out element shown in Fig. 2. In this case, the phase function of the focusing fan-out element is the combination of the periodic Fourier-transform fan-out function $\phi_f(x)$ and a spherical phase function $\phi_s(x)$. Using paraxial scalar diffraction theory[8], the focusing fan-out element is described by the complex-amplitude transmittance function

$$t(x; \lambda_o) = P(x) \exp\{ i[\phi_f(x) + \phi_s(x)] \} , \tag{4}$$

where λ_o is the design wavelength in free space, $P(x) = \mathrm{rect}(x/D)$ is the rectangular aperture of diameter D, and the spherical phase function $\phi_s(x)$ can be written in the paraxial approximation as

$$\phi_s(x) = -\frac{\pi x^2}{\lambda_o f} , \tag{5}$$

where f is the focal length. The field propagation to the detection plane is then described by the Fresnel diffraction integral

$$U(x', z) = \frac{\exp(ikz)}{\sqrt{i\lambda z}} \int_{-\infty}^{\infty} t(x; \lambda_o) \exp\left\{ i \frac{k}{2z} [x' - x]^2 \right\} dx , \tag{6}$$

where $k=2\pi/\lambda$ and λ is the read-out wavelength. Inserting Eqs. (4) and (5) into Eq. (6) and using $\lambda = \lambda_o$, the field distribution $U(x', z = f)$ in the focal plane at $z = f$ becomes essentially the Fourier transform (*FT*) of the fan-out phase function $\phi_f(x)$

$$U(x', z = f) \propto FT\{ \mathrm{rect}(x/D) \exp(i\phi_f(x)) \} = \sum_{p=-\infty}^{\infty} A_p \mathrm{sinc}\left(\frac{D}{\lambda_o f} [x' - p\lambda_o f/d] \right) , \tag{7}$$

where $\mathrm{sinc}(x) = \sin(\pi x)/(\pi x)$. The spot spacing $\Delta x'$ in the focal plane becomes

$$\Delta x' = \frac{\lambda_o f}{d} . \tag{8}$$

In order to separate the spots and not to introduce noise, several periods of the fan-out element have to be illuminated. In particular, we chose the aperture diameter D to be an integer multiple of the fan-out period d, i. e. $D = Md$ with $M > 10$. The efficiency η and the uniformity error u of the focused spot array are then determined by the quality of the initial fan-out function $\phi_f(x)$. Figure 3 shows the calculated irradiance distribution $I(x', z=f) = |U(x', z=f)|^2$ for a 9x1 focusing fan-out element with D = 2.56 mm, λ_o = 632.8 nm, d = 160 μm and f = 25 mm, which results in a spot

spacing in the focal plane of $\Delta x' = 99\ \mu m$. The 9x1 focusing fan-out element yields a maximum diffraction efficiency of $\eta = 99.3\%$ and perfect uniformity.

The realization of the transmittance function $t(x; \lambda_o)$ as a planar surface-relief DOE requires the wrapping of the phase function in Eq. (4) to an interval between 0 and an integer multiple of 2π. In the following, we restrict the discussion to the general case of a maximum modulation depth equal to 2π. Therefore, the maximum depth h of the corresponding surface-relief grating structure becomes

$$h = \frac{\lambda_o}{n(\lambda_o) - 1}, \tag{9}$$

where n is the refractive index of the grating material. The resulting phase function $\Psi(x)$ of the element can then be written as

$$\Psi(x) = \left(\phi_f(x) + \phi_s(x) + \varphi_o\right) \text{ modulo } 2\pi \ , \tag{10}$$

where φ_o is a constant phase offset. The consequence of the phase wrapping are discrete transitions from 0 to 2π in the phase profile. Using the phase offset φ_o in Eq. (10), the position of the transition points can be laterally shifted. This has no effect on the fan-out quality for an ideal element with the calculated phase function $\Psi(x)$ of Eq. (10). However, as we show in the next section, the fabrication error tolerances for the kinoform surface-relief element, that generates the phase function phase $\Psi(x)$, depend strongly on the position of the transition points. Therefore, the phase offset φ_o can be efficiently used to reduce the sensitivity of the kinoform element to fabrication errors.

3. Fabrication error tolerances

In this section, we consider the influence of vertical etch depth errors on the reconstruction quality of the ideal fan-out phase function $\Psi(x)$ and minimize the sensitivity of the fan-out function to such fabrication errors.

For the analysis, we assume a linear scaling of the phase function $\Psi(x)$, which can result from either a wavelength change ($\lambda \neq \lambda_o$) or a linear surface relief error. The scaling results in the new transmittance function

$$t_s(x; \lambda) = P(x) \exp\{i\alpha\Psi(x)\} , \tag{11}$$

where α represents the linear scaling factor which has for a surface-relief DOE in transmission the form

$$\alpha = \frac{\lambda_o[n(\lambda) - 1]}{\lambda[n(\lambda_o) - 1]} \beta . \tag{12}$$

The first factor in Eq. (12) takes into account the wavelength and material dispersion dependence[9] and β represents the relief depth scaling. In order to understand the influence of the scaling errors on the fan-out performance, it is useful to note that the scaled phase function $\alpha\Psi(x)$ has the same periodicity as the ideally wrapped phase function $\Psi(x)$. As a consequence, the transmittance function of the scaled element $t_s(x; \lambda)$ can be expressed by a generalized Fourier series expansion of the variable $\Psi(x)$ [10,11]:

$$t_s(x; \lambda) = P(x) \sum_{q=-\infty}^{\infty} B_q \exp\{iq\Psi(x)\} , \tag{13}$$

where the coefficients are given by

$$B_q = \frac{1}{2\pi} \int_0^{2\pi} \exp\{ i(\alpha - q)\Psi(x)\} \, d\Psi(x) = \exp\{ i\pi(\alpha - q)\} \, \mathrm{sinc}(\alpha - q) . \tag{14}$$

The term ($q = 1$) in Eq. (13) corresponds to the desired fan-out signal. As a consequence, scaling errors do not influence the optimized phase function $\Psi(x)$, but they reduce the power in the signal wave by a factor $|B_1|^2 = \mathrm{sinc}^2(\alpha - 1)$ and produce additional noise orders ($q \neq 1$) with amplitudes B_q, which affect the fan-out signal through interference. Inserting Eqs. (10) and (14) into Eq. (13), we can rewrite the transmittance function of the scaled element as

$$t_s(x; \lambda) = P(x) \sum_{q=-\infty}^{\infty} \exp\{ iq(\varphi_o - \pi)\} \mathrm{sinc}(\alpha - q) \exp\{ iq[\phi_f(x) + \phi_s(x)]\} , \tag{15}$$

where multiplicative phase factors have been omitted. The constant phase offset φ_0 changes the relative phase of the different orders (q) in Eq. (15) and can be used to minimize the interference effects without reducing the high diffraction efficiency η of the initial fan-out function $\phi_f(x)$.

In order to define a criterion for the sensitivity of the fan-out function to scaling errors, we calculate the average diffraction efficiency

$$\eta_s = 0.5\{\eta(\alpha = 0.9) + \eta(\alpha = 1.1)\} \tag{16}$$

and the average uniformity error

$$\sigma_s = 0.5\{\sigma(\alpha = 0.9) + \sigma(\alpha = 1.1)\} \ , \tag{17}$$

resulting from scaling factors $\alpha = 0.9$ and $\alpha = 1.1$.

This criterion corresponds to a large tolerable scaling error of ±10%, which can be achieved even in an industrial fabrication environment. It follows from Eq. (15), that the power in the signal fan-out order is reduced by the factor $|B_1|^2 = \text{sinc}^2(0.1) = 0.9675$, and the spurious noise orders contain 3.25% of the total power. In the next two sections, we have investigated numerically the sensitivity of the efficiency η_s and of the uniformity error σ_s to scaling errors for Fourier-transform and focusing fan-out elements.

Fourier-transform fan-out elements

We first have analyzed the scaling error sensitivity of Fourier-transform fan-out elements ($\phi_s(x) = 0$). Using direct write technologies, the continuous phase function $\phi_f(x)$ of a Fourier-transform fan-out element can either be directly realized or it can be wrapped to the interval $[0, 2\pi]$ for the fabrication. Both possibilities are shown in Fig. 1. In the ideal case, both approaches yield the same efficiency and uniformity. However, as will be shown in the following analysis, they have a fundamentally different behavior to scaling errors.

In the case of continuous-phase DOEs without discrete phase transitions, scaling errors modify directly the fan-out phase function $\phi_f(x)$ and therefore, affect directly the angular spectrum of the diffraction orders in Eq. (1). The generalized Fourier expansion in Eq. (15) is not valid for continuous phase functions. As a consequence, a strong dependence of the uniformity error on

scaling errors results. We have calculated the far-field of the scaled continuous fan-out phase function $\exp\{i\alpha\phi_f(x)\}$. The sensitivity criterion (Eq. (17)) produces an uniformity error of σ_s = 46% for the 9x1 fan-out element and of σ_s = 91% for a 45x1 fan-out element. In the absence of scaling errors (α = 1.0), both optimized fan-out elements generate an uniformity error σ below 0.1%.

In order to analyze Fourier-transform fan-out elements with the wrapped phase function, the Fraunhofer diffraction pattern of the scaled transmittance function $t_s(x; \lambda)$ in Eq. (15) has to be calculated. Since the fan-out phase function is periodic, the Fraunhofer diffraction pattern is a discrete function. Therefore, the fan-out diffraction orders and spurious noise orders are overlapping and interference effects are expected. The dashed curve in Fig. 4 shows the sensitivity σ_s of the uniformity error for the 9x1 fan-out element as a function of the phase offset φ_o. For comparison, we have also plotted the uniformity error sensitivity σ_s of the continuous phase function without discrete transitions. It is shown that by choosing an optimum value for φ_o, the interference effects between the fan-out orders and the spurious noise orders are minimized and the uniformity error sensitivity σ_s is reduced from over 40% to 8%. The phase function of the 9x1 fan-out element with the location of the transition points optimized to get minimum scaling error is represented in Fig. 1 by the solid line. Similar results have been obtained for fan-out elements with fan-out numbers $N \leq 9$. For larger fan-out numbers N, the uniformity error sensitivity u_s can be reduced by a similar amount, but no longer below 10%. This result can be seen in Fig. 5 for the 45x1 fan-out element, where only a minimum uniformity sensitivity of σ_s = 30% is achieved. The main problem for the remaining large uniformity error is the interference with the zero-order term of the generalized Fourier expansion in Eq. (15). The zero-order term is not spread out by the fan-out function $\phi_f(x)$ and produces in the far-field a single peak on the optical axis. Since the amplitude of one fan-out order scales as $(\eta/N)^{0.5}$ with increasing fan-out number N, the interference of the central fan-out order with the zero-order peak on the optical axis can no longer be compensated. As shown in Ref. 3, further improvement is possible by shifting the fan-out array off-axis and separating the fan-out orders from the zeroth order. A lateral shift of half the spot

spacing $\Delta x'$ in the far-field, which corresponds to the addition of a linear phase varying from 0 to π over one period of the fan-out function $\phi_f(x)$, is sufficient to reduce the uniformity error sensitivity σ_s of the 45x1 fan-out element to about 15%, as shown in Fig. 5. In this special case, the uniformity sensitivity σ_s dependence on the phase offset φ_0 has a periodicity of π, since only odd numbered (q) terms of the generalized Fourier expansion overlap with the fan-out diffraction orders in the far-field.

Scaling errors have only a small influence on the diffraction efficiency of fan-out elements in the far-field. This holds for continuous and wrapped fan-out phase functions. Note that due to the presence of uniformity errors, the efficiency can even increase above the efficiency of the ideal fan-out function η.

Focusing fan-out elements

Adding focusing power $\phi_s(x)$ to the fan-out function increases the number of 0-2π transitions in the phase function. Therefore, a further improvement of the uniformity error sensitivity to scaling errors can be expected. This behavior has been demonstrated experimentally in a previous publication[12]. For the analysis of focusing fan-out elements, we have calculated the Fresnel propagation of the scaled transmittance function into the detection plane. By inserting Eqs. (5) and (15) into Eq. (6), we obtain for the Fresnel propagation of the scaled transmittance function $t_s(x; \lambda)$

$$U(x', z) = \frac{1}{\sqrt{i\lambda z}} \sum_{q=-\infty}^{\infty} \exp\{ iq(\varphi_0 - \pi) \} \operatorname{sinc}(\alpha - q)$$

$$\int_{-\infty}^{\infty} P(x) \exp\{ iq\phi_f(x) \} \exp\left\{ i\pi x^2 \left[\frac{1}{\lambda z} - \frac{q}{\lambda_0 f} \right] \right\} \exp\left\{ -i \frac{2\pi}{\lambda z} x x' \right\} dx \quad , \quad (18)$$

where multiplicative phase factors have been omitted. Similar to the analysis of the blazed Fresnel zone plate[9,11], the diffraction orders (q) of the generalized Fourier series expansion are focused in different planes at the locations

$$z_q = \frac{\lambda_o f}{\lambda q} \quad . \tag{19}$$

The fan-out pattern is focused in the plane $z_1 = \lambda_o f/\lambda$. The spot spacing $\Delta x'(z = z_1)$ of the fan-out orders in the plane $z = z_1$ can be calculated from Eqs. (18) and (19)

$$\Delta x'(z = z_1) = \frac{\lambda z_1}{d} = \frac{\lambda_o f}{d} \quad . \tag{20}$$

Therefore, in contrast to Fourier-transform elements, focusing fan-out elements have the property that the spot spacing in the focal plane z_1 is independent of the read-out wavelength λ. However, focusing fan-out elements are not achromatic, because the focal plane position z_1 depends on the read-out wavelength λ.

The defocusing of spurious noise diffraction orders in the focal plane z_1 of the fan-out function produces a continuous noise distribution and increases the signal-to-noise ratio. We have calculated the uniformity error sensitivity σ_s and the efficiency η_s of the focusing 9x1 fan-out element as a function of the focal length $z_1 = f$ for the parameters $\lambda = \lambda_o = 0.6328$ μm, D = 2.56 mm and d = 160 μm. The results have been obtained for a fixed value of the phase offset φ_o and are represented in Figs. 6 (a) and (b). On the top axis in Figs. 6 (a) and (b), we have given the inverse of the Fresnel number $N_f = D^2/(4\lambda f)$ for the focusing term $\phi_s(x)$ in the phase function $\Psi(x)$. The transition between the far-field and the near-field behavior can clearly be seen in both curves. The fluctuations for $f < 10^3$ mm and $N_f > 2.6$ indicate that the zero-order term is sufficiently defocused over more than one fan-out order. Thus, the fan-out performance is determined by the interference with a continuously distributed background noise. The efficiency η_s converges for decreasing f to the value $\eta_s = \text{sinc}^2(0.1)\eta = 0.961$ predicted by Eq. (15). In this limit, the interference effects on the efficiency and the uniformity become negligible.

Similar to the case of Fourier-transform fan-out elements, the uniformity error sensitivity of focusing elements can be minimized by optimizing the phase offset φ_o. It is important to note, that already a weak focusing power adds sufficient supplementary transition points to the phase function, in order to create fan-out elements which are almost insensitive to scaling errors. This

result is shown in Fig. 7, where the uniformity error sensitivity σ_s is plotted as a function of the phase offset φ_0 for a focusing 9x1 fan-out element with a focal length of f = 10^3 mm, which corresponds to a small Fresnel number of $N_f = 2.6$. For an optimum choice of φ_0, an uniformity error sensitivity u_s below 2% can be achieved.

As shown in this section, the optimization of the position of the 0-2π transition points in the kinoform relief reduces efficiently the sensitivity of the uniformity error to profile scaling errors. The position of the transition points can be optimized through the phase offset φ_0 which is therefore an important parameter for the fabrication of high-quality fan-out elements by direct-write technologies.

4. Fabrication by laser beam writing

Our approach for the fabrication of kinoform DOEs is direct laser beam writing in photoresist. By using successive replication of the master photoresist micro-relief, this technology has the potential of a low cost mass-fabrication process. The laser beam writing system at the Paul Scherrer Institute is described in detail in Refs. [1,13,14]. It uses for the writing a x-y raster scan movement which allows the realization of arbitrary two-dimensional structures. The resist is exposed by a focused HeCd laser beam at the wavelength $\lambda = 442$ nm. The writing spot diameter has been determined to $\delta = 1.6$ μm at 1/e intensity points by knife edge measurements. For relief depths $h \leq 3$ μm the Shipley Microposit S1828 photoresist is used, which after exposure is developed for 30 s, using the Shipley AZ 303 developer diluted 1:10 with deionized water. This process results in a very linear relief depth to exposure energy characteristic. Therefore, small errors during the exposure and the development process produce the linear relief scaling errors, which we consider for the fabrication error analysis.

The finite spot size of the laser beam writer does not allow to produce sharp steps at the 0-2π transitions in the surface-relief profile. The resulting surface relief can be described by a convolution of the ideal shape and the focused writing spot of diameter δ. The smoothed transitions

have a width approximately equal to the diameter δ of the writing spot. For small diameters δ in the order of the wavelength, the smoothed transitions in the surface relief can no longer be accurately described by amplitude transmittance and paraxial scalar diffraction theory. However, if we assume that the minimum segment size s between two transitions is much larger than the writing spot diameter δ, paraxial scalar diffraction theory gives accurate results. In this limit, we describe the resulting phase function $\Psi_c(x)$ after the surface-relief element directly by a convolution of the ideal phase function $\Psi(x)$ and a Gaussian point spread function (PSF), namely,

$$\Psi_c(x) = \Psi(x) * g(x) \ , \tag{21}$$

where * represents the convolution operation and

$$g(x) = \sqrt{\pi}\frac{\delta}{2}\exp\left\{-\frac{4x^2}{\delta^2}\right\} \tag{22}$$

is the normalized PSF of the laser beam writing system. The consequences on the profile shape are shown in Fig. 8, where the ideal phase function $\Psi(x)$ and the resulting phase function $\Psi_c(x)$ after the convolution are shown. The laser beam writing process introduces rounded transitions and reduces the modulation depth. As a consequence, the diffraction efficiency and the uniformity of the ideal phase function are reduced. We have analyzed, how these PSF effects can be compensated. In addition, we have veryfied, whether they change the optimized scaling error behavior of the kinoform function, which was derived in section 3 for perfect transitions.

For this purpose, we have calculated the Fresnel propagation (Eq. (6)) of the convolved phase function $\Psi_c(x)$ for the focusing 9x1 fan-out element into the focal plane z_1. The calculated diffraction efficiency η and the uniformity error σ are shown in Figs. 9 (a) and (b) as a function of the focal length $z_1 = f$ and the inverse of the Fresnel number N_f of the focusing element. The results have been calculated for $\lambda = \lambda_0 = 0.6328$ µm, D = 2.56 mm, d = 160 µm, δ = 1.6 µm and for a fixed phase offset value φ_0. We observe a reduction of the diffraction efficiency η which is proportional to the number of transition points in the surface-relief profile. This efficiency loss becomes the major problem for the realization of focusing elements with F-numbers = f/D $\leq$ 10. In this case, PSF compensation[15] and clipping of the phase function $\Psi(x)$ to a multiple of 2π have to

be considered. The uniformity error decreases with the focal length f. Focusing kinoform elements behave already for weak focusing power similar to off-axis elements[3], where the signal phase is encoded by the position of the transition points (detour-phase principle). As a consequence, the rounding of the transitions has only a small influence on the uniformity provided that the center of the transition remains at the correct position. Therefore, the optimized set of transition points, obtained for the ideal phase function $\Psi(x)$, yields also the best scaling error tolerances and should be used for the fabrication of focusing fan-out elements.

For the analysis of Fourier-transform fan-out elements, we have calculated the Fraunhofer diffraction pattern of the convolved phase function $\Psi_c(x)$. The influence of the convolution with the writing spot size has been analyzed for continuous-phase fan-out elements and fan-out elements with optimized 0-2π transitions. Figure 10 represents the efficiency η and the uniformity error u for the 9x1 fan-out element after convolution for both types versus the ratio of the grating period d to the writing spot diameter σ.

For continuous-phase elements, the efficiency η (solid line) is almost independent of the ratio d/δ. However, the uniformity error σ (dashed line) increases for small ratios d/δ. For ratios $d/\delta > 200$, the remaining small uniformity error σ is essentially due to a small scaling error, which can be directly compensated to achieve again perfect uniformity. This is no longer possible for smaller ratios d/σ, because the convolution changes the profile shape. In this case, the convolution operation has to be directly included in the design algorithm for the fan-out phase function $\phi_f(x)$. For this purpose, we use an iterative approach, as described in Ref. [16], and can achieve perfect uniformity and high diffraction efficiency in the case of the 9x1 fan-out element for ratios $d/\delta \geq 10$. For ratios $d/\delta < 10$, uniform fan-out solutions can be found, but no longer with the optimized shape of Fig. 1 and therefore with lower diffraction efficiency.

For fan-out solutions with optimized transitions, the efficiency loss for low ratios $d/\delta < 30$ becomes the main problem. In addition, the optimized scaling error behavior starts to fail at about the same limit. For ratios $d/\delta < 100$, the position of the transition points for optimized scaling error behavior starts to depend on the width δ of the PSF. Therefore in this domain, the position of the

transition points has to be reoptimized by taking into account the convolution with the writing spot size. For still smaller ratios $d/\delta < 30$, the solution behaves similar as a continuous-phase function. In this case, the scaling error tolerances can no longer be optimized and only poor diffraction efficiencies are achieved.

In conclusion, it is reasonable to fabricate Fourier-transform fan-out elements with small ratios d/δ as continuous-phase gratings, in order to achieve high diffraction efficiency. For larger ratios d/δ, it is preferable to introduce discrete transitions to the phase function and optimize the scaling error behavior, as shown in section 3, in order to achieve better fabrication error tolerances. The above limits have been calculated for the 9x1 fan-out element. However, numerical simulations have shown that the critical values of ratio d/σ are proportional to the fan-out number N.

5. Experimental results

Experimental results have been achieved for the fabrication of cylindrically focusing 9x1 fan-out elements in photoresist. The elements have been designed for the wavelength $\lambda_0 = 0.6328$ µm, with a diameter D = 2.64 mm, a fan-out period d = 165 µm, and focal length f = 25 mm, which corresponds to a F-number ≈ 10. This results in a smallest segment size of s = 12 µm at the border of the structure. In order to use a standard fabrication process of the laser beam writer, the phase function has been rounded to a 1x1 μm^2 pixel grid. Smaller pixel sizes are possible but increase the writing time of the structure. The rounding shifts the position of the transition points and introduces detour-phase errors to the signal phase function. However, since the local phase error is not repetitive for focusing elements, the rounding operation produces a negligible uniformity error (< 1%). Figure 11 shows an atomic force microscope measurement of the profile shape in the central region of the focusing fan-out element. Clearly visible is the surface roughness, which is due to the varying overlap between neighboring scan lines due to positioning errors along the scan movement. We have fabricated on the same substrate 8 different fan-out elements with varying exposure energy, linearly scaled with factors α from 0.85 to 1.20. In Fig. 12, we have represented the measured efficiency η and the measured uniformity error σ of the 8 elements, as well as the

simulated scaling behavior of the ideal phase function convolved with the Gaussian PSF of diameter $\delta = 1.6$ μm. Good agreement between the experimental results and the theoretical data is observed. Note, that for a non-optimized choice of the transition points, the scaling error behavior can be 10 times worse. The measured uniformity error is smaller than 5%, even for a large scaling error of 20%. A maximum diffraction efficiency of 74% has been measured (compensated for the Fresnel reflection at the photoresist-air and glass-air interfaces). The 10% efficiency loss compared to the calculated values is due to the scattered light from the surface roughness. As shown in Fig. 12, the surface roughness has a basic periodicity equal to the interscan distance (1 μm). Therefore, the major quantity of scattered light is diffracted out of the fan-out signal pattern and does not affect the uniformity.

6. Conclusions

Continuous-phase DOEs can be calculated by using design concepts based on either geometrical optics or physical optics. The resulting continuous phase function can always be wrapped to an integer multiple m of 2π, in order to reduce the modulation depth and to enable the realization by a planar surface-relief DOE. In the ideal case, the phase wrapping has no influence on the optical performance of the element. However, the phase wrapping and, in particular, the position of the transition points determine the stability of the kinofom phase function against fabrication errors. In this paper, we have shown that in the case of kinoform DOEs which produce a discrete intensity distribution in a desired image plane, the position of the $0\text{-}2\pi m$ transition points in the phase function can be optimized, in order to achieve high tolerance of the kinoform reconstruction quality against vertical profile scaling errors. As a result of this optimization process, the sensitivity of fan-out kinoforms to profile scaling errors can be reduced by about a factor 10. Scaling errors represent a major problem in the fabrication of kinoform surface reliefs by direct-write techniques. As a consequence, fabrication error tolerances and scaling error optimization should be included in the design process of the phase function, in order to realize high-quality elements.

Numerical results have been presented for the design of Fourier-transform and focusing fan-out elements which enable high diffraction efficiency and have optimized profile scaling error tolerances. The fabrication of such elements by laser beam writing is discussed and limits for the validity of the fabrication error tolerance optimization are derived. Experimental results have been achieved for the fabrication of focusing 9x1 fan-out elements by laser beam writing in photoresist. Uniformity errors smaller than 5% for profile scaling errors up to 20% have been demonstrated.

References

[1] M.T. Gale, M. Rossi, H. Schütz, P. Ehbets, H.P. Herzig, and D. Prongué, "Continuous-relief diffractive optical elements for two-dimensional array generation," Appl. Opt. **32**, 2526-2533 (1993).

[2] J. M. Miller, M. R. Taghizadeh, J. Turunen, N. Ross, E. Noponen, and A. Vasara, "Kinoform array illuminators in fused silica," J. of Mod. Opt. **40**, 723-732 (1993).

[3] J. Turunen, J. Fagerholm, A. Vasara, and M.R. Tagizadeh, "Detour-phase kinoform interconnects: the concept and fabrication considerations," J. Opt. Soc. Am. A **7**,1202-1208 (1990).

[4] M. Larsson, M. Ekberg, F. Nikolajeff, and S. Hard, "Successive-development optimization of resist kinoforms manufactured with direct-writing electron-beam lithography," Appl. Opt. **33**,1176-1179 (1994).

[5] Y. Oppliger, P. Sixt, J. M. Stauffer, J. M. Mayor, P. Regnault, and G. Voirin, "One-step shaping using gray-tone mask for optical and microelectronic applications," Microelectron. Eng. **23**, 449-454, (1994).

[6] U. Krackhardt, J.N. Mait, and N. Streibl, "Upper bound on the diffraction effciency of phase-only fan-out elements," Appl. Opt. **31**, 27-37 (1992).

[7] H. Lüpken, T. Peter, F. Wyrowski, and O. Bryngdahl, "Phase synthesis for array illuminator," Opt. Comm. **91**, 163-167 (1992).

[8] J. W. Goodman, *Introduction to Fourier optics* (McGraw-Hill, New York, 1968).

[9] D.A. Buralli, G.M. Morris, and J.R. Rogers, "Optical performance of holographic kinoforms," Appl. Opt. **28**, 976-983 (1989).

[10] J.W. Goodman and A.M. Silvestri, "Some effects of Fourier-domain phase quantization," IBM J. Res. Dev. **14**, 478-484 (1970).

[11] H. Dammann, "Blazed synthetic phase-only holograms," Optik **31**, 95 - 104 (1970).

[12] M. Rossi and R. Kunz, "Focusing fan-out elements based on phase-matched Fresnel lenses," Opt. Comm. **112**, 258-264 (1994).

[13] M.T. Gale, G.K. Lang, J.M. Raynor, H. Schütz, and D. Prongué, "Fabrication of kinoform structures for optical computing," Appl. Opt. **31**, 5712-5715 (1992).

[14] M.T. Gale, M. Rossi, J. Pedersen, and H. Schütz, "Fabrication of continuous-relief micro-optical elements by laser beam writing in photoresist," Opt. Eng. **33**, 3556-3566 (1994).

[15] M. Ekberg, F. Nikolajeff, M. Larsson, and S. Hard, "Proximity-compensated blazed transmission grating manufacture by direct-writing electron beam lithography," Appl. Opt. **33**, 103-107 (1994).

[16] J. Bengtsson, "Direct inclusion of the proximity effect in the calculation of kinoforms," Appl. Opt. **33**, 4993-4996 (1994).

Figure captions

Fig. 1. One period of the efficiency-optimized phase function for the 9x1 fan-out element: (dashed curve) continuous phase function, (solid curve) phase function with 0-2π transitions, optimized for highest profile scaling error tolerance.

Fig. 2. Read-out geometry for a transmissive focusing fan-out element.

Fig. 3. Calculated irradiance distribution in the focal plane of the focusing 9x1 fan-out element.

Fig. 4. Uniformity error sensitivity σ_s for the 9x1 fan-out element as a function of the phase offset parameter φ_o for a phase function with 0-2π transitions (dashed curve). The value of σ_s for the continuous phase function is indicated for comparison (solid curve).

Fig. 5. Uniformity error sensitivity σ_s for the 45x1 fan-out element as a function of the phase offset parameter φ_o: (dashed curve) phase function with 0-2π transitions, (dashed dotted curve) off-axis reconstruction of the fan-out function by half of the spot spacing distance $\Delta x'$. The value of σ_s for the continuous phase function is indicated for comparison (solid curve).

Fig. 6. Efficiency sensitivity η_s (a) and uniformity error sensitivity σ_s (b) for the focusing 9x1 fan-out element as a function of the focal length f and the inverse of the Fresnel number N_f. The curves are calculated for a fixed value of the phase offset parameter φ_o.

Fig. 7. Uniformity error sensitivity σ_s as a function of the phase offset parameter φ_o for the focusing 9x1 fan-out element with diameter D = 2.56 mm, fan-out period d =160 μm, wavelength λ = 0.6328 μm and focal length f = 1000 mm.

Fig. 8. Influence of the writing spot diameter δ on profile shape: (dashed curve) ideal phase function $\Psi(x)$, (solid curve) resulting phase function $\Psi_c(x)$ after the convolution with the Gaussian PSF of diameter δ = 1.6 μm at 1/e intensity points.

Fig. 9. Efficiency η (a) and uniformity error σ (b) as a function of the focal length f and the inverse of the Fresnel number N_f, produced by the phase function $\Psi_c(x)$ of the focusing 9x1 fan-out element after the convolution with the Gaussian PSF. The curves are calculated for a fixed value of the phase offset parameter φ_o.

Fig. 10. Efficiency η and uniformity error σ of the convolved phase $\Psi_c(x)$ as a function of the fan-out period d to the writing spot diameter δ ratio for the 9x1 fan-out element. (a) efficiency and (b) uniformity error of the continuous phase function; (c) efficiency and (d) uniformity error of the phase function with optimized 0-2π transitions.

Fig. 11. AFM measurement of the profile in the central region of a cylindrical focusing 9x1 fan-out element designed for the wavelength λ = 0.6328 μm with diameter D = 2.64 mm, fan-out period d = 165 μm and focal length f = 25 mm.

Fig. 12. Efficiency η and uniformity error σ of the fabricated element as a function of the scaling factor α. (solid curve) calculated efficiency, (dashed curve) calculated uniformity error, (o markers) measured efficiency, and (+ markers) measured uniformity error.

Peter Ehbets received the diploma in physical electronics from the University of Neuchâtel, Switzerland, in 1990. Then, he joined the Applied Optics Group at the Institute of Microtechnology of the University of Neuchâtel as a graduate research assistant. In 1995, he received the Ph.D. degree in Optics from the University of Neuchâtel. His current research deals with the design and fabrication of diffractive optical elements for beam shaping and optical interconnects.

Hans Peter Herzig received the diploma in physics from the Swiss Federal Institute of Technology in Zürich (ETHZ), Switzerland, in 1978. From 1978 to 1982 he was a scientist in the Optics Development Department of the company Kern in Aarau, Switzerland, where he worked in lens design and optical testing. In 1983, he joined the Applied Optics Group at the Institute of Microtechnology of the University of Neuchâtel, Switzerland, as a graduate research assistant, working in the field of holographic optical elements, especially scanning elements. In 1987, he received the Ph.D. degree in Optics from the University of Neuchâtel. Now, he is lecturing modern optics and is responsible for the research in microoptics, including diffractive optical elements and microlenses.

Markus Rossi received his MSc degree in physics at the Swiss Federal Institute of Technology (ETH), Zürich, Switzerland in 1990. He is currently working at the Paul Scherrer Institute in Zürich on the design, fabrication, and characterization of micro-optical elements. In 1995, he received the Ph.D. degree in Optics from the University of Neuchâtel, Switzerland. His work includes the study of novel types of planar optical elements in the form of phase-matched Fresnel elements and their fabrication by laser beam writing. Special interest is devoted to applications of micro-optical elements for optical interconnection systems.

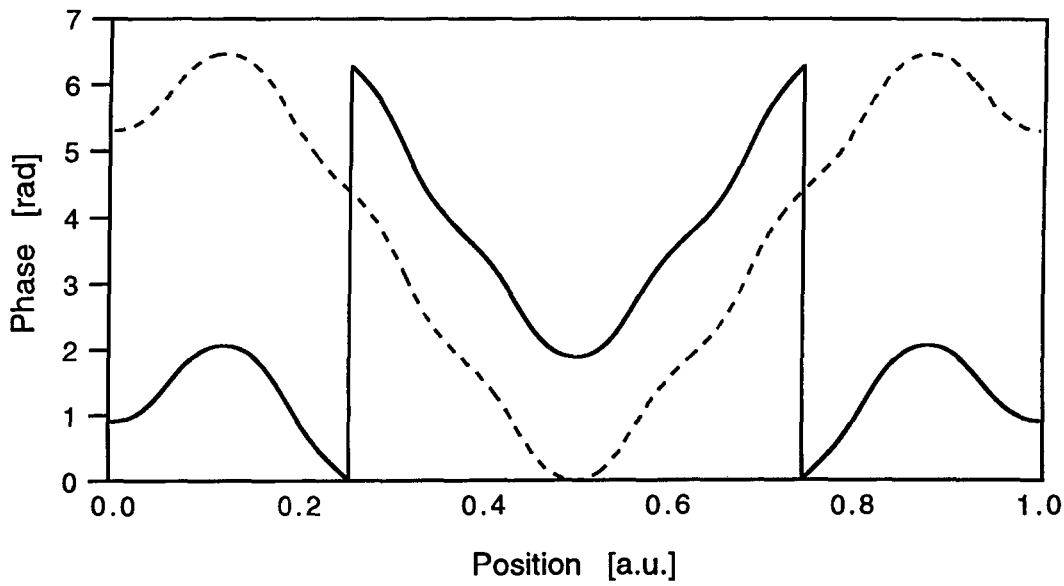

Ehbets/Fig. 1.

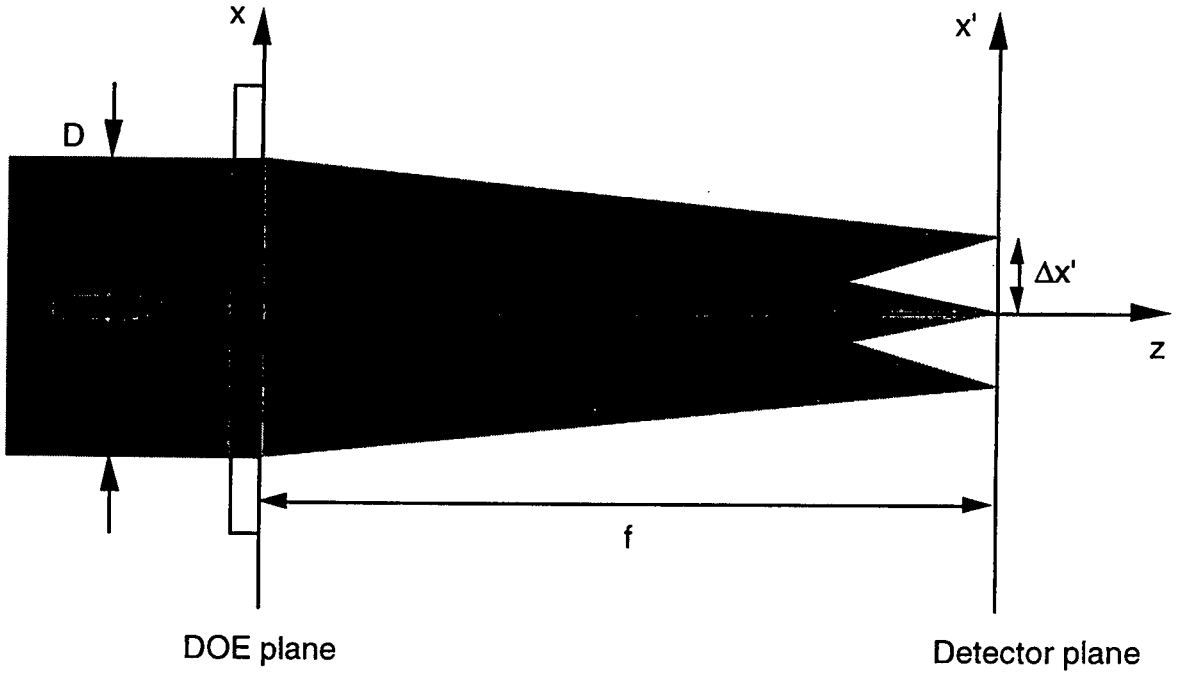

Ehbets/Fig. 2.

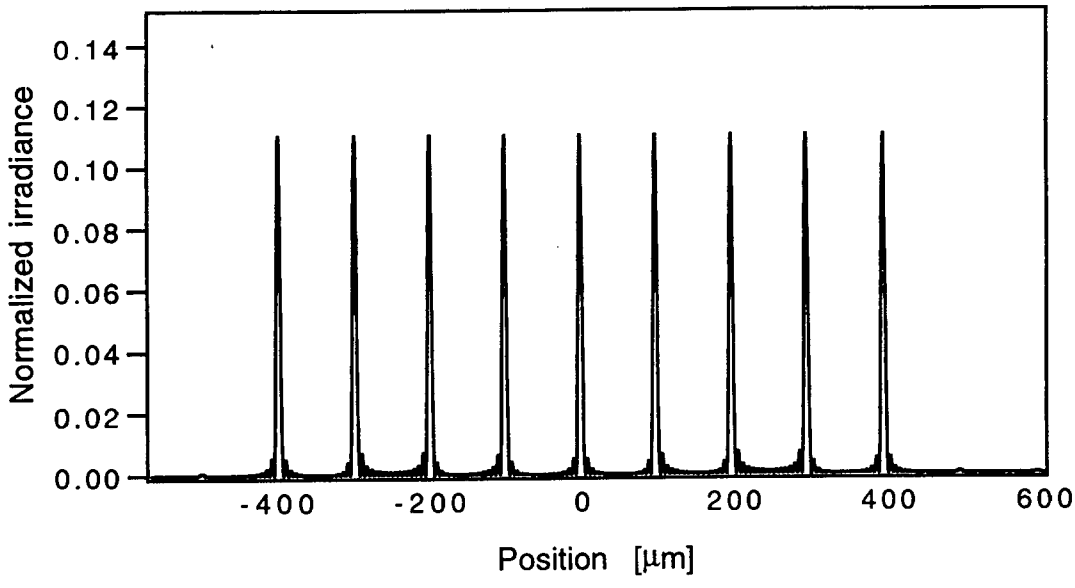
Normalized irradiance
0.14
0.12
0.10
0.08
0.06
0.04
0.02
0.00
-400
-200
0
200
400
600
Position [μm]

Ehbets/ Fig. 3.

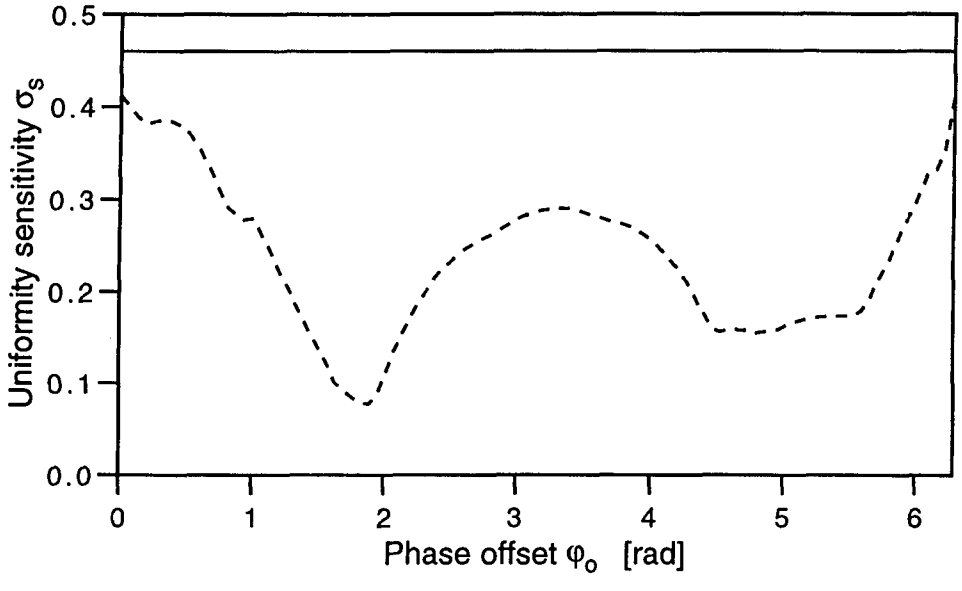
0.5
0.4
0.3
0.2
0.1
0.0
Uniformity sensitivity σ_s
0
1
2
3
4
5
6
Phase offset φ_o [rad]

Ehbets/Fig. 4.

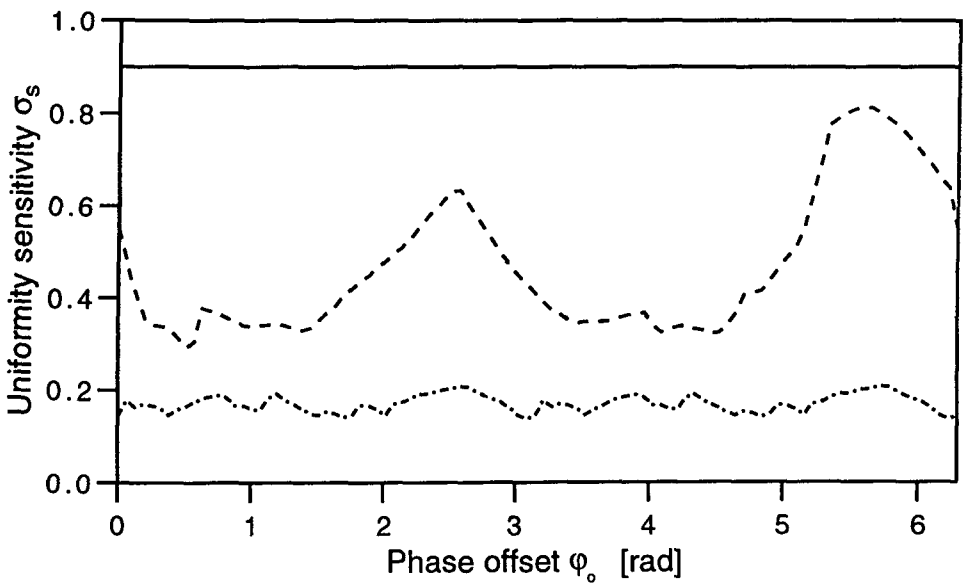
1.0
0.8
0.6
0.4
0.2
0.0
Uniformity sensitivity σ_s
0
1
2
3
4
5
6
Phase offset φ_o [rad]

Ehbets/ Fig. 5.

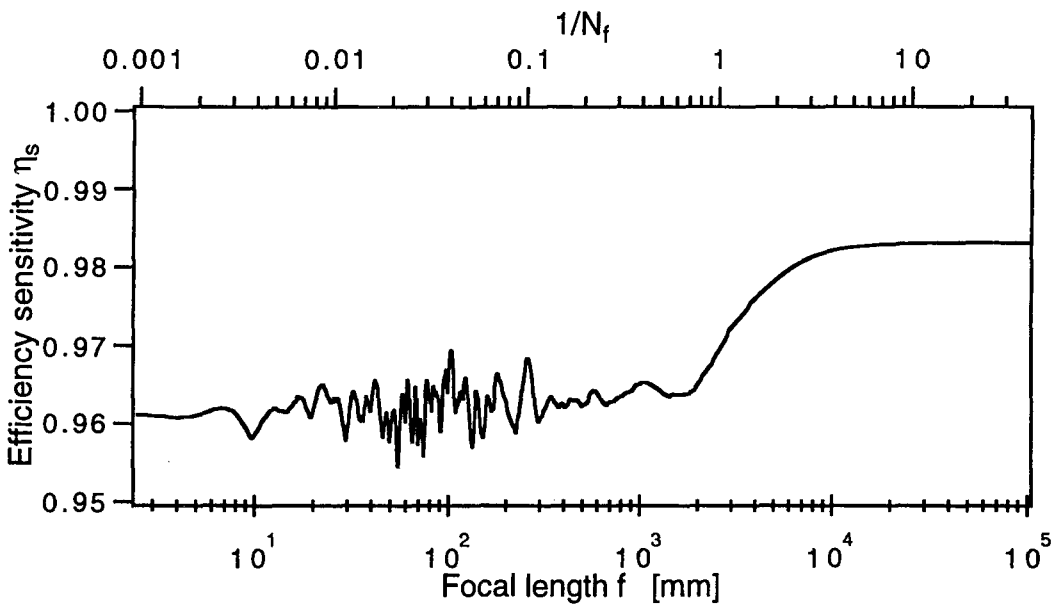

(a)

Ehbets/ Fig. 6 (a).

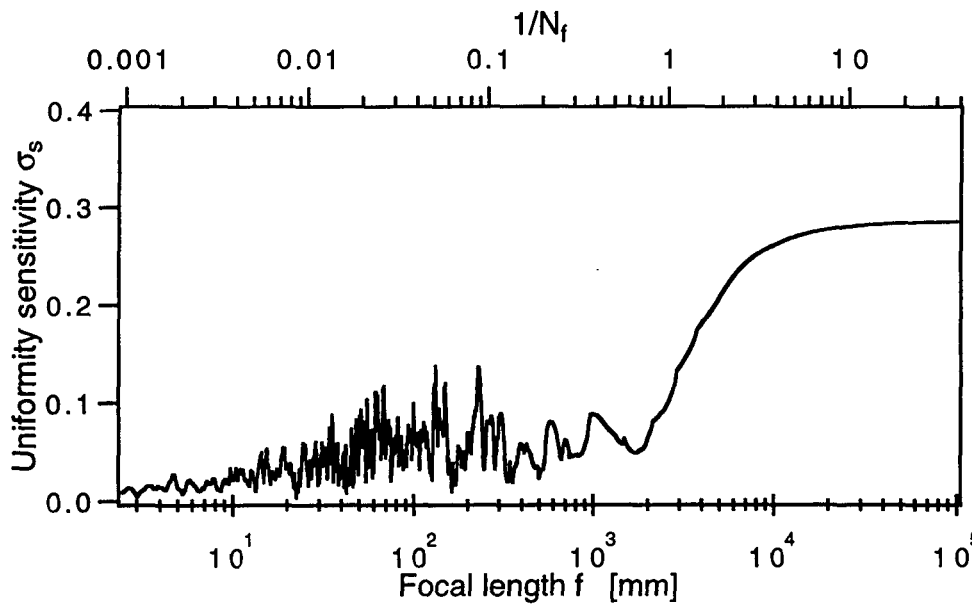

(b)

Ehbets/ Fig. 6 (b).

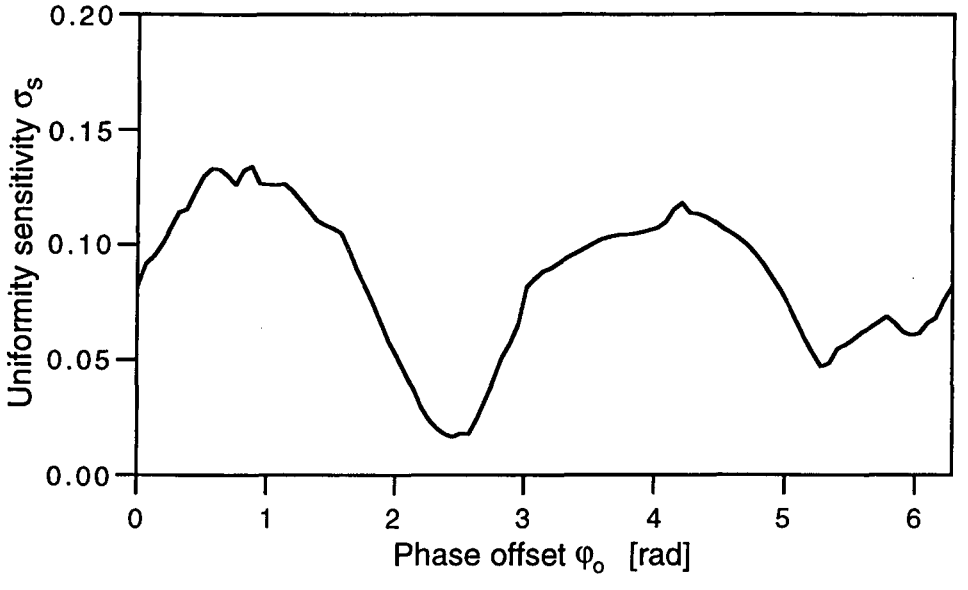
0.20
0.15
0.10
0.05
0.00
Uniformity sensitivity σ_s
0
1
2
3
4
5
6
Phase offset φ_o [rad]

Ehbets/ Fig. 7.

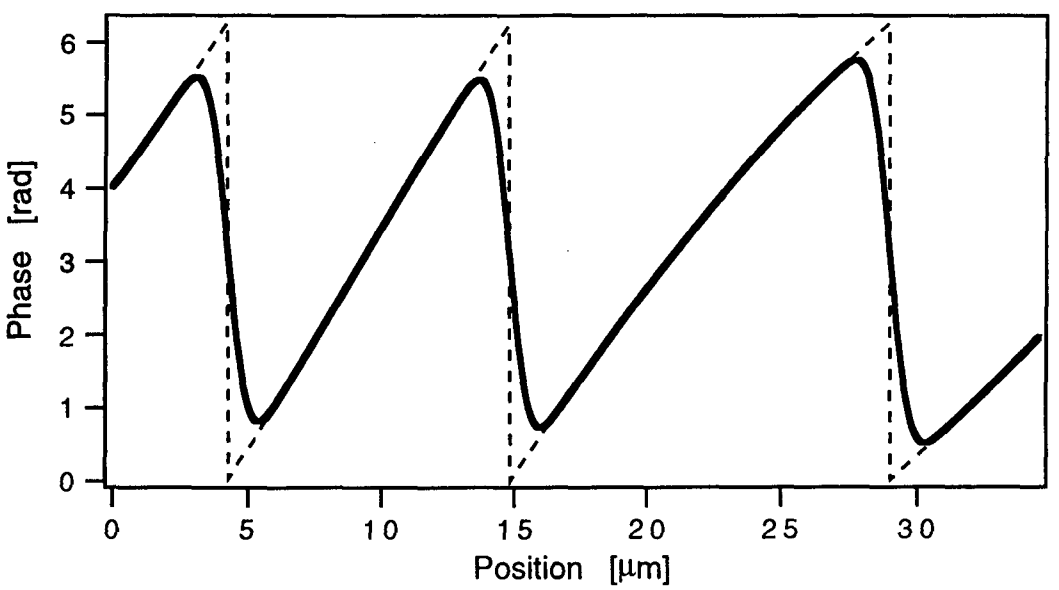

Ehbets/ Fig. 8.

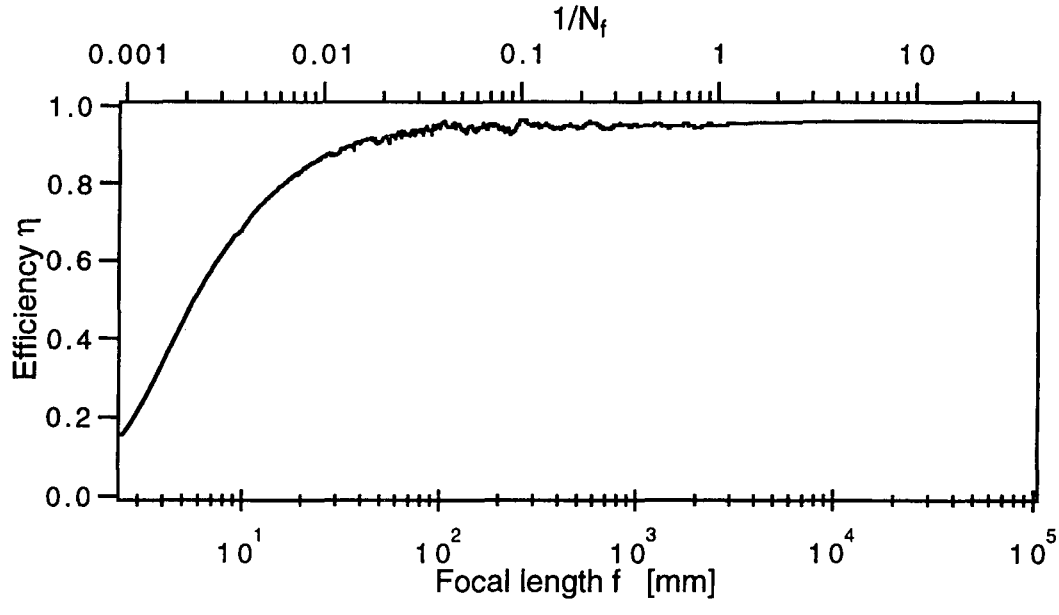

(a)

Ehbets/ Fig. 9 (a).

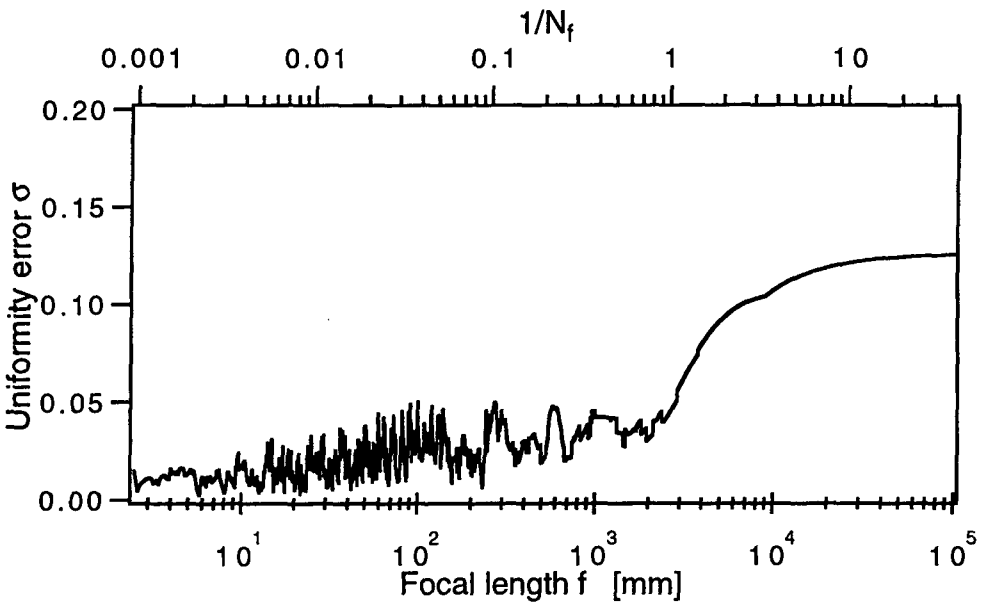

(b)

Ehbets/ Fig. 9 (b).

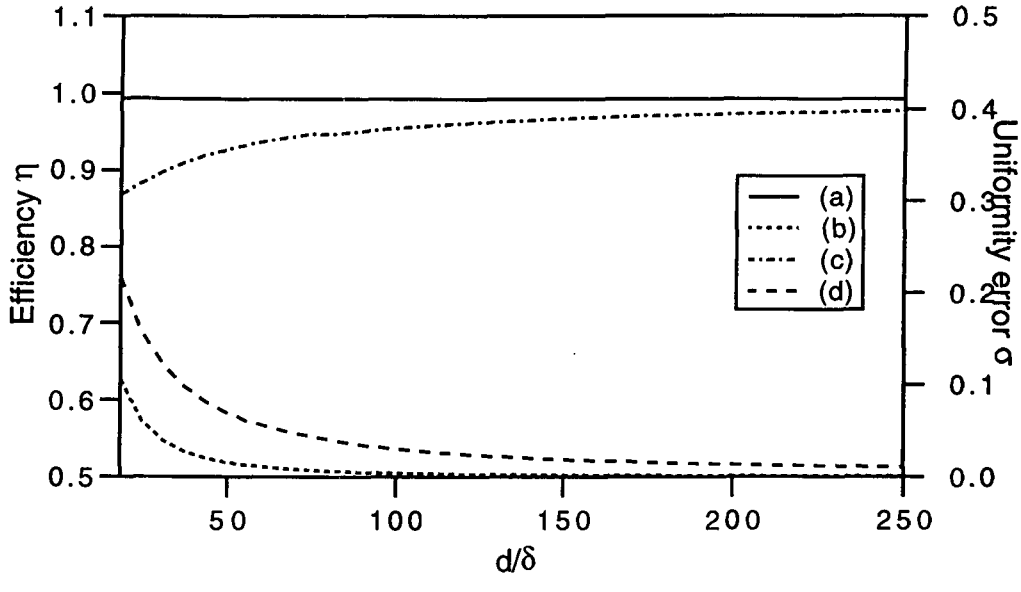

Ehbets/ Fig. 10.

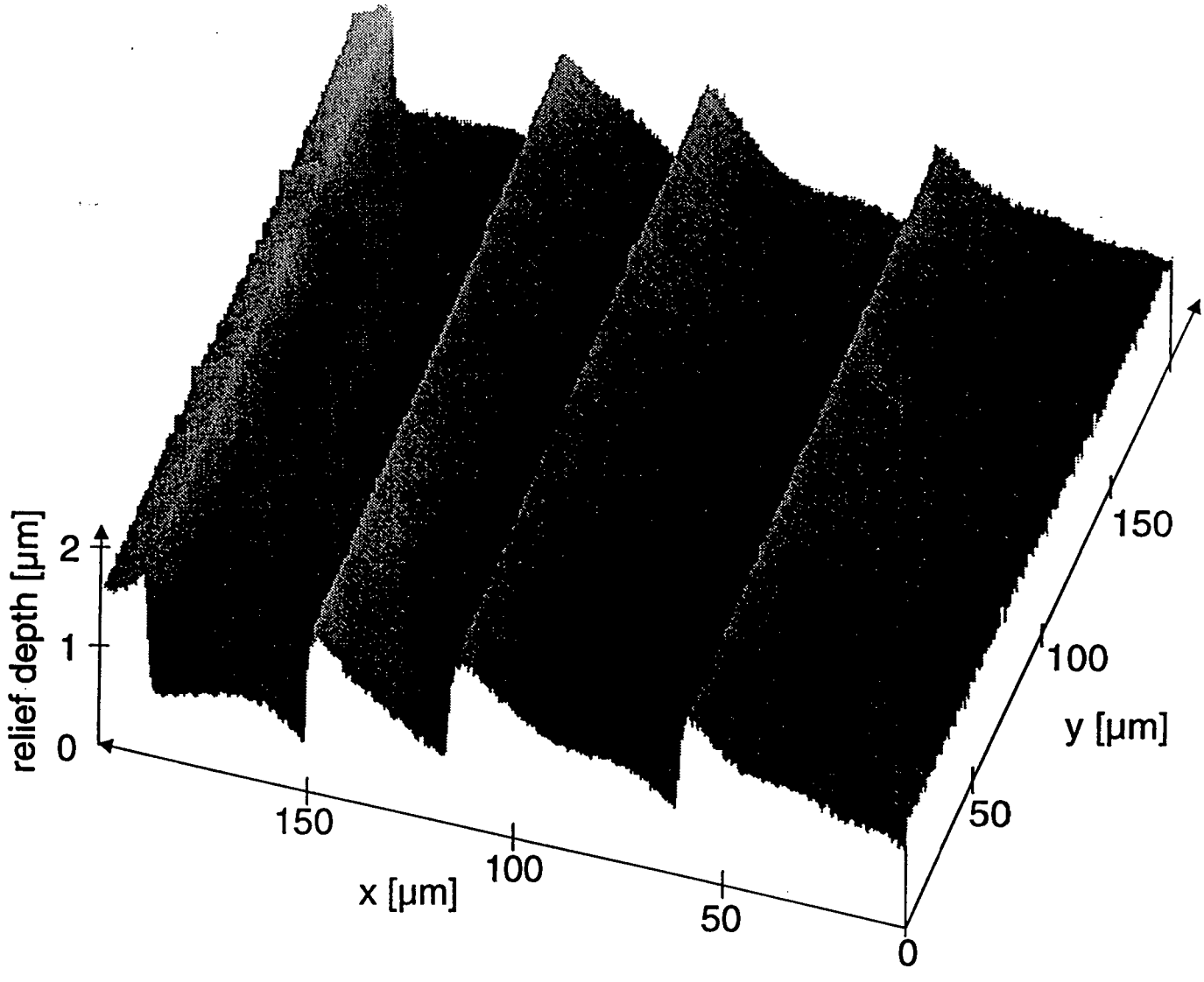

Ehbets/ Fig. 11.

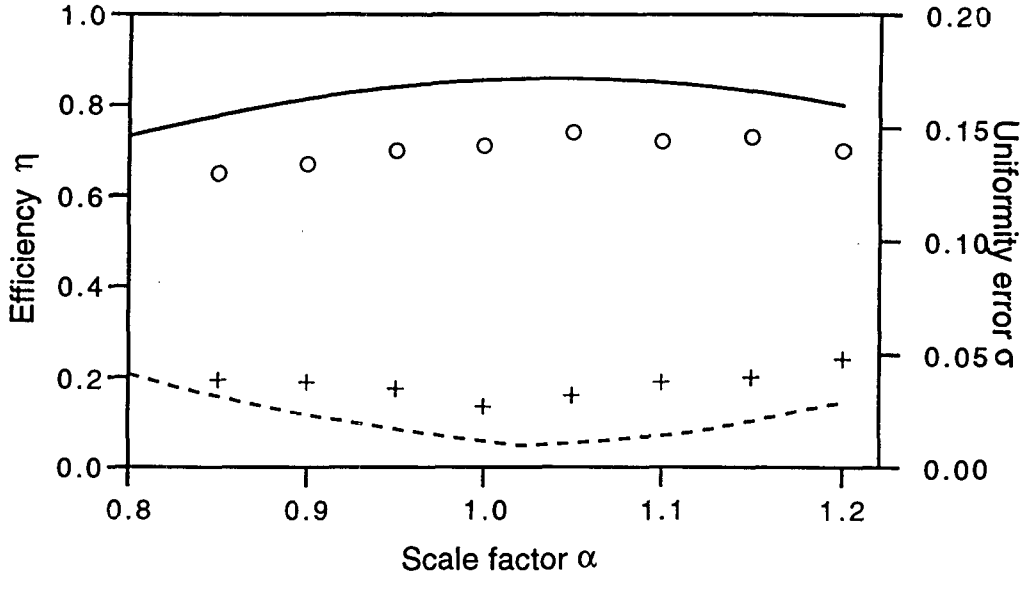

Ehbets/ Fig. 12.

JOURNAL OF MODERN OPTICS, 1993, VOL. 40, NO. 4, 637–645

Beam shaping of high-power laser diode arrays by continuous surface-relief elements

P. EHBETS†, H. P. HERZIG†, R. DÄNDLIKER†,
P. REGNAULT‡ and I. KJELBERG‡

† Institute of Microtechnology, University of Neuchâtel,
Rue A.-L. Breguet 2, CH-2000 Neuchâtel, Switzerland
‡ Centre Suisse d'Electronique et de Microtechnique S.A. (CSEM),
Maladière 41, CH-2007 Neuchâtel, Switzerland

(*Received 25 May 1992; accepted 22 July 1992*)

Abstract. A breadboard for beam shaping of high-power laser diode arrays (LDAs) has been realized. The coherent beams are added with the aid of a continuous surface-relief fan-in element. It results in a nearly symmetric single lobed beam of collimated light with maximum conversion efficiency. The theoretical efficiency is determined to be 96·7%. Experimentally, one third of the total power is now in the central peak.

1. Introduction

Semiconductor lasers are used in optics as compact, monochromatic light sources, that can be directly modulated. Some applications, such as communication between satellites and pumping of fibre lasers, require high power and near fundamental mode beam quality. High power can be achieved by phase-locked laser diode arrays (LDAs). Unfortunately, LDAs generate poor quality output beams, which cannot be collimated properly by conventional diode laser optics. In this paper we demonstrate the conversion of a multi-lobed near-field emitted by ten stripes of a LDA into a single-lobed Gaussian beam of collimated light.

The lateral modes of laser diode arrays are defined by the periodic gain and refractive index distribution across their widths. These modes can be described by coupled-wave theory [1]. The 180° out-of-phase mode seems to be the most stable mode in parallel filament arrays. Consequently, these lasers show a double lobed far-field. In order to improve the optical quality of the LDA output, different possibilities have been proposed. Using a phase plate, the 180° mode can be converted in a 0° mode [2], which leads to a relatively strong central lobe with smaller side lobes, as shown in figure 1. For one-dimensional arrays the light distribution is highly asymmetric. This is inadequate to fill the aperture of a collimator uniformly. The side lobes can be eliminated by an additional afocal system [3]. The system uses a d.c. phase shifter in the back focal plane of the first lens and a binary phase corrector element in the back focal plane of the second lens. However, the asymmetry of the light distribution is not removed. Another method uses a lens and a binary fan-in grating to superimpose N lasing apertures, converting the laser array into a single emitter with about N times the power density [4]. In this case the shape of the beam is determined by the aperture of a single laser stripe (figure 1). The coherent addition is only efficient when the beams are in the correct phase state. This has been achieved by an external cavity including the laser array and also the binary fan-in grating.

Higher efficiency close to 100% can be achieved by coherently adding N lasers with the aid of continuous surface-relief gratings [5]. Our approach is based on the

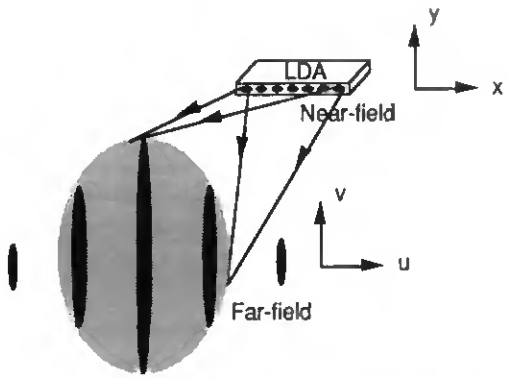

Figure 1. Far-field pattern of coupled laser diode array: the black pattern corresponds to the 0° mode; the grey pattern is the far-field of a single stripe.

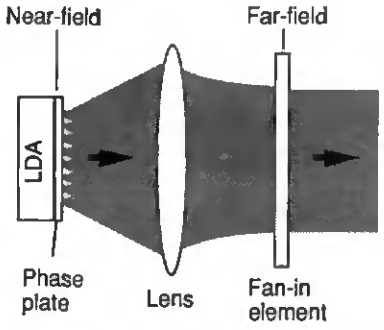

Figure 2. Basic arrangement for far-field shaping.

tandem component shown in figure 2. A phase-locked LDA is chosen that emits only one transversal mode. The LDA, that was used for the experiment, fulfilled this condition only near threshold. For higher driving currents, several lateral modes of the LDA started to lase. For this reason, an external cavity should be used for high power, in order to increase the modal separation and enhance the coherence. Other array structures, like Y-guides [6] or resonant-optical waveguides [7], provide much better spatial-mode selectivity and stability. Therefore, even at high power no external cavity is needed for an efficient beam shaping. The optimum phases are now introduced by a phase plate at the LDA output. The fan-in element has a continuous surface-relief profile enabling maximum conversion efficiency. A compact bread-board for beam shaping of high power LDAs has been realized. We summarize briefly the theory and then we present our experimental results.

2. Theory

The basic concept for the far-field shaping is shown in figure 2, where N beams emitted by a LDA are added coherently. The fan-in element is only efficient for a well defined phase relationship between the emitted beams. If the LDA operates in a stable single mode, these phases can be established with a phase plate in the near-field. In the following, we calculate the optimum phases and the corresponding fan-in element for an efficient beam shaping.

In our model, the near-field distribution $U(x, y)$ at the LDA output, after the phase plate, is approximated by an array of N Gaussian beams. We restrict the analysis to the case of one-dimensional arrays, but the same principle can be applied for two-dimensional arrays. Under these assumptions the near-field of the LDA can be written as

$$U(x,y)=\sum_{m=1}^{N} A_m \exp(\mathrm{i}\phi m)\exp\left[-\frac{(x-x_m)^2}{w_x^2}-\frac{y^2}{w_y^2}\right], \tag{1}$$

where A_m is the amplitude, ϕ_m the phase, and x_m the position of the mth Gaussian beam. We assume a constant spacing between two neighbouring beams, defined by $s=x_{m+1}-x_m$. For index-guided LDAs, the number of Gaussian beams in the near-field corresponds to the number of array elements and their beam waist radii w_x and w_y are mainly determined by the geometry of a single stripe [8]. Whereas, gain-guided LDAs can produce lateral modes with more lobes in the near-field than waveguides [9]. In such a situation, the number of Gaussian beams has to be increased, in order to describe the near-field distribution accurately.

The far-field distribution $\hat{U}(u, v)$ is related to the near-field $U(x, y)$ by a Fourier transform. Thus, we get for the far-field

$$\begin{aligned}\hat{U}(u,v)&=\int_{-\infty}^{\infty} U(x,y)\exp[2\pi\mathrm{i}(xu+yv)]\,\mathrm{d}x\,\mathrm{d}y\\&=c_1\exp[-\pi^2(w_x^2u^2+w_y^2v^2)]\sum A_m\exp(\mathrm{i}\phi_m)\exp(2\pi\mathrm{i}x_mu),\end{aligned} \tag{2}$$

or expressed in amplitude and phase

$$\hat{U}(u,v)=|\hat{U}(u,v)|\exp[\mathrm{i}\Psi(u,v)], \tag{3}$$

where $\Psi(u,v)=\arg\{\hat{U}\}$ and c_1 is a constant.

As the emission of every array element interferes with each other, interference patterns in the far-field intensity distribution with periodicities of $1/s$, $1/2s, \ldots,$ $1/(N-1)s$ can be observed. If the interference terms of equal spatial frequency are collected, the intensity distribution in the grating plane can be written as

$$\begin{aligned}I(u,v)=|\hat{U}|^2=c_2\exp[-2\pi^2(w_x^2u^2+w_y^2v^2)]\\\times\left[\sum_{m=1}^{N}A_m^2+2\sum_{p=1}^{N-1}B_p\cos(2\pi psu+\Phi_p)\right].\end{aligned} \tag{4}$$

For a given set A_i, ϕ_i, the coefficients B_p, Φ_p for one spatial frequency component of the interference pattern can be calculated from the equations

$$B_p^2=\left[\sum_{m=1}^{N-p}A_mA_{m+p}\cos(\phi_m-\phi_{m+p})\right]^2+\left[\sum_{m=1}^{N-p}A_mA_{m+p}\sin(\phi_m-\phi_{m+p})\right]^2, \tag{5}$$

$$\Phi_p=\arctan\left(\frac{\sum_{m=1}^{N-p}A_mA_{m+p}\sin(\phi_m-\phi_{m+p})}{\sum_{m=1}^{N-p}A_mA_{m+p}\cos(\phi_m-\phi_{m+p})}\right). \tag{6}$$

The envelope of the intensity distribution $I(u, v)$ determined by equation (4) is the desired Gaussian far-field distribution, corresponding to the far-field of a single stripe. If we are able to eliminate the variations in the interference patttern, the intensity distribution becomes equal to that Gaussian envelope. According to

equation (3), the remaining phase distribution could then be converted into a plane wave by a phase element with transmittance equal to $\exp[-i\Psi(u, v)]$. An interference term close to a constant value can be achieved by requiring minimum variance, namely

$$\int_{-\infty}^{\infty}\int_{-\infty}^{\infty}\left[\sum_k B_k \cos(2\pi ksu + \Phi_k)\right]^2 du\, dv \rightarrow \min. \tag{7}$$

Since the terms of different spatial frequency are orthogonal, the minimum condition becomes finally

$$\sum_k B_k^2 \rightarrow \min. \tag{8}$$

The minimization of equation (8) yields the optimized phases ϕ_m for a given set of amplitudes A_m.

We summarize the beam shaping process sketched in figure 2. A set of amplitudes A_m and phases ϕ'_m is known at the LDA output. The optimum set of phases ϕ_m can be found by minimization of equation (8). The phase differences between the optimum phases ϕ_m and the phases ϕ'_m of the LDA have to be added by a phase plate. The optimized intensity distribution $I(u, v)$ in the far-field is then given by equation (4) and the phase distribution $\Psi(u, v)$ by equations (2) and (3). In order to generate a plane wave a second phase element has to be added to compensate $\Psi(u, v)$ in the far-field. Its complex amplitude transmittance is

$$T(u, v) = \exp[-i\Psi(u, v)]. \tag{9}$$

The optimization of equation (8) is a numerical problem, which has been solved by using the Downhill Simplex Method [10].

3. Experimental results

Figure 3 shows the breadboard for far-field shaping of LDA mounted on a large heatsink. The continuous surface-relief fan-in element can be observed in front of the assembled prototype. The system includes a LDA, a phase plate, a lens, and a fan-in element as already depicted in figure 2.

For our experiments, we have used a SDL-2420 LDA from Spectra Diode Labs, which is a gain-guided device and offers ten phase coupled emitters spaced by 10 μm, operating at the wavelength $\lambda = 801$ nm. Spectral analysis of the near-field has shown that near threshold, the LDA operates in a single lateral mode, which is known as the $v = 10$ mode [8]. For this mode the emitters possess an alternating 0/180° phase state producing the double lobed far-field shown in figure 4.

The phase plate that should generate the optimized phases consists of 10 zones each of 10 μm width. The element is fabricated at CSEM by reactive ion etching (RIE) into fused silica. Repeated etching produces discrete levels. We have distributed the 10 optimum phases on 16 equally spaced levels between 0 and 2π. It results that in this special case the etch with depth corresponding to a phase delay of $\pi/4$ is not necessary and therefore, three etching steps were sufficient to generate the required levels.

The optimized phases ϕ_i are shown in the first row of the table. In the second row the quantized values for the phase plate are listed. Illuminated with the $v = 10$ mode the phase plate generates the optimized phases. The quantization error is within $\pm\lambda/40$. Theoretically 97·3% of the power emitted by the LDA can be collimated into

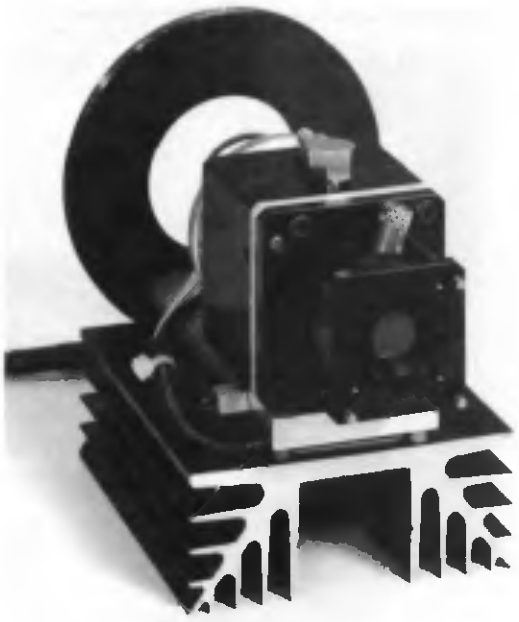

Figure 3. Breadboard of LDA shaping mounted on a heat-sink.

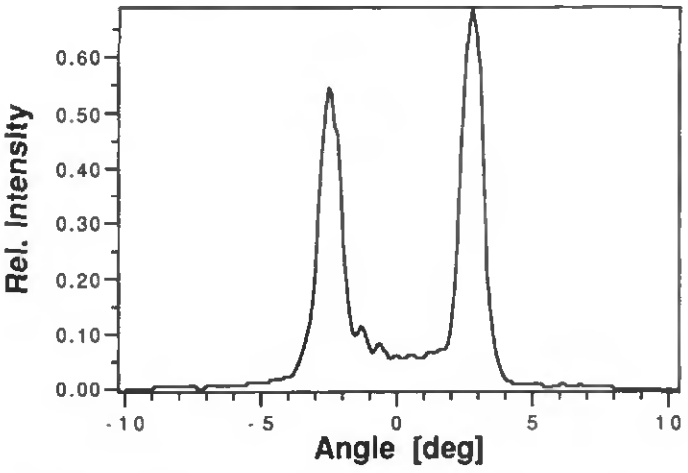

Figure 4. Measured double lobed far-field of 180° mode.

a single Gaussian beam. Due to the quantization of the optimized phases the efficiency drops slightly to 96·7%. Figure 5 shows the calculated profile of the phase plate. In comparison, figure 6 shows a scanning electron microscope (SEM) picture of the fabricated phase plate. The accuracy of the depth profile is better than 1%.

A lens with short focal length of $f = 14{\cdot}5$ mm has been chosen to get a compact system. This defines the periodicity of the fan-in element in the Fourier plane of the lens (figure 2) to be $p = \lambda f / s = 1{\cdot}16$ mm. The number of periods illuminated in the far-field is inversely proportional to the fill-factor of the LDA, which is defined by

Calculated phases in the near-field.

Beam no.	Optimum phases [rad]	Quantized phase plate [rad]	Quantization error [rad]
1	0·00	0·00	0·00
2	0·52	3·53	−0·13
3	0·24	0·39	0·16
4	5·11	1·96	0·00
5	5·05	5·11	0·05
6	1·41	4·71	0·17
7	1·52	1·57	0·05
8	4·58	1·57	0·13
9	2·02	1·96	−0·06
10	4·61	1·57	0·10

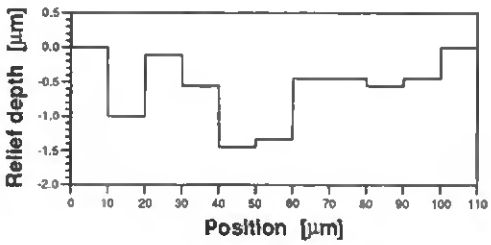

Figure 5. Calculated profile of the phase plate.

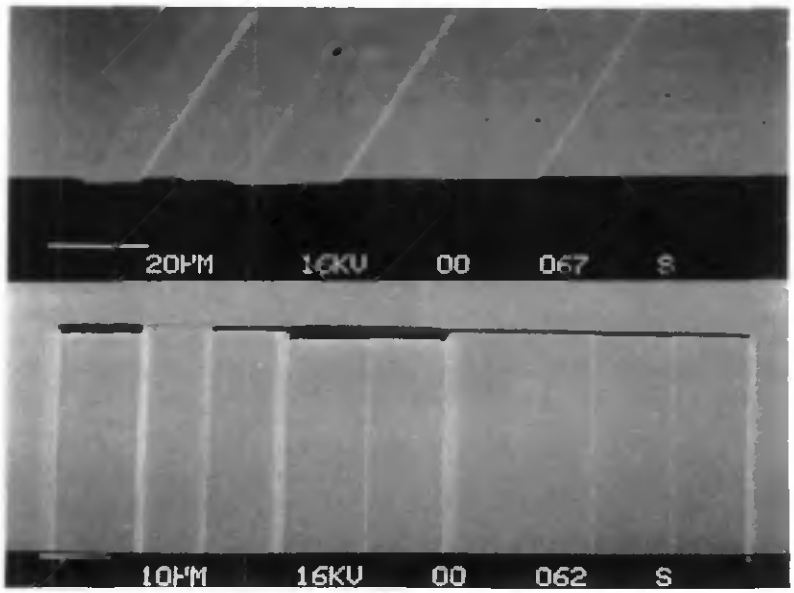

Figure 6. SEM pictures of the fabricated phase plate: side view, top view.

the ratio of the Gaussian beam diameter and the stripe spacing. In our case, about three periods of the fan-in element were illuminated.

According to equation (9) the fan-in element has to generate a phase distribution of $-\Psi(u, v)$ in the far-field. This is achieved by a continuous surface-relief element in the back focal plane of the lens (figure 2). The thickness modulation is obtained from the phase distribution by the following relation

$$d(x, y) = d_0 + \Psi(x = \lambda f u, y = \lambda f v) \frac{\lambda}{2\pi(n-1)}, \tag{10}$$

where d_0 is a constant thickness and $(n-1)$ is the refractive index difference between medium and air. In our experiment, we have calculated the far-field from equations (2) and (3) for constant amplitudes A_m and for the quantized optimized phases ϕ_m. The resulting thickness variation is the continuous function shown in figure 7 (*a*). It is known that for even numbered arrays the profile of fan-in elements has phase steps of π (e.g. [11]). In order to avoid discontinuity in the profile we have translated our LDA by half a period, i.e. by $s/2$ with respect to the fan-in element. This is equivalent to an additional wedge in the Fourier plane, which slightly deflects the outgoing beam.

The element is written in photoresist using the laser-beam writing system at the Paul Scherrer Institute, Zurich [12]. The photoresist is exposed with a scanning laser beam of controllable intensity and then etched by a developer. The fidelity of

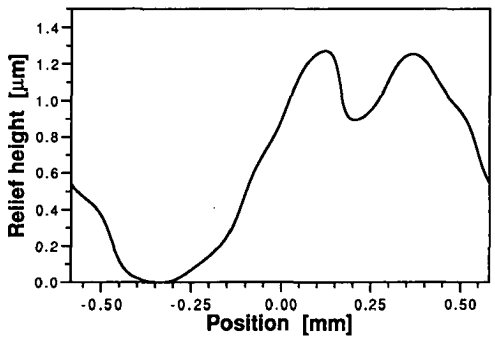

(*a*)

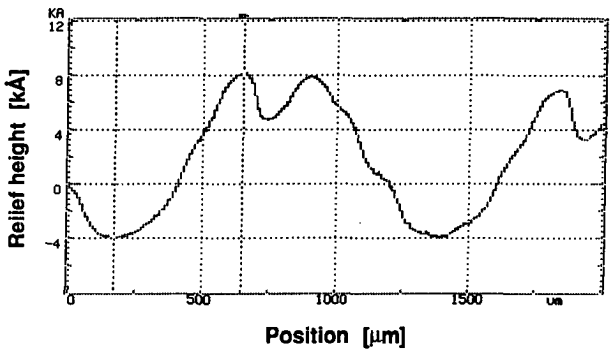

(*b*)

Figure 7. Profile of the fan-in element: (*a*) theory, (*b*) measured.

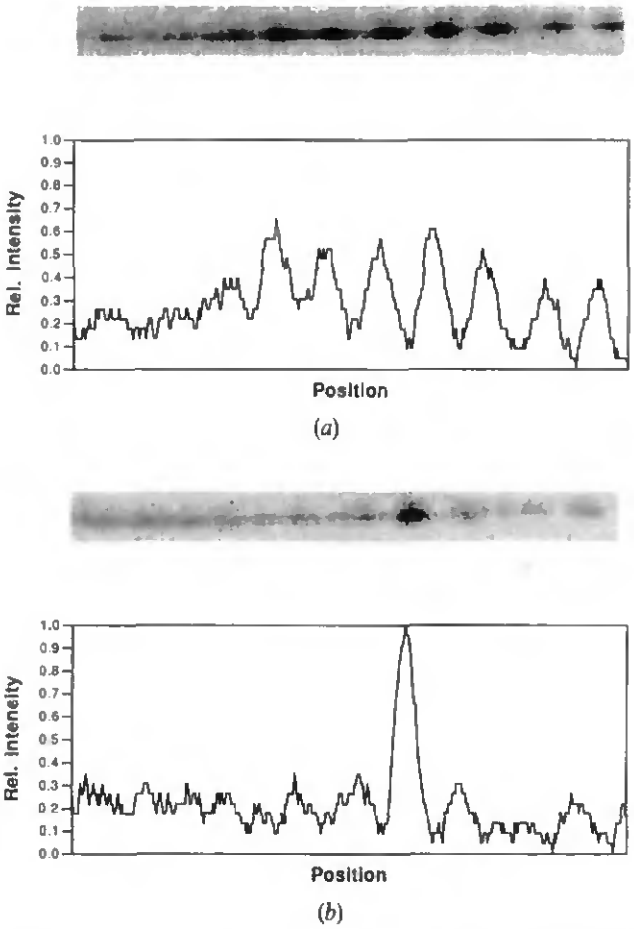

Figure 8. Source array (*a*) before shaping and (*b*) after shaping. It results in a nearly symmetric single lobed beam.

the resulting relief profile relies on the knowledge and reproducibility of the photoresist response. Finally, the phase element is baked and measured with a stylus profilometer. One typical measured profile is shown in figure 7 (*b*).

In the case of perfect shaping one collimated beam should come out of the shaping system (figure 2). We have focused this beam on to a CCD camera, where we can observe the virtual source. Figure 8 (*a*) shows the source array before shaping. In this case, we have removed the fan-in grating. Then the ten array elements can be identified. Unfortunately, the LDA does not emit a nice symmetric near-field. The first three lobes are hardly detectable. This asymmetry might be due to the effects of non-uniform heat sinking, non-uniform gain across the array, or unwanted back reflection from the phase plate, which was not antireflective coated. Figure 8 (*b*) shows the virtual source after adding the fan-in element. It results in a single bright spot as predicted by theory with nearly symmetric aspect. One third of the total power is now in the central peak.

The poor performance cannot be explained by the quality of the shaping elements. The phase plate and the fan-in element are sufficiently accurate. The fact

that the amplitude distribution of the source array was not uniform, as assumed for the design of the element, seems not to be important, either. Numerical simulations show that the efficiency should only drop down to 96·0% for the observed near-field amplitude distribution (figure 8(*a*)) and to 87·5% for the theoretical half-sinus amplitude modulation of the $v=10$ mode. The efficiency of the shaping depends much more on the relative phases of the emitters. For this reason, it is assumed that the phase plate was placed at a position where the different beams did already partially overlap. For future use, antireflection coatings on the elements are recommended to avoid feedback into the LDA.

4. Conclusions

We have shown that stable eigenmodes emitted by LDAs can be shaped and collimated with very small inherent losses. The proposed method produces a nearly symmetric single lobed beam of collimated light with maximum conversion efficiency. A compact breadboard has been built for shaping an array of ten elements. The system includes a multilevel phase plate at the LDA output to produce in the far-field a smooth intensity distribution, which corresponds to the far-field of a single stripe of the laser array. The structure of the array is converted into a phase distribution in the far-field. This phase distribution is then corrected by a continuous surface-relief fan-in grating. The theoretical efficiency for this set-up is 96·7%. Experimentally, we have found one third of the total power in the central peak.

References

[1] MEHUYS, D., and YARIV, A., 1988, *Optics Lett.*, **13**, 571.
[2] HEIDEL, J. R., RICE, R. R., and APPELMAN, H. R., 1986, *Quant. Electron. Lett.*, **22**, 749.
[3] LEGER, J. R., SWANSON, G. J., and HOLZ, M., 1987, *Appl. Phys. Lett.*, **50**, 1044.
[4] LEGER, J. R., SWANSON, G. J., and VELDKAMP, W. B., 1987, *Appl. Optics*, **26**, 4391.
[5] HERZIG, H. P., DÄNDLIKER, R., and TEIJIDO, J. M., 1989, *Holographic Systems, Components and Applications*, Bath, UK, Conference Publication No. 311 (London: Institution of Electrical Engineers), pp. 133–137.
[6] WELCH, D. F., CROSS, P., SCIFRES, D., STREIFER, W., and BURNHAM, R. D., 1986, *Electron. Lett.*, **22**, 293.
[7] MAWST, L. J., BOTEZ, D., JANSEN, M., ROTH, T. J., TU, C., and ZMUDZINSKI, C., 1991, *Electron. Lett.*, **27**, 1586.
[8] BOTEZ, D., 1988, *IEEE J. quant. Electron.*, **24**, 2034.
[9] HADLEY, G. R., HOHIMER, J. P., and OWYOUNG, A., 1986, *Appl. Phys. Lett.*, **49**, 684.
[10] PRESS, W. H., FLANNERY, B. P., TEUKOLSKY, S. A., and VETTERLING, W. T., 1989, *Numerical recipes in Pascal* (Cambridge University Press).
[11] MORRISON, R. L., 1992, *J. opt. Soc. Am.* A, **9**, 464.
[12] GALE, M. T., LANG, G. K., RAYNOR, J. M., SCHÜTZ, H., and PRONGUÉ, 1992, *Appl. Optics*, **31**, 5712.

a reprint from Applied Optics

Interferometric fabrication of modulated submicrometer gratings in photoresist

Peter Ehbets, Hans Peter Herzig, Philippe Nussbaum, Peter Blattner, and René Dändliker

Interferometric recording is applied to the fabrication of modulated submicrometer gratings in photoresist. High diffraction efficiency requires optimized recording conditions, which are obtained by the use of an on-axis continuous surface-relief grating for the generation of the object beam. The optimized phase function is copied into the resist layer by means of a self-aligned two-step recording process with an intermediate copy in a volume photopolymer hologram. As a result, we demonstrate high carrier frequency surface-relief off-axis fan-out gratings for illumination in transmission with visible light.

Key words: Holography, photoresist, submicrometer gratings, diffractive optical elements, optical interconnects.

1. Introduction

Modern microfabrication techniques permit the realization of highly efficient diffractive optical elements (DOE's) that have multilevel or continuous microreliefs.[1] However, difficulties still arise for the fabrication of off-axis elements in rigid materials such as glass or quartz with submicrometer carrier grating periods. These elements are of interest for building compact optical systems with a folded optical path.[2] Furthermore, they are attractive because high efficiency can already be achieved with a two-level phase profile. Therefore recent research has focused on the design and fabrication of modulated high carrier frequency gratings.[3–5]

Modulated submicrometer gratings have been fabricated by use of electron-beam (e-beam) lithography for the patterning of the resist. This technique offers high flexibility for the generation of arbitrary structures. The accuracy of e-beam writing is mainly limited by stitching errors of the order of 100 μm between scan fields when the elements exceed the size of a single scan field, i.e., when they are larger than 0.8–1.0 mm.[6] Within one scan field the positioning errors are typically of the order of 10–50 nm. These positioning errors introduce detour phase factors for off-axis elements that affect the encoded object phase function and limit the performance in the case of submicrometer carrier grating periods.[4]

Here we present an alternative fabrication method for binary off-axis DOE's based on optimized interferometric recording in photoresist. This approach has the advantage of a parallel writing process that can be used directly for the fabrication of larger quantities. In addition, wave fronts can be generated with high accuracy over large fields, which results in a better positioning accuracy of the modulated grating lines. However, interferometric recording is less flexible compared with e-beam writing.

Most of the research in photoresist recording has involved the fabrication of regular, high-resolution gratings. Conditions for high first-order diffraction efficiency have been derived and experimentally demonstrated.[7–10] However, only a few studies have investigated the recording of more general object beams in photoresist. The recording of photoresist holograms was studied by Bartolini.[11] He observed a strong trade-off between efficiency and reconstruction fidelity and could achieve only low efficiencies of the order of 5%. The reconstruction fidelity is mainly affected by the intermodulation noise, which is due to the recorded object-beam intensity variations in the hologram. Better performance can only be achieved if these intermodulations are reduced or even eliminated. For the recording this requires the use of optimized object beams, which can in general be produced by computer-generated holograms. The

The authors are with the Institute of Microtechnology, University of Neuchâtel, Rue Breguet 2, Neuchâtel CH-2000, Neuchâtel, Switzerland.

Received 12 August 1994; revised manuscript received 24 October 1994.

0003-6935/95/142540-08$06.00/0.

copying of an optimized wave front with an off-axis reference beam into a hologram led to the concept of hybrid holograms.[12] Bartelt and Case[12] achieved diffraction efficiencies of the order of 50% and good fidelity by recording an object beam with random phase in a volume hologram. High diffraction efficiencies over 90% were then obtained for the copying of fan-out elements in dichromated gelatin.[13,14] In this case the intermodulations were minimized by the application of numerical optimization techniques. We have applied the same concept for the recording of efficient surface-relief holograms in photoresist.

In Section 2 we discuss the recording conditions for efficient photoresist holograms. In Section 3 the generation of optimized object beams is considered and the recording setup for the copying is discussed. Accurate positioning of the photoresist plate in the optimum recording plane is crucial. To achieve precise alignment we applied a two-step approach for the copying. In Section 4 experimental results are presented for the fabrication of an off-axis 9 × 9 fan-out element. Fan-out elements are key components for optical interconnects. In this research we use them as test elements, because the generated spot array in the far field of the fan-out element can be easily characterized. The accuracy of the fabrication process can be deduced from the uniformity error of the generated array.

2. Optimized Holographic Recording in Photoresist

The basic configuration for interferometric recording is shown in Fig. 1. The interference pattern of a plane reference wave and an object beam is recorded in a thin photoresist layer. Symmetric incidence of the two beams is required in order to produce interference fringes perpendicular to the hologram plane. Incidence angle θ defines the period of carrier grating s with $s = \lambda/(2 \sin \theta)$, where λ is the free-space wavelength of the recording light. After development a modulated surface-relief grating is obtained. At readout the grating is illuminated at Bragg angle θ_B, which is defined by $\sin \theta_B = \lambda/(2s)$. The object-beam wave front is regenerated in the minus-first diffraction order of the carrier grating and produces the desired intensity pattern in the far field. In the case of high carrier frequency gratings, the angular spread of the object beam, α, is much smaller compared with Bragg angle θ_B.

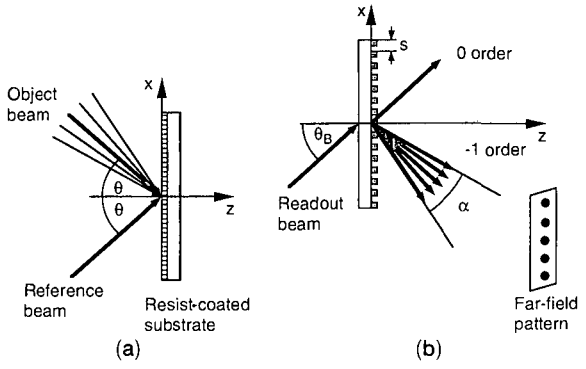

Fig. 1. Geometries of (a) recording and (b) readout for interferometric recording in photoresist.

We restrict the following analysis to one-dimensional object beams, but the same principle can be applied to the two-dimensional case. The plane of incidence is the (x, z) plane as shown in Fig. 1, and TE polarization is assumed. The reference plane wave can then be written as

$$E_r(x, z) = A_r \exp\{ik[\sin(\theta)x + \cos(\theta)z]\}, \quad (1)$$

where $k = 2\pi/\lambda$. The electric field of the object beam can be expressed by a spatially varying amplitude and phase function, i.e.,

$$E_o(x, z) = \exp[-ik \sin(\theta)x]A_o(x, z)\exp[i\Phi_o(x, z)], \quad (2)$$

where the linear phase factor determines the off-axis incidence. In the general case the propagation of Eq. (2) can be calculated by the use of the angular spectrum approach.[15] We are particularly interested in the recording of fan-out gratings. In this case the object amplitude and phase functions, $A_o(x, z)$ and $\Phi_o(x, z)$, are periodic with respect to the x axis and can be written as a discrete superposition of propagating diffraction orders, i.e.,

$$E_o(x, z) = \exp[-ik \sin(\theta)x] \sum_{m=-M}^{N} A_m \exp(i\varphi_m) \times \exp[i(mKx + \gamma_m z)], \quad (3)$$

where $(M + N + 1)$ is the total number of diffraction orders retained in the analysis, $K = 2\pi/\Lambda$, Λ is the period of the fan-out element, and γ_m is the propagation constant of the mth diffraction order along the z axis, defined by

$$\gamma_m = \{k^2 - [k \sin(\theta) + mK]^2\}^{1/2}. \quad (4)$$

The diffraction orders are characterized by their amplitudes, A_m, and phases, φ_m. The central N_s diffraction orders form the fan-out signal and create the spot array in the Fourier plane. All the higher diffraction orders correspond to undesired noise. The quality of a fan-out element is characterized by two parameters: the signal diffraction efficiency, η, and the uniformity error, e, of the generated array. The signal diffraction efficiency is the fraction of the total power in the N_s signal diffraction orders. Uniformity error e can be defined by the contrast function,

$$e = \frac{I_{\max} - I_{\min}}{I_{\max} + I_{\min}}, \quad (5)$$

where $I_{\max}$ and $I_{\min}$ are the maximum and minimum spot intensities of the N_s signal beams.

Using Eqs. (1) and (2) we can write the interference of the reference wave with the modulated object beam

in a form similar to the two-wave case, i.e.,

$$I(x, z) = |E_r(x, z) + E_o(x, z)|^2$$
$$= A_r^2 + A_o(x, z)^2 + 2A_rA_o(x, z)$$
$$\times \cos[Qx - \Phi_o(x, z)], \quad (6)$$

where $Q = 2\pi/s = 2k \sin \theta$. Optimized recording conditions are obtained if the intensity variations of object-beam amplitude $A_o(x, z)$ are minimized in the hologram plane at $z = 0$. This is identical to the design of an on-axis phase-only DOE. Assuming $A_o(x, z)$ and $\Phi_o(x, z)$ to be slowly varying with respect to the wavelength λ, we can apply the paraxial scalar diffraction theory. Many different optimization schemes have been proposed in the literature for this task, based on either iterative phase-retrieval algorithms[16–18] or parametric optimization techniques.[19] In the case of regular fan-out elements, continuous phase functions as shown in Fig. 2 for a 9 × 1 fan-out element can be determined.[20] This phase-only solution produces in the far field a uniform spot array with a high signal diffraction efficiency of 99.3%. The corresponding interference pattern of Eq. (6) is shown in Fig. 3. For the representation, a low carrier frequency $Q = 4\pi N_s/\Lambda$ has been chosen. The whole object information is encoded in phase function $\Phi_o(x, z = 0)$, which modulates frequency Q of the carrier grating.

The recorded sinusoidal intensity distribution, shown in Fig. 3, is transformed by the photoresist development into a surface-relief grating. The physics of the photoresist development process is described in Ref. 11. Depending on the type of developer and the dilution, either a binary or a rather linear characteristic between the exposure energy and the photoresist relief depth can be achieved. In the case of binary development the sinusoidal interference pattern is hard clipped, and a rectangular-shaped surface relief results. For linear development the sinusoidal form is more or less maintained. It has been shown that high diffraction efficiencies with a rectangular or sinusoidal grating require carrier grating periods of the order of the optical wavelength.[7,10] In this case only the zeroth and the minus-first diffraction order are propagating for incidence at the Bragg angle. As a consequence the diffraction at the high frequency carrier surface-relief grating has to be analyzed by the use of rigorous diffraction theories. This is a demanding task because the period of the modulated grating is defined by the period of the paraxial object function, which typically has a size of $\Lambda > 100$ μm. As a consequence, a large number of diffraction orders has to be retained in the model. A rigorous analysis of this type of binary high frequency carrier DOE's was recently published by Noponen and Turunen.[3] They analyzed the validity of the hybrid encoding scheme and found that the fan-out phase function would be correctly encoded in the binary carrier grating if the period of the highest frequency component in the fan-out function was at least 10 times larger than the period of carrier grating s, i.e.,

$$\frac{\Lambda}{N_s s} > 10. \quad (7)$$

In the reported experiments we use a factor 10 above this limitation, and therefore encoding errors can be neglected. The first-order diffraction efficiency is then optimized by the consideration of the regular carrier grating. We used a model based on rigorous coupled-wave theory[7] and determined the optimum relief depth, h, of the grating for TE polarization. The efficiency curves are shown in Fig. 4 for the two cases of a rectangular and a sinusoidal relief profile illuminated in transmission from resist to air at the Bragg angle. The results were calculated for a wavelength of $\lambda = 633$ nm, a typical photoresist index of $n = 1.63$, and a grating period of $s = 577.4$ nm. High diffraction efficiencies over 90% can be achieved for both relief types and require a modulation depth in the range of $0.8\ \mu\text{m} < h < 1.0\ \mu\text{m}$.

Optimized phases of the recording fan-out beam achieve minimum intermodulations in a single plane ($z = 0$). As the object beam propagates out of this optimum plane, intermodulations will appear and deteriorate the recording conditions. To specify the

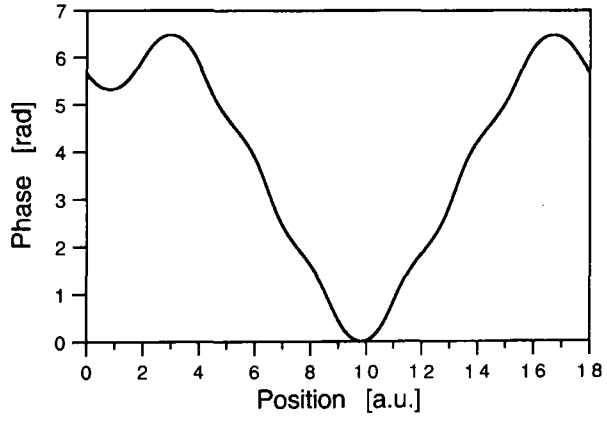

Fig. 2. One period of the optimized phase function for an on-axis 9 × 1 fan-out element.

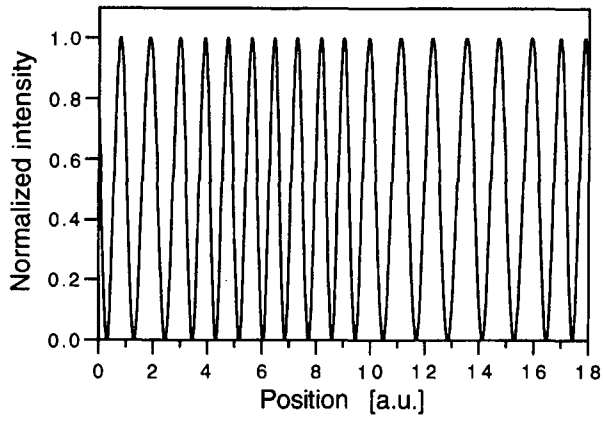

Fig. 3. One period of the optimized interference pattern in the recording plane for the 9 × 1 fan-out element.

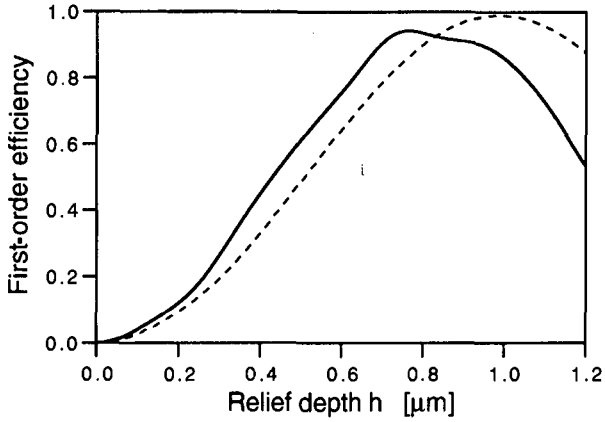

Fig. 4. Calculated first-order diffraction efficiency η_{-1} as a function of relief depth h for a rectangular relief profile (solid curve) and for a sinusoidal relief profile (dashed curve).

alignment tolerances for a successful recording, we determined the depth of the optimum plane. The propagation of the object beam is described by Eqs. (3) and (4). We assumed off-axis propagation at a recording angle of $\theta = 25°$ and calculated the evolution of the intermodulations $A_o(x, z)$ for the optimized 9×1 fan-out element, shown in Fig. 2. The calculated contrast of intermodulations V resulting from a displacement $z = d$ out of the optimum plane is shown in Fig. 5 for different fan-out periodicities Λ equal to 100, 200, and 400 μm. Intermodulation contrast V was defined by $V = (I_{max} - I_{min})/(I\,max + I_{min})$, where I_{max} and I_{min} are the maximum and minimum intensities of the object beam in the plane $z = d$. Gratings recorded under the conditions for high diffraction efficiency cannot linearly reproduce object intermodulations $A_o(x, z = d)$. Small intensity variations caused by intermodulations are clipped to a constant value because of nonlinear development and because of the strongly nonlinear behavior of the diffraction efficiency curve near its maximum. However, object phase function $\Phi_o(x, z = d)$ is accurately recorded by the relative phase of the carrier grating. The clipping of the amplitude function to $A_o(x, z = d) = \text{const}$. discards some object information.

The result of the clipping can best be analyzed by the calculation of the uniformity error of the spot array generated from phase-only function $\Phi_o(x, z = d)$. The results are shown in Fig. 6. For most applications a uniformity error of $e < \pm 10\%$ can be tolerated. Therefore, using Figs. 5 and 6, one can estimate the depth of the optimum plane and tolerable clipping level. Significant intermodulations occur of the diffraction orders at the border of the fan out loose the optimum phase relation with the central beam. The interference between one marginal diffraction order of the fan out and the central fan-out beam results in a periodic function. The period of this interference pattern in the direction of the z axis gives a good estimation for the depth of the optimum recording plane. For small fan-out angles α, the relation

$$t = c\,\frac{\cos(\theta)\Lambda^2}{\pi\lambda N^2} \tag{7}$$

is obtained for the depth as a function of the fan-out parameters, where c is a constant defined by the tolerable uniformity error and $N \approx (N_s - 1)/2$. The depth of the optimum plane is mainly determined by the quadratic dependence on fan-out period Λ and on the number of signal diffraction orders N_s. Oblique incidence at angle θ results only in the cosine factor and has little influence.

3. Two-Step Recording Setup

The problems at recording are the generation and the accurate alignment of the optimized object beam with respect to the hologram plane. Different possibilities exist for the generation of the optimized object beam in the hybrid recording arrangement introduced by Bartelt and Case. The most common approach is to encode the optimized wave front in a low-resolution computer-generated hologram[13,20] and then copy it in the hologram plane by means of a $4f$ imaging system. For the generation of large spot

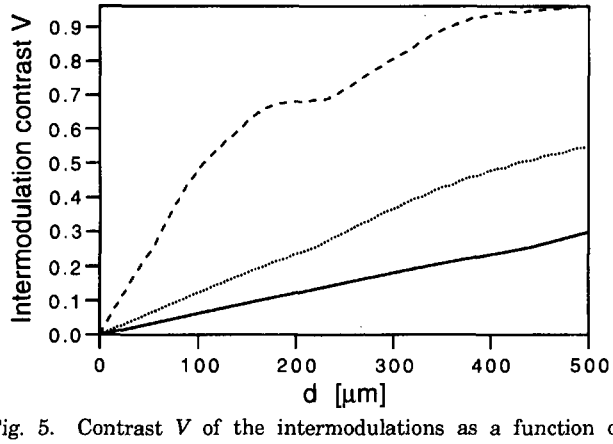

Fig. 5. Contrast V of the intermodulations as a function of displacement d out of the optimum plane calculated for different fan-out periods of $\Lambda = 100$ μm (dashed curve), $\Lambda = 200$ μm (dotted curve), and $\Lambda = 400$ μm (solid curve).

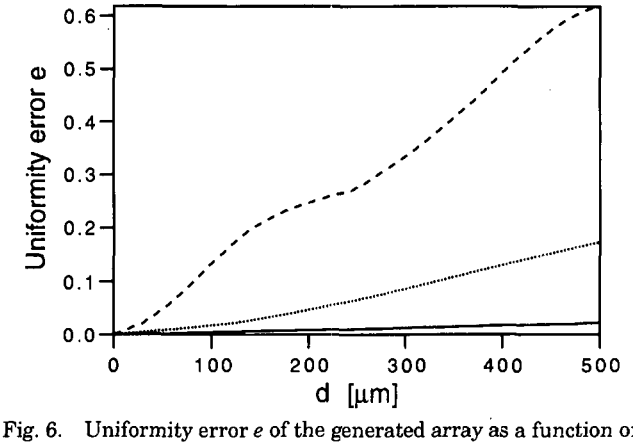

Fig. 6. Uniformity error e of the generated array as a function of displacement d out of the optimum plane calculated for different fan-out periods of $\Lambda = 100$ μm (dashed curve), $\Lambda = 200$ μm (dotted curve), and $\Lambda = 400$ μm (solid curve).

arrays, the self-imaging properties of periodic fields become interesting. By considering the free-space propagation after a pinhole array, one can find planes of low intermodulations.[21] In this research we chose a third approach by copying the optimized phase function of an existing on-axis phase-only DOE into the hologram plane. Problems appear with the hybrid recording approach if, for the desired far-field pattern, phase functions with low diffraction efficiencies are found. In this case higher diffraction orders besides the N_s signal diffraction orders become important and are necessary to describe the phase-only solution. As a consequence, spatial filtering of the imaging system has to be taken into account to achieve low intermodulation.[13] For regular, discrete patterns such as fan-out elements, high diffraction efficiencies can be achieved with continuous or multilevel DOE's. In the reported experiment we used a continuous surface-relief grating as the master element for the interferometric copying. The fabrication of continuous surface-relief gratings is a critical process, but good results have been obtained by laser-beam writing.[22]

For the required relief depth for transmission gratings to be achieved, interference fringes perpendicular to the resist surface are required. Therefore, the optimized plane of low-intensity variations is tilted with respect to the propagation direction of the object beam, and the alignment of the imaging system becomes a difficult task. The alignment tolerances are shown in Fig. 6 and can be estimated from relation (7). We have avoided these problems by using a two-step recording approach for the copying. The two-step recording process is schematically represented in Figs. 7 and 8. The optimized phase function of the on-axis fan-out element is first copied in a volume hologram. This intermediate copy does not have to be recorded for high diffraction efficiency. Therefore a linear recording process can be used, which can restore the intermodulations.[12] This hologram is recorded with a high reference-to-object-beam ratio. As we can see in Fig. 7, we imaged fan-out phase function $\Phi_o(x, z = 0)$ into the hologram plane by using a single lens. This transformation adds a quadratic phase term to the fan-out phase but introduces no intensity variations.

Because of the linear recording conditions of the volume hologram, small intermodulations can be tolerated, and the alignment requirements in the image plane become less severe. We used a photopolymer as the holographic recording medium for the intermediate copy. The photopolymer material has the advantage that it is self-developing during the exposure. The holographic plate can therefore be kept in place during the whole process and is automatically aligned. At readout the photopolymer hologram is illuminated by the conjugate reference beam, as shown in Fig. 8. This illumination generates the conjugate object beam, which passes inversely through the same imaging system and compensates on its way all the acquired aberrations. The complex conjugate of the fan-out phase function, i.e., $-\Phi_o(x, z = 0)$, is then reconstructed in the plane where the original fan-out element was placed. The Fourier transform properties show that complex conjugation of a phase function introduces an inversion symmetry in the far field, but it does not change the intensity distribution. As a result, the conjugate phase function is again a uniform fan-out element and the photoresist hologram can be recorded in this predefined plane with a symmetric off-axis reference beam.

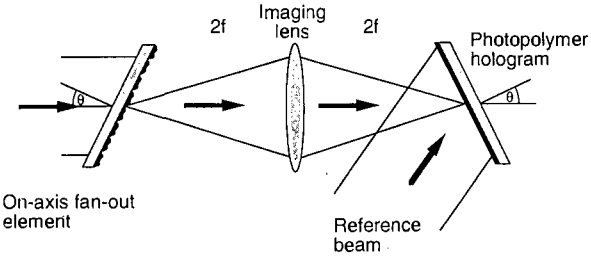

Fig. 7. Recording geometry of the intermediate copy in the photopolymer hologram.

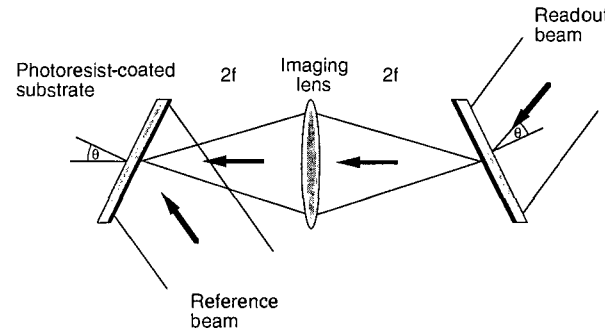

Fig. 8. Recording geometry of the resist hologram.

4. Experimental Results

Experimental results were obtained by the use of this two-step recording approach for copying a continuous surface-relief 9 × 9 fan-out element into a modulated binary resist grating. We obtained the two-dimensional phase function by crossing two symmetric one-dimensional solutions, which are shown in Fig. 2. The design and the fabrication by laser-beam writing of this element have been described in previous publications.[22,23] The fan-out gratings were realized with a period of $\Lambda = 400$ μm and for a wavelength of $\lambda = 488$ nm. For normal incidence, phase function $\Phi_o(x, z = 0)$ and relief height $d(x)$ are related by

$$\Phi_o(x, z = 0) = \frac{2\pi}{\lambda}(n - 1)d(x), \tag{8}$$

where n is the refractive index of the medium. Propagation through the same phase grating at oblique incidence results in phase modulation errors. The main error is a linear increase of the optical path length difference, which can be compensated by the rescaling of relief profile $d(x)$ calculated for normal incidence. The corrected relief height $d_c(x)$ for ob-

lique incidence is obtained by

$$d_c(x) = d(x)\frac{n-1}{n\cos(\theta_n) - \cos(\theta)}, \qquad (9)$$

where θ and θ_n are the incidence angles in air and in the medium. In general, higher-order phase errors will appear. Because of the large ratio between the fan-out period and the modulation depth, these local phase deformations are smaller than $\pi/100$ and thus far below the fabrication accuracy. We fabricated a continuous surface-relief 9 × 9 fan-out element in photoresist with a refractive index of $n = 1.64$ for the required recording angle of $\theta = 25°$. This requires a relief depth correction, Eq. (9), of 0.94. The far-field characterization of the fabricated element yields a uniformity error of $e = \pm 10\%$ over the whole 9 × 9 array.

For the imaging system shown in Fig. 7, a lens with focal length of $f = 100$ mm and an aperture diameter of 50 mm were chosen. With this configuration, spatial filtering effects can be neglected. The intermediate volume hologram copy was made in the photopolymer material HRS352 from Du Pont de Nemours[24] by the use of an argon laser at the wavelength $\lambda = 488$ nm. The photopolymer layer was spin coated to a thickness of 17 μm on a BK-7 glass substrate with antireflection coating on the opposite surface. Symmetric incidence between the reference beam and the object beam was chosen for the recording. Because the image plane of the fan-out element is again a plane of low intermodulations, a high reference-to-object-beam ratio is not necessary for a linear recording process.[25] We used a beam ratio equal to unity. Typical exposure parameters have been an energy of $E = 150$ mJ/cm^2, followed by a diffusion time of ~8 min, and a uniform postexposure to fix the hologram. Efficiencies of the order of 40% were obtained without heating the photopolymer hologram after exposure. Under these conditions an excellent linear recording was achieved. The intermediate photopolymer hologram reconstructed the 9 × 9 spot array in the far field with the same uniformity error as the original fan-out element.

The final copy was made in Shipley Microposit 1400-37 photoresist. A layer of 2.8 μm thickness was spin coated on a glass substrate and baked at 95 °C for 30 min. For the exposure an absorber was index matched on the backside of the substrate to avoid backreflections, and symmetric incidence at ±25° was chosen. Because the photoresist material has low sensitivity at the wavelength of $\lambda = 488$ nm, high exposure energies of the order of 1.5 J/cm^2 are required. The consequence of using expanded beams are exposure times of several minutes. Under these circumstances, fringe stabilization becomes important. We obtained the best performance by stabilizing the large interference fringes produced from a reference grating with equal period, which was fixed on the same substrate holder. During the exposure the piezocorrection signal of the fringe stabilization system varied by the order of $\lambda/20$. Because the average position of the fringes is recorded, the position accuracy of the recorded pattern is still better. After exposure the resist holograms were developed during 30 s in the AZ-303 developer from Hoechst diluted 1:4. According to Bartolini,[11] this process results in rather linear development characteristics. The form of the resulting surface relief for a modulated fan-out grating can be seen on the scanning electron microscopy picture of Fig. 9. Grating period $s = \lambda/(2\sin\theta) = 577.4$ nm results from the incidence angle of $\theta = 25°$. We achieved maximum relief depths of the order of 600 nm by using this process. The position modulation of the grating grooves is only of some nanometers and cannot be distinguished in Fig. 9.

The modulated fan-out gratings were designed for readout in transmission with the He–Ne laser wavelength $\lambda = 633$ nm. The achieved relief depths of 600 nm are not optimum, as one can seen from the efficiency curves in Fig. 4. The wavelength change between recording and readout shifts the Bragg angle to $\theta_B = \lambda/(2s) = 33.2°$. An overall first-order efficiency of $\eta_{-1} = 69\%$ was measured for the grating shown in Fig. 9. This value includes the Fresnel reflection loss of $R = 6\%$ at the first substrate interface and absorption of the order of 2% in the photoresist. The generated 9 × 9 spot array in the far field of the minus-first diffraction order is shown in Fig. 10. The CCD picture is saturated so that the small sidelobes of the Airy function around each spot are visible. One can see that no significant higher diffraction orders appear outside of the signal array. The 9 × 9 spot array contains 65% of the total incident power. The 4% efficiency loss compared with the first order efficiency is mainly due to light that is scattered at the rough photoresist surface. The surface roughness results from coherent noise that is generated from backreflections. Improvements are possible by the reduction of the coherence length of the recording laser and by the use of an incoherent preexposure. The uniformity of the array was measured for illumination with a collimated

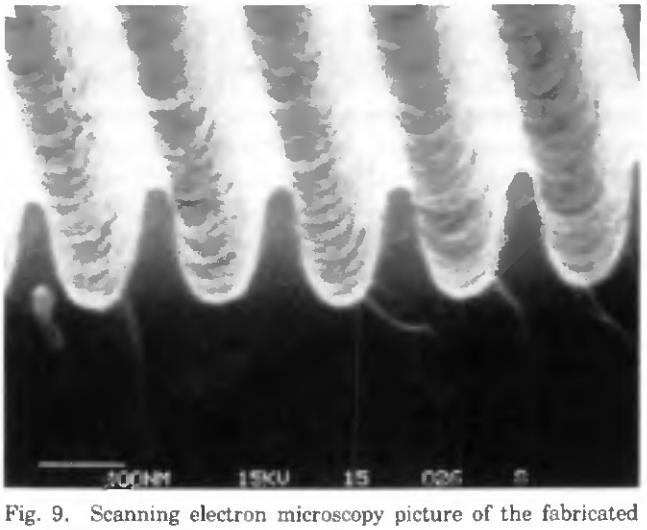

Fig. 9. Scanning electron microscopy picture of the fabricated surface relief in photoresist.

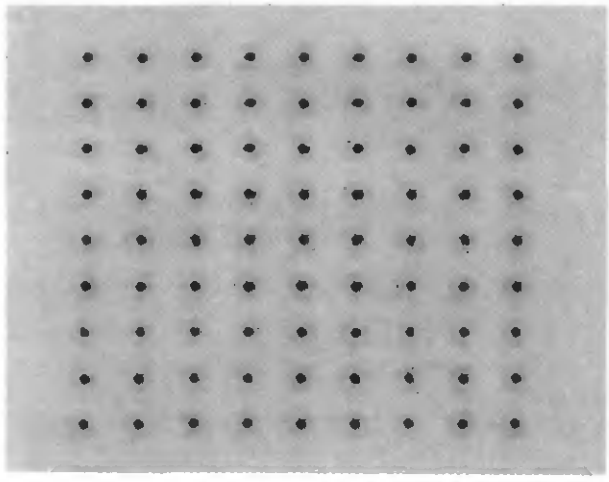

Fig. 10. 9 × 9 array of generated spots in the minus-first diffraction order of the carrier grating.

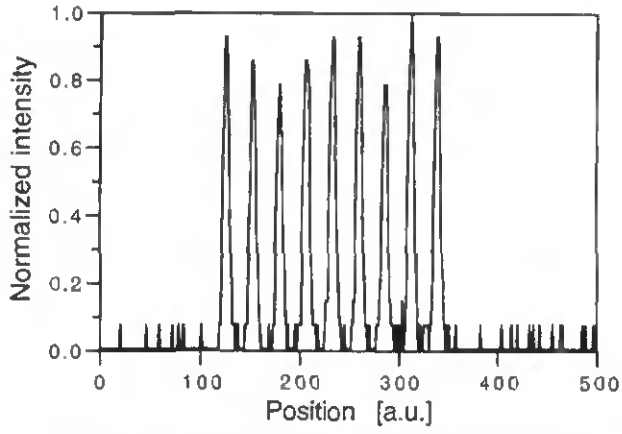

Fig. 11. Intensity line scan through the row of the 9 × 9 array with the highest uniformity error.

beam that was 4 mm in diameter. Each row of the array was scanned individually by a detector. The intensity distribution of the row with the worst uniformity is shown in Fig. 11. We measured a uniformity error of $e = \pm 13\%$. Compared with the uniformity error of $e = \pm 10\%$ of the original fan-out element, we achieved an accurate copy of the fan-out phase function. Higher diffraction efficiencies require slightly deeper relief depths. One can obtain this by improving the photoresist processing or by etching the binary resist relief in the substrate material.[1]

5. Conclusions

We investigated interferometric recording for the fabrication of modulated binary gratings with submicrometer periods in photoresist. Optimized recording conditions require minimum intermodulations in the hologram plane. This was achieved when the optimized phase function of an on-axis phase-only DOE was copied into the hologram plane. Alignment problems were solved by the use of an intermediate copy in a volume photopolymer hologram. After development a modulated binary surface-relief grating results, which can be transferred in a stable substrate material by the use of etching or material deposition techniques and which is also suitable for mass replication. The method has the potential to achieve ultrahigh carrier frequencies with high position accuracy. The far-field copying arrangement works well for object beams with high signal diffraction efficiencies. Off-axis 9 × 9 fan-out elements in transmission with a carrier frequency of 1700 lines/mm and first-order diffraction efficiencies in the range of 70% are demonstrated. Because of the high carrier frequency, these elements clearly show Bragg diffraction behavior and offer high first-order diffraction efficiency. Because they are thinner compared with standard volume holograms, they are much less sensitive to deviations of the readout angle. Therefore, these elements are interesting for optical interconnection systems, which require the generation of the fan-out signal not only for readout with a single reference beam but also for readout with a more complex input pattern.[26]

References

1. H. P. Herzig, M. T. Gale, H. W. Lehmann, and R. Morf, "Diffractive components: computer-generated elements," in *Perspectives for Parallel Optical Interconnects*, Ph. Lalanne and P. Chavel, eds. (Springer-Verlag, New York, 1993), pp. 71–107.
2. D. Prongué and H. P. Herzig, "Total internal reflection holography for optical interconnections," Opt. Eng. **33**, 636–642 (1994).
3. E. Noponen and J. Turunen, "Binary high-frequency-carrier diffractive optical elements: electromagnetic theory," J. Opt. Soc. Am. A **11**, 1097–1109 (1994).
4. J. Turunen, P. Blair, J. M. Miller, M. R. Tagizadeh, and E. Noponen, "Bragg holograms with binary surface-relief profile," Opt. Lett. **18**, 1022–1024 (1993).
5. E. Tervonen, J. Turunen, and J. Pekola, "Pulse-frequency-modulated high-frequency-carrier diffractive elements for pattern projection," Opt. Eng. **33**, 2579–2587 (1994).
6. M. J. Verheijen, "E-beam lithography for digital holograms," J. Modern Opt. **40**, 711–721 (1993).
7. M. G. Moharam and T. K. Gaylord, "Diffraction analysis of dielectric surface-relief gratings," J. Opt. Soc. Am. **72**, 1385–1392 (1982).
8. R. C. Enger and S. K. Case, "High-frequency holographic transmission gratings in photoresist," J. Opt. Soc. Am. **73**, 1113–1118 (1983).
9. M. G. Moharam, T. K. Gaylord, G. T. Sincerbox, and B. Yung, "Diffraction characteristics of photoresist surface-relief gratings," Appl. Opt. **23**, 3214–3220 (1984).
10. K. Yokomori, "Dielectric surface-relief gratings with high diffraction efficiency," Appl. Opt. **23**, 2303–2310 (1984).
11. R. A. Bartolini, "Characteristics of relief phase holograms recorded in photoresist," Appl. Opt. **13**, 129–139 (1974).
12. H. Bartelt and S. K. Case, "High-efficiency hybrid computer generated holograms," Appl. Opt. **21**, 2886–2890 (1982).
13. B. Robertson, J. Turunen, H. Ichikawa, J. M. Miller, M. R. Tagizadeh, and A. Vasara, "Hybrid kinoform fanout holograms in dichromated gelatin," Appl. Opt. **30**, 3711–3720 (1991).
14. H. P. Herzig and R. Dändliker, "Diffractive components: holographic optical elements," in *Perspectives for Parallel*

Optical Interconnects, Ph. Lalanne and P. Chavel, eds. (Springer-Verlag, New York, 1993), pp. 43–69.
15. J. W. Goodmann, *Introduction to Fourier Optics* (McGraw-Hill, New York, 1968), pp. 48–54.
16. R. W. Gerchberg and W. O. Saxton, "A practical algorithm for determination of phase from image and diffraction plane pictures," Optik (Stuttgart) **35,** 237–246 (1972).
17. J. R. Fienup, "Iterative method applied to image reconstruction and to computer-generated holograms," Opt. Eng. **19,** 297–305 (1980).
18. F. Wyrowski and O. Bryngdahl, "Iterative Fourier-transform algorithm applied to computer holography," J. Opt. Soc. Am. A **5,** 1058–1065 (1988).
19. J. Turunen, A. Vasara, and J. Westerholm, "Kinoform phase relief synthesis: a stochastic method," Opt. Eng. **28,** 1162–1167 (1989).
20. H. P. Herzig, D. Prongué, and R. Dändliker, "Optimized kinoform structures for highly efficient fan-out elements," Jpn. J. Appl. Phys. **27,** 1307–1309 (1990).
21. I. Seyd-Darwisch, J. Taboury, and P. Chavel, "Recording conditions of an array-illuminator hologram based on the Talbot effect," Appl. Opt. **32,** 7135–7144 (1993).
22. M. T. Gale, M. Rossi, H. Schütz, P. Ehbets, H. P. Herzig, and D. Prongué, "Continuous-relief diffractive optical elements for two-dimensional array generation," Appl. Opt. **32,** 2526–2533 (1993).
23. P. Ehbets, H. P. Herzig, D. Prongué, and M. T. Gale, "High-efficient continuous surface-relief gratings for two-dimensional array generation," Opt. Lett. **17,** 908–910 (1992).
24. W. J. Gambogi, W. A. Gerstadt, S. R. Mackara, and A. M. Weber, "Holographic transmission elements using improved photopolymer films," in *Computer and Optically Generated Holographic Optics,* I. Cindrich and S. H. Lee, eds., Proc. Soc. Photo-Opt. Instrum. Eng. **1555,** 256–267 (1991).
25. H. P. Herzig, P. Ehbets, D. Prongué, and R. Dändliker, "Fan-out elements recorded as volume holograms: optimized recording conditions," Appl. Opt. **31,** 5716–5723 (1992).
26. A. V. Krishnamoorthy, G. Yayla, and S. C. Esener, "A scalable optoelectronic neural system using free-space optical interconnects," IEEE Trans. Neural Net. **3,** 404–413 (1992).

a reprint from Applied Optics

Fan-out elements recorded as volume holograms: optimized recording conditions

H. P. Herzig, P. Ehbets, D. Prongué, and R. Dändliker

The recording of efficient fan-out elements as volume holograms is investigated by using the coupled-wave theory. In contrast to the results published in the standard literature, we find that the efficiency and the uniformity of regular fan-out elements depend strongly on the relative phases of the object waves, at least, if the thickness of the hologram is less than ~50 wavelengths. High efficiency and uniformity can be achieved by optimized recording conditions. At the same time, the required dynamic range of the holographic material becomes minimum.

Key words: Fan-out element, coupled-wave theory, volume hologram.

I. Introduction

Optical fan-out elements divide a single laser beam into a regular array of equally intense light spots in one or two dimensions. They are used in many applications of modern optics, such as parallel optical processing and fiber-optic communication. Currently fan-out elements are fabricated synthetically as surface-relief phase structures by using microfabrication techniques (e.g., see Ref. 1, Sec. 6). Such elements are Dammann gratings,[2] multilevel gratings,[3] or continuous surface-relief structures.[4] However, proper modulation at large carrier frequencies (> 1000 lines/mm) is difficult to achieve by mask projection. Therefore interferometrically recorded holograms are still of interest for realizing off-axis elements and large fan-out numbers. This paper deals with the recording of efficient fan-out elements in thick volume holograms. We have applied the coupled-wave theory for studying recording conditions for high diffraction efficiency and uniformity of the generated beam array.

Papers on the coupled-wave theory for multiple beam recording predict high efficiency for replaying N waves, and only a weak dependence of interactions between the beams because of the highly selective Bragg condition.[5] This would suggest that the recording of fan-out elements is an easy task. However, experimental results show the difficulties in recording uniform fan-out elements as volume holograms and the precautions that are necessary for generating a uniform distribution of the irradiance in the hologram plane.[6] Fundamental difficulties are explained in terms of recording nonlinearity. By using the coupled-wave theory, we have found that even in the case of prefect linearity a hologram does not generate a uniform fan-out.[7] We demonstrate how to apply the coupled-wave theory to the special problem of regular fan-out elements. These elements are called degenerated because all gratings with equal periodicity diffract light in the same direction and must be added coherently. As a consequence, the results for efficiency and uniformity depend strongly on the relative phases of the recorded object waves.

II. Simultaneous Recording with Minimum Intermodulations

A fan-out element can be fabricated by recording a hologram of N object waves $E_i(\mathbf{x}) = A_i \exp(-j\mathbf{k}_i\mathbf{x} + j\phi_i)$ with a reference wave $E_0(\mathbf{x}) = A_0 \exp(-j\mathbf{k}_0\mathbf{x} + j\phi_0)$. The basic configuration is shown in Fig. 1. The waves are characterized by wave vectors $\mathbf{k}_i = (k_i^y, k_i^z)$, amplitudes A_i, and phases ϕ_i, where $\mathbf{x} = (y, z)$ are the coordinates. Only the s polarization is considered.

We assume that the recording material responds linearly to the accumulated energy during exposure, i.e.,

$$\epsilon(y, z) = \epsilon_a + \delta \left| \sum_{i=1}^{N} E_i + E_0 \right|^2. \quad (1)$$

The authors are with the Institute of Microtechnology, University of Neuchâtel, Rue A.-L. Breguet 2, Neuchâtel CH-2000, Switzerland.

Received 19 June 1991.
0003-6935/92/265716-08$05.00/0.

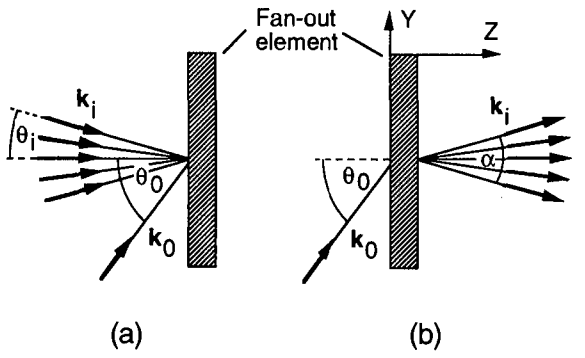

Fig. 1. (a) Recording and (b) readout of fan-out elements. The angles are defined inside the recording medium with refractive index $n = \sqrt{\epsilon_a}$ [see Eq. (1)]; α is the full fan-out angle.

The dielectric permittivity $\epsilon(y, z)$ after exposure then becomes

$$\epsilon(y, z) = \epsilon_a' + \sum_{i=1}^{N} \Delta\epsilon_{0i} \cos(\mathbf{K}_{0i}\mathbf{x} - \Phi_{0i}) + \sum_{q>p=1}^{N} \Delta\epsilon_{pq} \cos(\mathbf{K}_{pq}\mathbf{x} - \Phi_{pq}), \quad (2)$$

where $\Phi_{pq} = \phi_p - \phi_q$ and $\Delta\epsilon_{pq} = 2\delta A_p A_q$. Besides the desired N primary gratings $\mathbf{K}_{0i} = \mathbf{k}_0 - \mathbf{k}_i$, $N(N-1)/2$ unwanted intermodulation gratings $\mathbf{K}_{pq} = \mathbf{k}_p - \mathbf{k}_q$ are recorded. At readout, they generate intermodulation waves, which are coupled with the desired reconstruction beams. As a consequence, efficiency and uniformity of the fan-out suffer.

One possibility of reducing the intermodulations with respect to the primary gratings is to increase the reference-to-object beam ratio B (see Ref. 5), which is defined by

$$B = \frac{{A_0}^2}{\sum_{i=1}^{N} A_i^2}. \quad (3)$$

Then the modulations of the desired primary gratings become dominant ($\Delta\epsilon_{0i} \gg \Delta\epsilon_{pq}$). Unfortunately this method requires a high dynamic range of the recording material.

It was shown in an earlier paper that for on-axis regular fan-out elements the intermodulation gratings can be nearly perfectly eliminated.[4] In the case of regular elements, the projections ${K_{pq}}^y$ of the grating vector $\mathbf{K}_{pq}$ in the hologram plane (y axis) are all integer multiples of the lowest frequency $2\pi\nu$, which is formed by the interference between two neighboring object beams. Thus we can write the intermodulation term in Eq. (2) as

$$\sum_{q>p}^{N} \Delta\epsilon_{pq} \cos(\mathbf{K}_{pq}\mathbf{x} - \Phi_{pq}) = \sum_{q>p}^{N} \Delta\epsilon_{pq} \cos(2\pi m\nu y + {K_{pq}}^z z - \Phi_{pq}), \quad (4)$$

where $m = p - q$. There are $N - 1$ gratings with $m = 1$, $N - 2$ gratings with $m = 2$, etc. By adding the gratings with the same frequency but with optimized phase shifts Φ_{pq}, one can minimize the intermodulations.[4] Note that the grating with the highest frequency ($m = N - 1$) cannot be canceled because it appears only once.

The intermodulations vary in the z direction with ${K_{pq}}^z$ [Eq. (4)]. Consequently, they can be minimized for only one specific plane parallel to the hologram plane (z = constant). For on-axis object beams, as shown in Fig. 1, the z variation is rather slow, i.e., ${K_{pq}}^z$ is small. The largest component ${K_{pq}}^z$ is formed by the interference between the central beam propagating in the direction of the z-axis and the marginal beams of the fan-out. We obtain

$$({K_{pq}}^z)_{\max} = \frac{2\pi}{\lambda} n \left(1 - \cos\frac{\alpha}{2}\right) = \frac{2\pi}{\Lambda}, \quad (5)$$

where λ is the wavelength, α is the full angle ($\mathbf{k}_1$, $\mathbf{k}_N$) of the fan-out, n is the refractive index, and Λ is the periodicity of the grating $({K_{pq}}^z)_{\max}$. The intermodulations remain small within a depth h of $\pm\Lambda/10$, i.e.,

$$h = \frac{\Lambda}{5} = \frac{\lambda}{5n[1 - \cos(\alpha/2)]}. \quad (6)$$

We can conclude that for the geometry shown in Fig. 1 the hologram plane must be normal to the z axis within the tolerances given by Eq. (6). This restricts the optimum recording geometry.

For thick holograms the off-Bragg interactions become negligible, and, therefore, the phases of the object waves are irrelevant. In this case the recording geometry is not restricted by Eq. (6).

III. Coupled-Wave Equations

Below we derive the coupled-wave equations for regular fan-out elements. The electrical field has to fulfill the Helmholtz equation

$$\Delta E(y, z) + k^2\epsilon(y, z)E(y, z) = 0, \quad (7)$$

where $k = (2\pi/\lambda)$, and $\epsilon(y, z)$ as determined by Eq. (2).

The total electric field inside the hologram is written as a sum of M plane waves diffracted in different directions:

$$E(y, z) = E_0(y, z) + \sum_{i=1}^{N} E_i(y, z) + \sum_{i=N+1}^{M} E_i(y, z), \quad (8)$$

where the first N waves are the desired object waves. Each component of the electric field is of the form

$$E_i(y, z) = B_i(z)\exp(-j\mathbf{k}_i\mathbf{x}), \quad (9)$$

where $B_i(z)$ are complex amplitudes.

The waves $E_i(y, z)$ are generated by diffraction of an incident beam ($\mathbf{k}_m$) at a grating $\mathbf{K}_{pq}$. The wave vectors $\mathbf{k}_i$ are then determined by the beta-value construction, namely

$$k_i^y = {k_m}^y - {K_{pq}}^y, \quad q > p = 0, \ldots, N-1; \quad i, m = 0, \ldots, M. \quad (10)$$

For the z components we obtain

$$k_i^z = [k^2\epsilon_a - (k_i^y)^2]^{1/2}. \quad (11)$$

The coupled-wave equations are now obtained by introducing the electric field [Eq. (8)] into the Helmholtz equation (7). This yields

$$\frac{dC_m}{dz}\cos\theta_m = -j\sum_{n=0}^{M}\mathscr{W}_{mn}C_n, \qquad m = 0, \ldots, M, \quad (12)$$

where $C_i = B_i \exp(-jk_i^z)$. The reason for this substitution is to separate the wave parameters, which are described by the coefficients C_i, and the independent grating parameters, which are described by the matrix $\mathscr{W}_{mn}$. Note that the matrix must be Hermitian, i.e., $\mathscr{W}_{mn} = \mathscr{W}_{nm}^*$, and that the diagonal elements are equal to zero, i.e., $\mathscr{W}_{mm} = 0$.

For a simple coupling between two waves E_m and E_n through one grating $\mathbf{K}_{pq}$, we get

$$\mathscr{W}_{mn} = \chi_{pq} = \kappa_{pq}\exp[j(-K_{pq}^z + \Phi_{pq})]. \quad (13)$$

$\kappa_{pq} = k\Delta\epsilon_{pq}/4$ is Kogelnik's coupling coefficient for the grating $\mathbf{K}_{pq}$.

We have to consider that each beam E_m diffracts at all gratings. In our degenerated case all gratings with equal periodicity, i.e., equal K_{pq}^y, diffract light in the same direction. Their coupling coefficients have to be added coherently, which means that

$$\mathscr{W}_{mn} = \sum \chi_{pq}, \quad (14)$$

for $q - p$ = constant.

Figure 2 shows the spectrum of the waves included in our model for a fan-out of $N = 3$ and possible interactions for object wave (O wave) number 2 through the three primary gratings $\mathbf{K}_{01}$, $\mathbf{K}_{02}$, and $\mathbf{K}_{03}$, and the three intermodulation gratings $\mathbf{K}_{12}$, $\mathbf{K}_{23}$, and $\mathbf{K}_{13}$. For further reading, I waves are the intermodulation waves generated by diffraction of the readout wave at the intermodulation gratings $\mathbf{K}_{pq}$, and S waves are the secondary waves generated by diffraction of the object waves at the intermodulation gratings $\mathbf{K}_{pq}$.

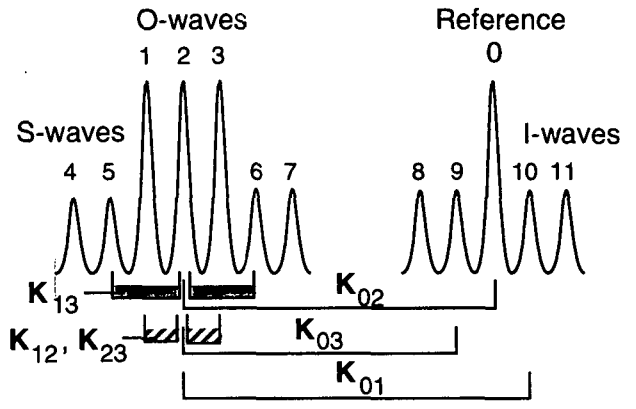

Fig. 2. Spectrum of the waves included in our model for a fan-out of $N = 3$, and possible interactions for object wave (O wave) no. 2 through primary gratings $\mathbf{K}_{0i}$ and intermodulation gratings $\mathbf{K}_{pq}$.

For a fan-out of N waves, we have made the following assumptions for our coupled-wave model:

- Simultaneous recording of N object waves and one reference wave leads to N primary gratings $\mathbf{K}_{0i}$ and $N(N-1)/2$ intermodulation gratings $\mathbf{K}_{pq}$, where $q > p = 1, \ldots, (N-1)$.
- The primary gratings are thick; only one diffraction order is considered.
- The intermodulation gratings are considered to be optically thin; the ± first diffraction orders are included.
- At readout, N object waves (O waves), $2(N-1)$ secondary waves (S waves), and $2(N-1)$ intermodulation waves (I waves) are generated.
- Any possible coupling between the waves E_m through the gratings $\mathbf{K}_{0i}$ and $\mathbf{K}_{pq}$ are accepted.
- Coupling coefficients χ_{pq} of gratings with equal periodicity, i.e., equal K_{pq}^y, are added coherently.

IV. Numerical Results

The coupled-wave equations (12) have been solved by numerical integration with a Runge–Kutta equation. The boundary conditions for transmission holograms at $z = 0$ are $C_0 = 1$ and $C_i = 0$ for $i = 1, \ldots, M$.

The diffraction efficiency η_T of all object waves is obtained from Eq. (15):

$$\eta_T = \sum_{i=1}^{N}\eta_i,$$

with

$$\eta_i = \frac{\cos\theta_i}{\cos\theta_0}|C_i|^2, \qquad i = 1, \ldots, N. \quad (15)$$

The uniformity error e, which is important for fan-out elements, is described by

$$e = \frac{\eta_{i_{max}} - \eta_{i_{min}}}{\langle\eta_i\rangle}. \quad (16)$$

Below we distinguish between the corrected case and the uncorrected case. The corrected case has optimized phases Φ_{pq} for minimum intermodulations at the point $z = 0$, i.e., at the surface of the holographic emulsion. Except in the trivial case of three waves, the phases Φ_{pq} have been determined by numerical optimization.[4] In the uncorrected, worst case, a constant phase is assumed. We have calculated the results for a fan-out of $N = 3$ (Fig. 3 and Table I) and $N = 9$ (Fig. 4 and Table II). The following values have been used for the calculations:

- For three object beams: $\phi_1 = \phi_3 = 0$, $\phi_2 = \pi/2$.
- For nine object beams: $\phi_1 = \phi_9 = 1.77219$, $\phi_2 = \phi_8 = 0.13512$, $\phi_3 = \phi_7 = 3.88710$, $\phi_4 = \phi_6 = 2.45465$, $\phi_5 = 3.14159$ rad.
- Uncorrected worst case: $\phi_i = 0$.

Note that $\Phi_{pq} = \phi_p - \phi_q$.

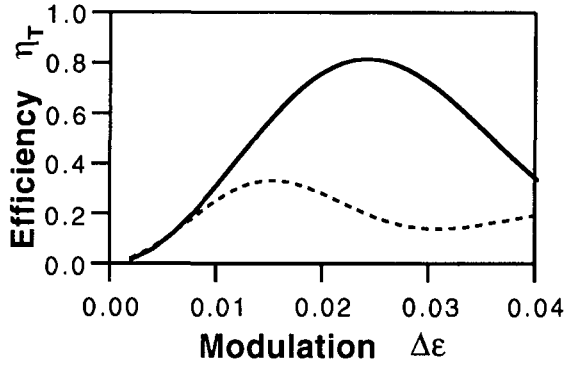

(a)

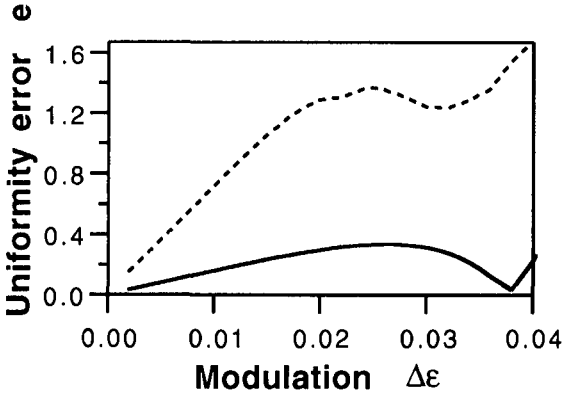

(b)

Fig. 3. Results for a fan-out of $N = 3$: (a) Total useful diffraction efficiency η_T versus the modulation amplitude $\Delta\epsilon$. The solid curve corresponds to the case of corrected phases and the dashed curve corresponds to the worst case; (b) uniformity error e versus $\Delta\epsilon$. The recording parameters are $\lambda = 0.488$ μm, $n = 1.5$, $B = 1$, $\theta_0 = 30°$, $\Delta\alpha = 1°$, and $d = 15$ μm.

Figures 3 and 4 show the total useful diffraction efficiency η_T and the uniformity error e as a function of the modulation amplitude $\Delta\epsilon = \Delta\epsilon_{0i}$ of one primary grating for $N = 3$ and $N = 9$, respectively. The corrected cases (solid curve) show a high diffraction efficiency and a good uniformity. The efficiency increases up to a maximum with increasing modulation, similar to the behavior of a single grating in a volume hologram. In the uncorrected cases (dashed curve), the efficiency is low and the uniformity is poor. Note that the modulation amplitude $\Delta\epsilon$ that is necessary for optimum efficiency is approximately $\sqrt{N}$ smaller than in the case of a single grating.

The angular separation of the fan-out is indicated by the angle $\Delta\alpha = \theta_{i+1} - \theta_i$ between two neighboring object beams. Tables I and II present the maximum diffraction efficiency η_T for different interbeam angles $\Delta\alpha$ and different beam ratios B, again for $N = 3$ and $N = 9$, respectively. From the numerical results we can clearly see the importance of using corrected phases for the object beams. For a reference-to-object beam ratio equal to unity, the fan-out element already possesses good characteristics. For example, for $N = 9$ and $\Delta\alpha = 0.1°$ the maximum diffraction efficiency becomes $\eta_{T_{max}} \sim 94\%$ with a relatively good uniformity of $e < 0.2$.

Table I. Results for a Fan-out of $N = 3$[a]

Interbeam Angle, $\Delta\alpha$	Beam Ratio, B	Modulation, $\Delta\epsilon$	Maximum Useful Diffraction Efficiency, η_T	Uniformity Error, e	
0.1°	1	0.013	0.23	0.63	uncorrected
	5	0.017	0.40	0.15	
	10	0.018	0.44	0.12	
0.1°	1	0.021	0.62	0.20	corrected
	5	0.022	0.78	0.28	
	10	0.024	0.81	0.30	
0.1°	1	0.021	0.62	0.20	corrected[b]
1°	1	0.016	0.32	1.10	uncorrected
	5	0.020	0.55	0.58	
	10	0.021	0.60	0.41	
1°	1	0.024	0.82	0.33	corrected
	5	0.026	0.94	0.16	
	10	0.026	0.95	0.12	
1°	1	0.024	0.82	0.32	corrected[b]
5°	1	0.024	0.75	1.73	uncorrected
	5	0.026	0.94	0.75	
	10	0.026	0.97	0.51	
5°	1	0.025	0.85	1.35	corrected
	5	0.026	0.96	0.80	
	10	0.026	0.97	0.60	
5°	1	0.025	0.96	0.60	corrected[b]

[a]The recording parameters are $\lambda = 0.488$ μm, $n = 1.5$, $\theta_0 = 30°$, and $d = 15$ μm.
[b]See Section V.

All calculations have been made with the following parameters: wavelength $\lambda = 0.488$ μm, refractive index of the holographic medium $n = 1.5$, thickness of the medium $d = 15$ μm, and reference beam angle $\theta_0 = 30°$.

V. Discussion

Here we try to explain the results obtained by our coupled-wave model. We have found that for small interbeam angles $\Delta\alpha$ the corrected phases give a much better efficiency. For larger angles the effect is less significant. A similar behavior is observed for the uniformity error e, except that for large $\Delta\alpha$ the uniformity may become bad.

In the ideal case, the Bragg condition is fulfilled for only the reconstruction of the desired N object waves through the primary gratings $\mathbf{K}_{0i}$. In reality, an unwanted cross coupling between the object waves (O waves) and intermodulation waves (I waves) through the efficient gratings $\mathbf{K}_{0i}$ also occur, as shown in Fig. 2. These interactions are influenced by the phases Φ_{0i}, but not by the beam ratio B (see results for $\Delta\alpha = 0.1°$). For fan-out elements, neighboring beams are rather close; thus the interactions are still close to the Bragg condition. Figure 5 shows the typical off-Bragg behavior of a thick volume grating. We

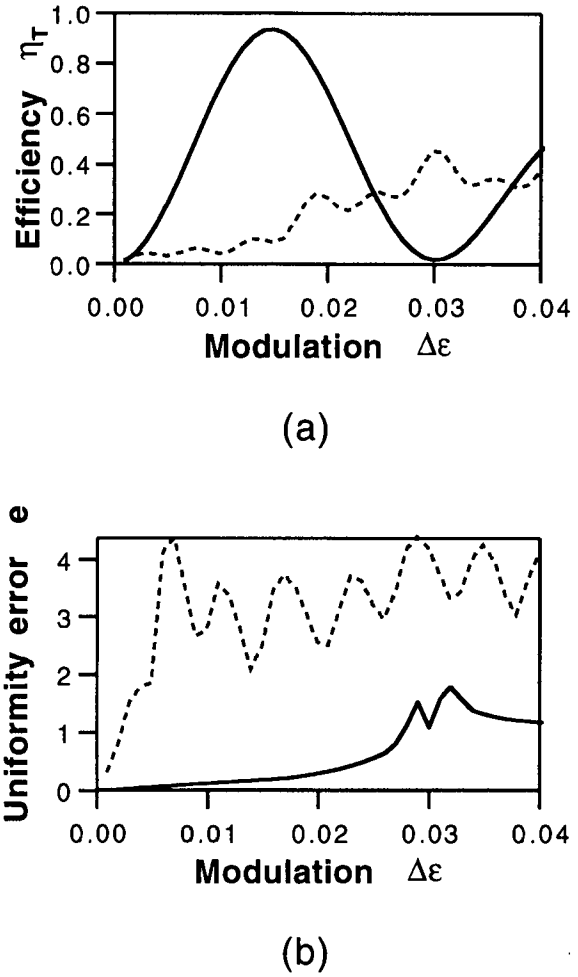

Fig. 4. Results for a fan-out of $N = 9$: (a) Total useful diffraction efficiency η_T versus the modulation amplitude $\Delta\epsilon$. The solid curve corresponds to the case of corrected phases and the dashed curve corresponds to the worst case; (b) uniformity error e versus $\Delta\epsilon$. The recording parameters are $\lambda = 0.488$ μm, $n = 1.5$, $B = 1$, $\theta_0 = 30°$, $\Delta\alpha = 0.1°$, and $d = 15$ μm.

assume that wave i fulfills the Bragg condition. It has been generated by diffraction at the grating $\mathbf{K}_{0i}$. The neighboring wave $i + 1$ can also receive light through the same grating $\mathbf{K}_{0i}$, but this interaction is now off-Bragg. The coupling remains efficient if the phase mismatch is less than 2π. We have applied this criterion to the arrangement shown in Fig. 1. It turns out that these off-Bragg interactions are important for a hologram thickness that is smaller than

$$t = \lambda/(n \tan \theta_0 \Delta\alpha), \tag{17}$$

where $\Delta\alpha = \alpha/(N - 1)$ is the interbeam angle between two neighboring beams, θ_0 is the reference beam angle, λ is the wavelength, and n is the refractive index. Consequently for a larger interbeam angle $\Delta\alpha$ and thicker holograms the fan-out properties become less sensitive to the phases. This can be observed for the efficiencies but not for the uniformities.

Table II. Results for a Fan-out of $N = 9$[a]

Interbeam Angle, $\Delta\alpha$	Beam Ratio, B	Modulation, $\Delta\epsilon$	Maximum Useful Diffraction Efficiency, η_T	Uniformity Error, e	
0.1°	1	0.030	0.45	4.20	uncorrected
	5	0.050	0.34	4.10	
	10	0.038	0.47	3.91	
0.1°	1	0.015	0.94	0.19	corrected
	5	0.015	0.97	0.12	
	10	0.015	0.98	0.12	
0.1°	1	0.015	0.94	0.19	corrected[b]
1°	1	0.021	0.30	3.21	uncorrected
	5	0.036	0.41	2.93	
	10	0.042	0.42	4.70	
1°	1	0.015	0.96	1.51	corrected
	5	0.015	0.97	0.73	
	10	0.015	0.98	0.57	
1°	1	0.015	0.98	0.35	corrected[b]
3°	1	0.024	0.77	1.09	uncorrected
	5	0.016	0.89	0.86	
	10	0.016	0.94	0.79	
3°	1	0.016	0.83	3.95	corrected
	5	0.015	0.95	1.68	
	10	0.015	0.97	1.11	
3°	1	0.016	0.83	2.44	corrected[b]

[a]The recording parameters are $\lambda = 0.488$ μm, $n = 1.5$, $\theta_0 = 30°$, and $d = 15$ μm.
[b]See Section V.

We have assumed that, at recording, the N amplitudes of the object beams are equal $A_i = 1$. For small interbeam angles $\Delta\alpha$, a perfect uniformity ($e < 0.01$) is achieved by adjusting the amplitudes A_i.

There are different reasons for uniformity errors. One reason is that the coupling coefficients depend on the directions of the wave propagation. Another reason is that, for optimized phases, the intermodulation gratings $\mathbf{K}_{pq}$ are canceled only within a depth h, which is given by Eq. (6). For larger fan-out angles α, the depth h becomes short, and therefore undesired intermodulation gratings are recorded. As a result the uniformity error increases, as observed for $\Delta\alpha = 5°$, i.e., $\alpha = 10°$ (Table I), and $\Delta\alpha = 3°$, i.e., $\alpha = 24°$

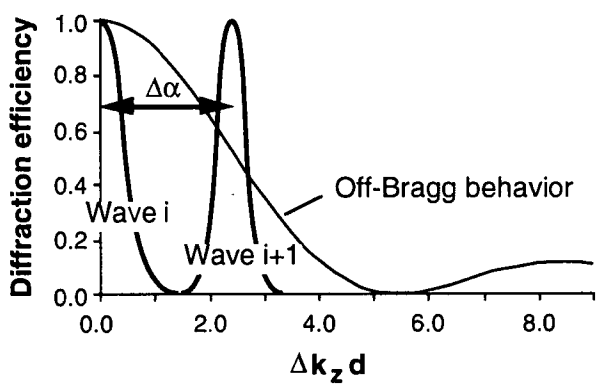

Fig. 5. Wave i fulfills the Bragg condition when diffracted at the grating $\mathbf{K}_{0i}$, whereas wave $\mathbf{K}_{i+1}$ is off-Bragg. If the phase mismatch becomes 2π, the coupling is no longer efficient.

(Table II). This error can be reduced by the beam ratio B or by the position of the plane of minimum intermodulations. As already mentioned above, the corrected case has optimized phases Φ_{pq} for minimum intermodulations at the point z = 0, i.e., at the surface of the holographic emulsion. If we would place the plane with minimum intermodulation in the center of the hologram at z = $d/2$, the uniformity error decreases significantly (see footnotes *b* in Tables I and II).

The uniformity problems observed for large angles between the beams are created by the thin intermodulation gratings $\mathbf{K}_{pq}$. We think that these gratings are not sufficiently described in our model by taking into account the ±1st orders only. A more rigorous theory is necessary to treat them exactly for large angles also.

Note that for sequentially recorded holograms the intermodulation gratings $\mathbf{K}_{pq}$ are not recorded, whereas the strong cross coupling through primary gratings $\mathbf{K}_{0i}$ is present.

VI. Dynamic Range

A holographic emulsion has a limited dynamic range that depends on the material and the thickness. For an optimum hologram recording the exposure energy must be within the dynamic range. If the exposure is increased about saturation, the emulsion does not generate a higher index modulation. For a high reference-to-object beam ratio and large fan-outs the limited dynamic range becomes important. We show that recording with optimized phases requires a lower dynamic range.

During recording, N object waves $E_i(\mathbf{x}) = A \times \exp[-j(\mathbf{k}_i\mathbf{x} + \phi_i)]$ and one reference wave $E_0(\mathbf{x}) = A_0 \exp[-j(\mathbf{k}_0\mathbf{x} + \phi_0)]$ are present. As shown in Eq. (1), the irradiance $I(\mathbf{x})$ in the hologram plane is given by

$$I(\mathbf{x}) = \left|\sum_{i=1}^{N} E_i + E_0\right|^2$$

$$= A_0^2 + NA^2 + 2A_0A\sum_{i=1}^{N}\cos(\mathbf{K}_{0i}\mathbf{x} - \Phi_{0i})$$

$$+ 2A^2\sum_{q>p=1}^{N}\cos(\mathbf{K}_{pq}\mathbf{x} - \Phi_{pq}), \qquad (18)$$

with $\Phi_{pq} = \Phi_p - \Phi_q$ and $\mathbf{K}_{pq} = \mathbf{k}_p - \mathbf{k}_q$.

Figure 6 shows the irradiance $I(\mathbf{x})$ in the hologram plane (y axis) for optimized phases and for the worst case ($\Phi_{0i} = \Phi_{pq} = 0$), respectively. Both cases are calculated for maximum contrast, i.e., $I_{\min} = 0$ and for the same maximum irradiance $I_{\max}$. In the uncorrect case ($\Phi_{0i} = \Phi_{pq} = 0$) all gratings are in phase at $x = 0$ and $y = 0$; thus all amplitudes add up and produce a high maximum intensity. In the corrected case with the optimized phases, however, the primary gratings $\mathbf{K}_{0i}$ are never all in phase at the same position, and the intermodulation term, which contains the gratings $\mathbf{K}_{pq}$, disappears nearly perfectly.

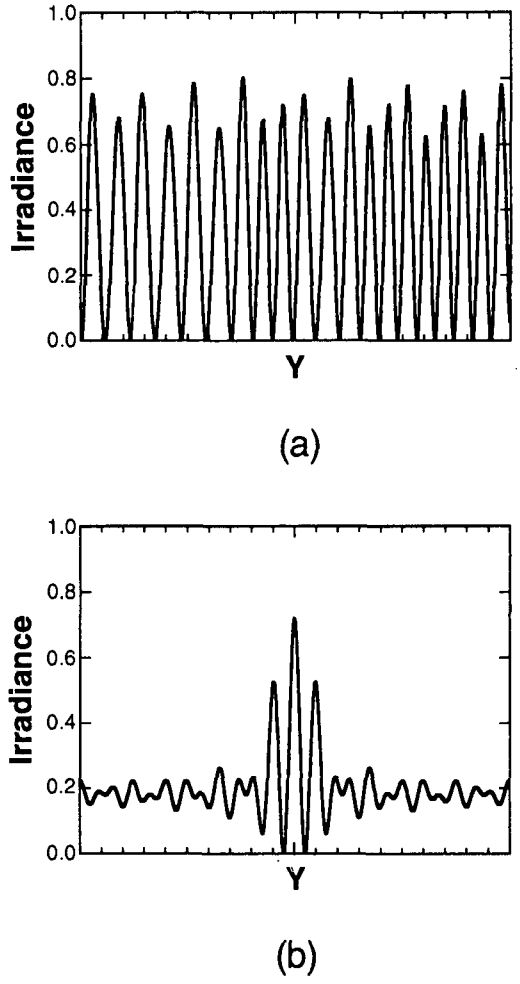

Fig. 6. Interference pattern in the hologram plane (y axis) of nine object beams with a reference wave for (a) optimized phases, (b) worst case, for the same maximum modulation level.

Then the first summation in Eq. (18) yields $2A_0A\sqrt{N}$ and the second summation, i.e., the intermodulations, can be omitted. The maximum and minimum values of the irradiance are found to be

$$I_{\max} = (A_0 + \sqrt{N}A)^2, \qquad I_{\min} = (A_0 - \sqrt{N}A)^2, \qquad (19)$$

for the corrected case, and

$$I_{\max} = (A_0 + NA)^2, \qquad I_{\min} = (A_0 - NA)^2, \qquad (20)$$

for the uncorrected case, where N is the number of fan-out beams and A is the amplitude of the object waves for the recording. Maximum contrast is obtained for $I_{\min} = 0$, which gives the relations $A_0 = \sqrt{N}A$ and $A_0 = NA$ for the two cases, respectively. Then we get a reference-to-object ratio of $B = 1$ for the optimized phases from Eq. (3), whereas $B = N$ for the uncorrected case, which means that the corrected case requires considerably less reference irradiance.

The modulation of the dielectric permittivity $\Delta\epsilon_{0i}$ for the primary gratings $\mathbf{K}_{0i}$, as shown in Eq. (2), is proportional to $2A_0A$. Assuming that the recording

material saturates at a level corresponding to an irradiance of $I_{max} = I_s$, we then find from Eqs. (19) and (20), with $I_{min} = 0$, that

$$\Delta\epsilon_{0i} \propto 2A_0A = 2\sqrt{N}A^2 = I_s/2\sqrt{N} \qquad (21)$$

for the corrected case, and

$$\Delta\epsilon_{0i} \propto 2A_0A = 2NA^2 = I_s/2N \qquad (22)$$

for the uncorrected case, which means that the recorded modulation $\Delta\epsilon_{0i}$ for the primary gratings is $\sqrt{N}$ times higher for the optimized phases. Besides the fact that the fan-out is more efficient in the case of corrected phases, as shown in Figs. 3 and 4, the required modulation amplitude $\Delta\epsilon$ for maximum efficiency can be obtained more easily within the limited dynamic range of the recording material.

VII. Recording Optimized Fan-Out Elements

Figure 7(a) shows the recording setup for on-axis fan-out holograms. The object is an array of coherent sources. The optimized phases ϕ_i can be obtained by different techniques. One possibility is to illuminate a pinhole array, followed by an appropriate phase plate. Another is to use computer-generated holograms or kinoforms to generate the desired array (see Figs. 6 and 7 in Ref. 4). If the sources are in the front focal plane of the lens ($d = f$), the recorded element is nonfocusing; for greater object distances ($d > f$) it becomes focusing. Figure 7(b) shows the off-axis equivalent. Because of the limited depth of the optimum plane [Eq. (6)], the source array and the holographic optical element must be parallel.

If the lens is removed, we get a focusing fan-out element. However, the optimized phases generate a uniform illumination only if the hologram is in the far field, i.e., at a distance $d > (Ns)^2/\lambda$ [see Fig. 8(a)]. Another method of fabricating focusing fan-out elements without a lens uses the self-imaging properties of large periodic structures.[8] In this case the object is a regular array of coherent sources with identical phases $\phi_i = 0$. Considering the beam propagation in free space, we find planes of reduced intermodulations that are suitable for recording efficient holograms. These planes are parallel to the object plane, as in the case of optimized phases. In Fig. 8(b) we incline the object; thus we must also incline the hologram. The self-imaging (Talbot) distance is proportional to s^2 and for inclined objects is proportional to $(s \cos\theta)^2$. If we incline a regularly spaced two-dimensional array (same spacing s in the x and the y directions) with respect to the y axis, we get two different distances for the optimum planes, depending on s^2 and $(s \cos\theta)^2$, respectively. However, a common minimum plane can be determined. This problem can be avoided if the initial array has two different periods Λ in the x and the y directions, namely $\Lambda_x = s$ and $\Lambda_y = s/\cos\theta$.

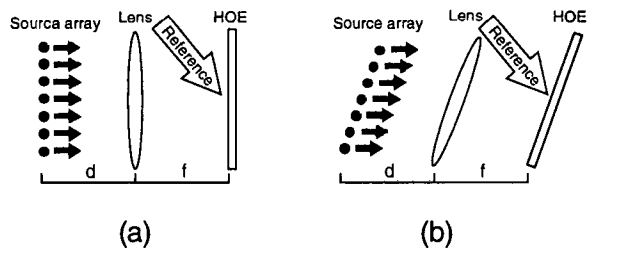

Fig. 7. Object waves (a) on-axis and (b) off-axis; the holographic optical element (HOE) becomes focusing for $d > f$ and nonfocusing for $d = f$.

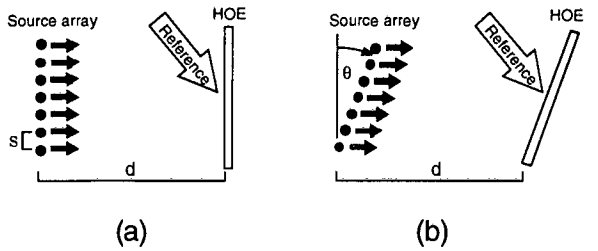

Fig. 8. Recording without a lens with spherical object waves by using the self-imaging properties of large periodic structures: (a) on axis, (b) off axis.

Because of the self-imaging properties, this method is suitable for large arrays only. Note that, depending on the position of the recording plane, this element becomes either a fan-out (overlapping) or a lenslet array (nonoverlapping beams).

Fan-out elements in volume holograms can be fabricated also by copying the phase structure of already existing fan-out elements as such, e.g., Dammann gratings. A simple image formation with a single lens would destroy the phase structure and therefore the properties of the fan-out. This can be avoided by using a 4-f imaging system, as shown in Fig. 9, which twice applies a Fourier transform, thereby conserving the phase distribution.[6] Analogous to Figs. 7 and 8, there also exists an off-axis arrangement of Fig. 9.

VIII. Conclusions

We have investigated the recording of efficient fan-out elements as volume holograms by using the coupled-wave theory. In contrast to the results published in the standard literature, we have found that the efficiency and uniformity of regular fan-out elements depend strongly on the relative phases of the object waves, if the thickness of the holographic emulsion is smaller than $t = \lambda/(n \tan\theta_0\Delta\alpha)$, where θ_0 is the angle of the reference wave and $\Delta\alpha$ the angle between the fan-out beams. A typical value is $t = 32$

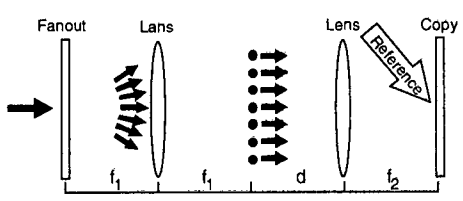

Fig. 9. 4-f system for copying fan-out elements, with magnification $m = f_2/f_1$, where $d = f_2$. Focusing power can be included if $d > f_2$.

μm for $\lambda = 488$ nm, $n = 1.5$, $\theta_0 = 30°$ and $\Delta\alpha = 1°$. High efficiency and uniformity can be achieved by optimized phases of the object beams, which minimize the intermodulations. At the same time the required dynamic range of the holographic material also becomes minimum.

The recording conditions are optimum if the irradiance of the object beam is uniform in the hologram plane. This can be achieved only in specific planes that are parallel to the object plane. As a consequence, only specific recording geometries are allowed. Several possible recording techniques for fabricating efficient and uniform fan-out elements have been presented.

IX. References

1. H. P. Herzig and R. Dändliker, "Holographic optical elements for use with semiconductor lasers," in *International Trends in Optics*, J. W. Goodman, ed., (Academic, New York, 1991), pp. 57–75.
2. H. Dammann and K. Görtler, "High-efficiency in-line multiple imaging by means of multiple phase holograms," Opt. Commun. **3,** 312–315 (1971).
3. S. J. Walker and J. Jahns, "Array generation with multilevel phase gratings," J. Opt. Soc. Am. A **7,** 1509–1513 (1990).
4. H. P. Herzig, D. Prongué, and R. Dändliker, "Design and fabrication of highly efficient fan-out elements," Jpn. J. Appl. Phys. **29,** L 1307–L 1309 (1990).
5. R. K. Kostuk, "Comparison of models for multiplexed holograms," Appl. Opt. **28,** 771–777 (1989).
6. B. Robertson, M. R. Taghizadeh, J. Turunen, and A. Vasara, "High-efficiency, wide-bandwidth optical fanout elements in dichromated gelatin," Opt. Lett. **15,** 694–696 (1990).
7. H. P. Herzig, P. Ehbets, D. Prongué, and R. Dändliker, "Fan-out elements by multiple beam recording in volume holograms," in *Holographic Optics III. Principles and Applications,* G. M. Morris, ed., Proc. Soc. Photo-Opt. Instrum. Eng. **1507,** 247–255 (1991).
8. I. Seyd-Darwish, P. Chavel, J. Taboury, and Y. Malet, "Array illuminator hologram based on the Talbot effect," in *Conference Record of the 1990 International Topical Meeting on Optical Computing* (Japan Society of Applied Physics, Tokyo, 1990), pp. 294–296.

Optics Communications 89 (1992) 5–11
North-Holland

OPTICS
COMMUNICATIONS

TIR holography analyzed with coupled wave theory

P. Ehbets, H.P. Herzig and R. Dändliker
Institute of Microtechnology, University of Neuchâtel, Neuchâtel, Switzerland

Received 6 August 1991; revised manuscript received 5 November 1991

A coupled wave model is presented to describe the diffraction behavior of thick total-internal reflection (TIR) holograms. We have transformed the coupled wave equations into a transfer matrix formalism, enabling a general treatment of the boundary conditions. The off-Bragg characteristic of TIR holograms is found to be completely different from normal volume holograms. The diffraction efficiency depends strongly on the phase of the total internal reflection and the optical pathlength through the hologram. High efficiency at the same angle as used for the recording requires careful control of all parameters.

1. Introduction

Total-internal reflection (TIR) holography offers a method to realize transmission holograms with object planes in the near-field. This holographic recording geometry was first investigated by Stetson [1] and has become of recent interest due to its applications to photolithography [2,3] and optical interconnects [4].

Fig. 1 shows the typical recording set-up for TIR holography. The object beam interferes with the reference beam, which is fed through a prism under 45° into the holographic layer and totally reflected at the film–air interface. The interface pattern of three beams, namely the object beam, the reference beam and the total internal reflection of the reference (TIR), is recorded in the holographic film. In general three thick diffraction gratings are formed. Two of them involve the object beam, while the third is a Lippmann grating formed by the interference of the reference with the TIR beam. The electric field vectors of the reference and the TIR beam are orthogonal for recording with p polarized light, therefore no Lippmann grating is formed.

We are interested in the conditions for replaying the object wave with high diffraction efficiency. Using coupled wave theory, we shall study the influence of the relative phases of the gratings, the phase shift due to total reflection at the backside, and the phase propagation through the hologram.

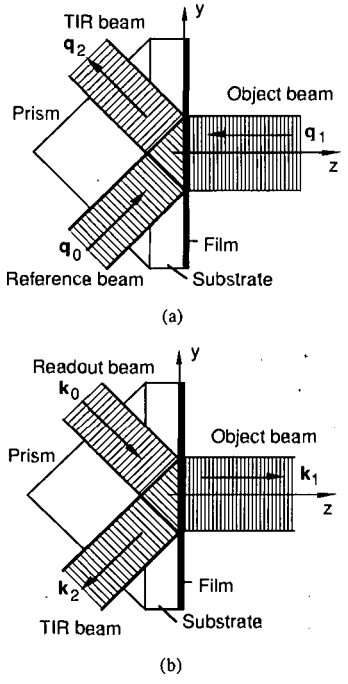

Fig. 1. (a) Recording and (b) readout geometry for TIR holography.

2. Coupled wave analysis

The following coupled wave model is developed for plane waves of infinite extent. The plane of incidence is the yz plane, as shown in fig. 1. At recording, three waves are present. They can be written as

$$\boldsymbol{E}_i(y, z) = A_i \boldsymbol{u}_i \exp[-\mathrm{i}(\boldsymbol{q}_i \cdot \boldsymbol{x} - \varphi_i)], \quad i = 0, 1, 2, \tag{1}$$

where $\boldsymbol{q}_i$ are the wavevectors at recording, A_i the real amplitudes, $\boldsymbol{u}_i$ the unity vectors in the direction of the polarizations, and φ_i the constant phase factors defined at $y = z = 0$. The index i denotes the reference wave ($i=0$), the object wave ($i=1$), and the TIR wave ($i=2$). Note that $A_2 = A_0$ and that for the s polarization $\boldsymbol{u}_i = (1, 0, 0)$.

Since the TIR beam is generated at the film–air interface, its constant phase at $y = z = 0$ is determined by

$$\varphi_2 = \varphi_0 + \Omega_{\mathrm{TIR}}(\theta) - 2\beta d \cos(\theta), \tag{2}$$

where θ is the angle of incidence of the reference wave, d is the thickness of the holographic film, β is the length of the wavevectors at recording and $\Omega_{\mathrm{TIR}}(\theta)$ is the phase shift due to the total reflection at $z = d$. The last term in eq. (2) is the propagation phase of the reference beam through the holographic film.

If we assume that there is no absorption and that the response of the recording material is proportional to the incident energy during exposure, the resulting dielectric permittivity becomes

$$\epsilon(y, z) = \epsilon_{\mathrm{a}} + \delta |\boldsymbol{E}_0 + \boldsymbol{E}_1 + \boldsymbol{E}_2|^2, \tag{3}$$

where δ is the proportionality factor and ϵ_{a} is the average dielectric permittivity of the recording material before exposure.

After substitution of eq. (1) in eq. (3) the recorded permittivity can be written as

$$\epsilon(y, z) = \epsilon_{\mathrm{a}} + \delta \sum_{i=0}^{2} A_i^2 + \sum_{i<j=1}^{2} \Delta\epsilon_{ij} \cos(\boldsymbol{K}_{ij} \cdot \boldsymbol{x} - \Phi_{ij}). \tag{4}$$

Three gratings are recorded simultaneously. Their grating vectors $\boldsymbol{K}_{ij}$, relative phases Φ_{ij} and modulation amplitudes $\Delta\epsilon_{ij}$ are given by

$$\boldsymbol{K}_{ij} = \boldsymbol{q}_i - \boldsymbol{q}_j,$$

$$\Phi_{ij} = \varphi_i - \varphi_j, \quad i<j=1, 2,$$

$$\Delta\epsilon_{ij} = 2\delta A_i A_j \boldsymbol{u}_i \cdot \boldsymbol{u}_j. \tag{5}$$

Note that for p polarization the effective modulation level is $\boldsymbol{u}_i \cdot \boldsymbol{u}_j$ times smaller than for s polarization. The recording process of the hologram changes the average value ϵ_{a} of the dielectric permittivity to a new average value ϵ'_{a}.

Furthermore, we have considered the possibility of shrinkage or swelling of the holographic film during processing. Since we do not exactly know the influence of thickness variations on the recorded permittivity, we have used a simple geometrical model. Shrinkage or swelling in the z-direction alters only the z-component of the grating vectors:

$$\boldsymbol{K}_{ij}^{y}|_{\mathrm{new}} = \boldsymbol{K}_{ij}^{y}|_{\mathrm{old}},$$

$$\boldsymbol{K}_{ij}^{z}|_{\mathrm{new}} = \left(\frac{1}{1+s}\right) \boldsymbol{K}_{ij}^{z}|_{\mathrm{old}}, \tag{6}$$

where s is the relative thickness variation and $s>0$ stands for swelling and $s<0$ for shrinkage.

At readout, the hologram is illuminated with the plane wave $\boldsymbol{k}_0$, as shown in fig. 1b. According to the criteria derived in ref. [5], the three gratings work in the Bragg diffraction regime and will reconstruct only one diffraction order of significant amplitude. Thus, we describe the electric field inside the hologram by

$$\boldsymbol{E}(y, z) = \sum_{i=0}^{2} B_i(z)\, \boldsymbol{u}_i \exp(-\mathrm{i}\boldsymbol{k}_i \cdot \boldsymbol{x}), \tag{7}$$

where the index $i=0$ stands for the readout beam, $i=1$ for the reconstructed object beam, and $i=2$ for the TIR of the readout beam. The coefficients $B_i(z)$ are complex amplitudes, which vary in the z-direction due to the coupling between the waves.

At recording (fig. 1), the wavevectors $\boldsymbol{q}_i$ are assumed to be in the (y, z)-plane, namely

$$\boldsymbol{q}_0 = \beta(0, \sin\theta, \cos\theta), \quad \boldsymbol{q}_1 = \beta(0, 0, -1),$$

$$\boldsymbol{q}_2 = \beta(0, \sin\theta, -\cos\theta), \tag{8}$$

where θ is the incidence angle of the reference wave. The hologram is reconstructed with the readout wave $\boldsymbol{k}_0 = \beta'(0, \sin\theta', \cos\theta')$, where θ' is the incidence

angle. For the choice of readout wave indicated in fig. 1b, $\theta' < 0$. Due to the change of the average dielectric permittivity ϵ_a, the length $\beta' = (2\pi\sqrt{\epsilon'_a})/\lambda$ is different from β at recording, even for the same wavelength λ. The directions of the reconstructed wavevectors $\boldsymbol{k}_i$ are then determined by the β-value method [6]:

$$
\begin{aligned}
&k_1^y = k_0^y - K_{12}^y = \beta' \sin\theta' + \beta \sin\theta \,, \\
&k_1^z = \sqrt{\beta'^2 - (k_1^y)^2} \,, \\
&k_2^y = k_0^y - K_{02}^y = \beta' \sin\theta' \,, \\
&k_2^z = \sqrt{\beta'^2 - (k_2^y)^2} \,. \qquad (9)
\end{aligned}
$$

The coupled wave equations are now derived by introducing the electric field, eq. (7), and the dielectric permittivity, eq. (4), into the wave equation

$$
\Delta \boldsymbol{E}(y, z) + (2\pi/\lambda)^2 \, \epsilon(y, z) \, \boldsymbol{E}(y, z) = 0 \,. \qquad (10)
$$

The modulation of the refractive index is assumed to be small, therefore the weak coupling approximation can be used [7]. We obtain the following coupled wave equations:

$$
\begin{aligned}
\frac{\mathrm{d}}{\mathrm{d}z} B_0 &= -\mathrm{i} \frac{\kappa_{01}}{\cos\theta'} \exp[\mathrm{i}(\Delta k_{12} z + \Phi_{12})] \, B_1 \\
&\quad - \mathrm{i} \frac{\kappa_{02}}{\cos\theta'} \exp[\mathrm{i}(\Delta k_{02} z + \Phi_{02})] \, B_2 \,, \\
\frac{\mathrm{d}}{\mathrm{d}z} B_1 &= -\mathrm{i}\kappa_{10} \exp[-\mathrm{i}(\Delta k_{12} z + \Phi_{12})] \, B_0 \\
&\quad - \mathrm{i}\kappa_{12} \exp[\mathrm{i}(\Delta k_{01} z + \Phi_{01})] \, B_2 \,, \\
\frac{\mathrm{d}}{\mathrm{d}z} B_2 &= \mathrm{i} \frac{\kappa_{20}}{\cos\theta'} \exp[-\mathrm{i}(\Delta k_{02} z + \Phi_{02})] \, B_0 \\
&\quad + \mathrm{i} \frac{\kappa_{21}}{\cos\theta'} \exp[-\mathrm{i}(\Delta k_{01} z + \Phi_{01})] \, B_1 \,, \qquad (11)
\end{aligned}
$$

where θ' is the incidence angle of the readout beam $\boldsymbol{k}_0$. The off-Bragg factors are defined by

$$
\begin{aligned}
&\Delta k_{12} = k_0^z - k_1^z - K_{12}^z \,, \\
&\Delta k_{02} = k_0^z - k_2^z - K_{02}^z \,, \\
&\Delta k_{01} = k_1^z - k_2^z - K_{01}^z \,. \qquad (12)
\end{aligned}
$$

The z-components of the grating vectors $\boldsymbol{K}_{12}$ and the wavevectors $\boldsymbol{k}_i$ are obtained from eqs. (5), (8) and (9).

In the case of the special geometry shown in fig. 1, with $A_0 = A_2$, we found for the coupling coefficients in eq. (11) $\kappa_{01} = \kappa_{10} = \kappa_{12} = \kappa_{21} = \kappa_1$ and $\kappa_{02} = \kappa_{20} = \kappa_2$, with

$$
\kappa_1 = \beta' \Delta\epsilon_{01} / 4\epsilon'_a \,, \quad \kappa_2 = \beta' \Delta\epsilon_{00} / 4\epsilon'_a \,, \qquad (13)
$$

for the s polarization and

$$
\kappa_1 = (\beta' \Delta\epsilon_{01} / 4\epsilon'_a) \boldsymbol{u}'_0 \cdot \boldsymbol{u}'_1 \,, \quad \kappa_2 = 0 \,, \qquad (14)
$$

for the p polarization. In addition to the coupled wave equations (11), the components of the electric field in eq. (7) must satisfy the following boundary conditions for $z = 0$ and $z = d'$:

$$
\begin{aligned}
&B_0(0) = \exp(\mathrm{i}\varphi'_0) \,, \\
&B_1(0) = 0 \,, \\
&B_2(d') = B_0(d') \exp\{\mathrm{i}[\Omega_{\mathrm{TIR}}(\theta') - 2\beta' d' \cos(\theta')]\} \,, \qquad (15)
\end{aligned}
$$

where $\Omega_{\mathrm{TIR}}(\theta')$ is the phase shift of the total internal reflection, and d' is the thickness of the hologram after processing.

The influence of the different phase factors φ_q can be seen more clearly when the complex amplitudes B_p are substituted by

$$
C_p(z) = B_p(z) \exp(\mathrm{i}\varphi_q) \,, \quad p, q = 0, 2; 1, 1; 2, 0 \,. \qquad (16)
$$

From eq. (11) we get the new coupled wave equations

$$
\begin{aligned}
(\mathrm{d}/\mathrm{d}z) C_0 &= -\mathrm{i}(\kappa_1/\cos\theta') \exp(\mathrm{i}\Delta k_{12} z) C_1 \\
&\quad - \mathrm{i}(\kappa_2/\cos\theta') \exp(\mathrm{i}\Delta k_{02} z) C_2 \,, \\
(\mathrm{d}/\mathrm{d}z) C_1 &= -\mathrm{i}\kappa_1 \exp(-\mathrm{i}\Delta k_{12} z) C_0 \\
&\quad - \mathrm{i}\kappa_1 \exp(\mathrm{i}\Delta k_{01} z) C_2 \,, \\
(\mathrm{d}/\mathrm{d}z) C_2 &= \mathrm{i}(\kappa_2/\cos\theta') \exp(-\mathrm{i}\Delta k_{02} z) C_0 \\
&\quad + \mathrm{i}(\kappa_1/\cos\theta') \exp(-\mathrm{i}\Delta k_{01} z) C_1 \,. \qquad (17)
\end{aligned}
$$

The coupled wave equations (17) are now independent of the relative phases $\Phi_{pq} = \varphi_p - \varphi_q$ of the gratings. The relevant phase information is grouped in the new boundary conditions, obtained from eq. (15),

$$
C_0(0) = \exp[\mathrm{i}(\varphi'_0 + \varphi_2)] \,,
$$

$$C_1(0)=0\,,$$

$$C_2(d')=C_0(d')\exp(\mathrm{i}\Delta\psi)\,, \qquad (18)$$

with $\Delta\psi=\Omega_{\mathrm{TIR}}(\theta')-\Omega_{\mathrm{TIR}}(\theta) \quad -2[\beta' d'\cos(\theta') -\beta d\cos(\theta)]$.

The constant phase $\varphi_0'+\varphi_2$ of the coefficient C_0, describing the readout beam at $z=0$, has no importance, because it causes only a common phase shift of the three waves. The phase $\Delta\psi$ of the coefficient C_2 at $z=d'$, however, has a strong influence on the solutions, because it changes the phase relation between the waves. The phase shift $\Delta\psi$ is due to differences between recording and readout, i.e. the phase change of the total internal reflection and the change of the optical length through the hologram.

3. Transfer matrix for numerical solutions

For the numerical solution of the coupled wave equations (17), we have used a transfer matrix formalism. The advantage of this approach is that the coupled wave system can be easily combined with other transfer matrices. This allows to calculate the integration of the TIR hologram in a more complex system. In addition, the transfer matrix is independent of the boundary conditions. This allows a general treatment of possible boundary conditions, without being obliged to integrate the coupled wave equations again.

The coupled wave equations (17) represent a linear system of differential equations for the unknown coefficients $C_i(z)$. Such a system can be described by a transfer matrix $\mathbf{M}_{pq}$, that transforms an input vector $\boldsymbol{C}(0)=(C_0(0),\ C_1(0),\ C_2(0))$ at $z=0$ into an output vector $\boldsymbol{C}(d')$ at $z=d'$, namely

$$\boldsymbol{C}(d')=[\mathbf{M}_{pq}]\cdot\boldsymbol{C}(0)\,,\quad p,q=0,1,2\,. \qquad (19)$$

The transfer matrix $\mathbf{M}_{pq}$ can be derived by integrating the system of differential equations (17) for three different orthogonal boundary conditions at $z=0$, namely $\boldsymbol{C}(0)=(1,0,0)$, $(0,1,0)$ and $(0,0,1)$. Each solution $\boldsymbol{C}(d')$ defines then one column of the transfer matrix $[\mathbf{M}_{pq}]$. The differential equations (17) were integrated numerically by a Runge–Kutta algorithm.

We are finally interested in the diffraction efficiency, defined by

$$\eta_1=\frac{k_1^z}{k_0^z}\frac{|C_1(d')|^2}{|C_0(0)|^2}\,, \qquad (20)$$

which is the fraction of the incident power coupled into the reconstructed object beam. The substitution of the boundary conditions (18) into eq. (20) yields for $C_0(0)=1$

$$\eta_1=\frac{k_1^z}{k_0^z}\left|M_{10}+M_{12}\left(\frac{M_{00}-M_{20}\exp(-\mathrm{i}\Delta\psi)}{M_{02}-M_{22}\exp(-\mathrm{i}\Delta\psi)}\right)\right|^2. \qquad (21)$$

4. Discussion of the results

The figs. 2 to 4 present the diffraction efficiency, calculated from eq. (21), as a function of the readout angle θ', for both s and p polarized light. We have considered different values for the thickness variation, namely no shrinkage (fig. 2), 1% shrinkage (fig. 3), and 1% swelling (fig. 4). For all calculations the

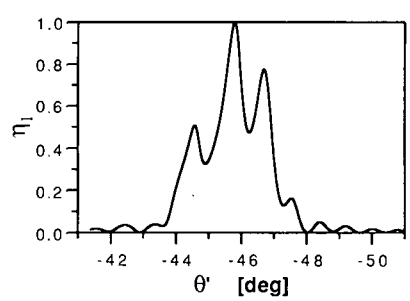

(a)

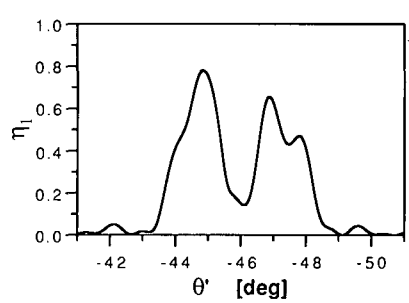

(b)

Fig. 2. Diffraction efficiency η_1 versus readout angle θ' for 0% shrinkage. (a) s polarization, (b) p polarization.

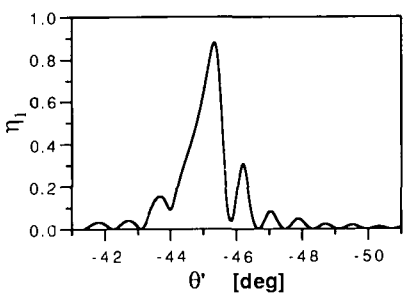

(a)

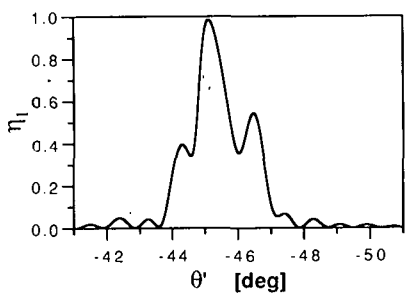

(b)

Fig. 3. Diffraction efficiency η_1 versus readout angle θ' for 1% shrinkage. (a) s polarization, (b) p polarization.

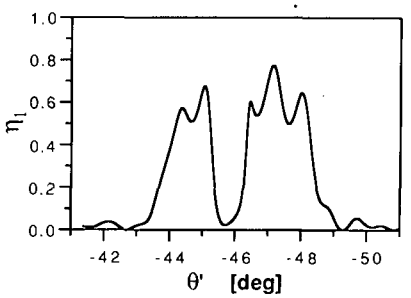

(a)

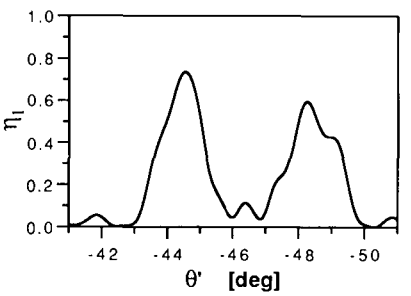

(b)

Fig. 4. Diffraction efficiency η_1 versus readout angle θ' for 1% swelling. (a) s polarization, (b) p polarization.

following parameters have been used: $\lambda = 0.488$ μm, $n_a = \sqrt{\epsilon_a} = 1.5$, $d = 15$ μm, $\theta = 45°$, and $A_0 = A_1$, which means equal intensity for the reference and the object beams. We have assumed the same value for the coupling factor κ_1 for both s and p polarization. This means for an interbeam angle of 45°, following eqs. (13) and (14), that the exposure has to be two times higher for p polarization than for s polarization. Therefore a modulation level of $\Delta\epsilon_{01} = 2\delta(A_0)^2 = 0.026$ for s polarization and $\Delta\epsilon_{01} = 2\delta(A_0)^2 \cos(\theta) = 0.037$ for p polarization has been chosen. The change of the average dielectric permittivity is calculated following eq. (4), using the same proportionality factor δ as for the exposure of the gratings. The resulting values for the refractive index are $n'_a = 1.51$ for s polarization and $n'_a = 1.53$ for p polarization.

A key element is the Lippmann grating $\boldsymbol{K}_{02}$, which couples light directly from the readout beam into the TIR beam. This grating is only present in the case of s polarization. This is the main reason for the differences between the results for p and s polarization.

The amplitude of the object beam $\boldsymbol{k}_1$ is coupled to the readout beam $\boldsymbol{k}_0$ and to the TIR beam $\boldsymbol{k}_2$ through the gratings $\boldsymbol{K}_{12}$ and $\boldsymbol{K}_{01}$, respectively. These two contributions are added coherently. Therefore the phase shift $\Delta\psi$ between the readout beam and the TIR is important. The phase shift $\Delta\psi$ is determined by the boundary condition of the hologram at $z = d'$, given by eq. (18). In figs. 2 to 4 we see rapid variations of the diffraction efficiency with the readout angle θ'. This can be explained by the angular dependence of $\Delta\psi$. For $\Delta\theta' = 1°$ the phase shift $\Delta\psi$ changes by more than 2π.

In the ideal case, i.e. if the recording and the readout parameters are identical, the Bragg angle for high diffraction efficiency is $\theta' = -45°$. Shrinkage or swelling (figs. 3 and 4), and also the change of the average permittivity ϵ'_a (figs. 2, 3 and 4), shift the Bragg angles at readout. The shift is different for the three gratings $\boldsymbol{K}_{ij}$. Large shrinkage or swelling will separate the angular regions where the gratings $\boldsymbol{K}_{01}$ and $\boldsymbol{K}_{12}$ are efficient, and therefore the influence of the coherent grating coupling will diminish. The out-

put of the hologram becomes insensitive to the phase shift $\Delta\psi$. This can already be seen in the case of 1% swelling in fig. 4. It shows two separated efficiency peaks centered at the shifted Bragg angles of the gratings $\boldsymbol{K}_{12}$ (left) and $\boldsymbol{K}_{01}$ (right). For readout angles near to one of the shifted Bragg angles only the corresponding grating will be efficient and as a consequence complete power transfer into the object beam should be possible. Using Kogelnik's two wave model [7], we can calculate the optimum modulation level $\Delta\epsilon_{01}$ for the transmission grating $\boldsymbol{K}_{12}$ at the shifted Bragg angle θ'. For 1% swelling we get $\theta' = -44.6°$ and $\Delta\epsilon_{01} = 0.042$ for s polarization, respectively $\theta' = -44.3°$ and $\Delta\epsilon_{01} = 0.058$ for p polarization. Fig. 5 shows that for this modulation level at the shifted Bragg angle all the incident power is transferred to the object beam ($\eta_1 = 1$).

For many practical applications, the object beam is not a plane wave but a focused beam or a more complex structure [2–4]. In these cases it is important that the object can be replayed at the same angle, because any change would introduce aberrations. It is difficult to record a hologram without a change of the average permittivity ϵ'_a, and therefore without a shift of the Bragg angle. Fortunately, as shown in fig. 3, it seems to be possible to compensate this shift by an appropriate shrink. The highest efficiency is again achieved near $\theta' = -45°$.

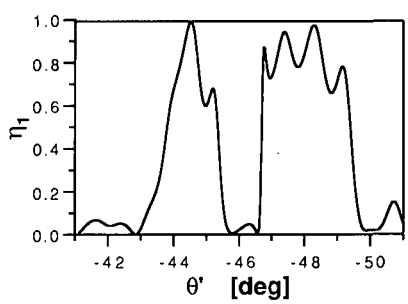

(a)

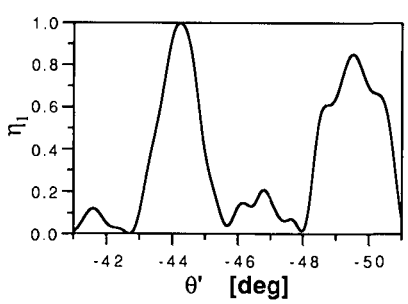

(b)

Fig. 5. Diffraction efficiency η_1 versus readout angle θ' for 1% swelling. Optimized transmission grating $\boldsymbol{K}_{12}$. (a) s polarization, (b) p polarization.

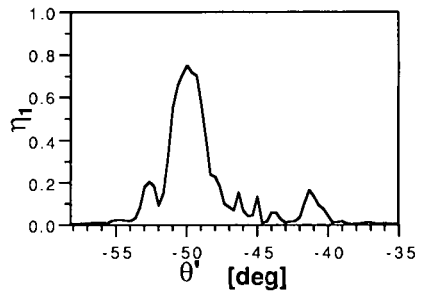

Fig. 6. Measured diffraction energy η_1 versus readout angle θ'. Material: photopolymer HRS 352, $d \approx 16$ μm, s polarization.

Actually, we have recorded only some few TIR holograms in dichromated gelatine and photopolymer. For the recording we have used the same geometry and the same parameters as for the numerical results. Fig. 6 shows the measured off-Bragg characteristics of a TIR hologram recorded in photopolymer. We observe a high Bragg peak with efficiency $\eta_1 \approx 80\%$ at $\theta' = -50°$ and a second smaller one at $\theta' = -41.5°$. The large shift of the Bragg angles indicates that during processing the thickness and the average permittivity have changed considerably. It is rather astonishing in comparison to figs. 4 and 5 that the second Bragg peak is much smaller than the first one. The main problem for quantitative comparison of theoretical and experimental results is the lacking detailed knowledge of the behavior of the holographic materials during recording and processing.

5. Conclusions

We have presented a coupled wave model, which allows to simulate the diffraction behavior of TIR holograms. For the numerical solution of the coupled wave equations we have used a transfer matrix formalism. This allows to separate the integration of the coupled wave equations and the treatment of the

boundary conditions. The transfer matrix representation of the coupled wave solution can also be used to calculate the behavior of the hologram in a more complex system.

In general, three gratings are recorded in a TIR hologram, except for the case of p polarization and 90° between the reference and the TIR beam. Nevertheless, high diffraction efficiency can be achieved in all cases. However, the efficiency depends strongly on the change of the refractive index (average permittivity), of the hologram thickness (shrinking or swelling), and of the incidence angle of the reference beam. The main influence results from the change $\Delta\psi$ of the total phase shift between incident and TIR beam at the film–air interface (eq. 18)). It has two contributions: the phase of the total internal reflection and the optical path length of the TIR through the hologram. The consequence of this phase shift are rapid variations in the efficiency.

For practical applications, the object has to be replayed at the same angle as the recording was done, otherwise aberrations occur [4]. However, any variations of the recording parameters introduce a shift of the Bragg angle and reduce the efficiency, therefore it is important to control exactly the changes of the average permittivity and the hologram thickness during processing. The simulations show that conditions can be found, where the angular shifts due to these changes can compensate each other and efficient readout at the original recording angle can be obtained. Experiments in photopolymers and DCG show efficiency curves similar to the calculated results.

References

[1] K. Stetson, Appl. Phys. Lett. 11 (1967) 225.
[2] J. Brook and R. Dändliker, Microelectron. Eng. 11 (1990) 127.
[3] R.T. Chen, L. Sadovnik, T.M. Aye and T. Jannson, Optics Lett. 15 (1990) 869.
[4] D. Prongué and H.P. Herzig, Proc. SPIE 1281 (1990) 113.
[5] M.G. Moharam, T.K. Gaylord and R. Magnusson, Optics Comm. 32 (1980) 14.
[6] R.R.A. Syms, Practical volume holography (Oxford University Press, Oxford, 1990) p. 45.
[7] H. Kogelnik, Bell Syst. Tech. J. 48 (1969) 2909.

High-carrier-frequency fan-out gratings fabricated by total internal reflection holographic lithography

Peter Ehbets, MEMBER SPIE
Hans Peter Herzig
Markku Kuittinen*
University of Neuchâtel
Institute of Microtechnology
Rue Breguet 2
CH-2000 Neuchâtel, Switzerland
E-mail: ehbets@imt.unine.ch

Francis S. M. Clube
Yves Darbellay
Holtronic Technologies SA
Champs-Montant 12B
CH-2074 Marin, Switzerland

Abstract. Total internal reflection (TIR) holographic lithography is applied to the fabrication of binary diffractive optical elements with submicrometer surface relief features. The recording conditions for the intermediate TIR volume hologram, used for high-resolution proximity printing, are discussed. In particular, the fabrication of efficient high-carrier-frequency fan-out gratings is considered and experimental results are presented for an off-axis 9×1 fan-out element in photoresist with a carrier frequency of 1000 lines/mm.

Subject terms: lithography; holography; gratings; optical interconnects.

Optical Engineering 34(8), 2377–2383 (August 1995).

1 Introduction

Fan-out elements split an incoming beam into a regular array of equally intense beams.[1] They are key components for optical interconnects, and off-axis elements, in particular, are of interest for the realization of integrated planar micro-optical systems.[2] In this paper, the fabrication of efficient binary off-axis fan-out gratings for visible and near-IR light is investigated. This is a challenging task, because it requires a fabrication process with submicrometer resolution and also with high position accuracy over the entire surface of the diffractive optical element (DOE).

Highly efficient off-axis fan-out elements can be fabricated by holographic recording in dichromated gelatin or photopolymer.[3] In this case, volume diffraction in the thick grating structure enables high diffraction efficiency for incidence at the Bragg angle. Unfortunately, the high angular selectivity of volume holograms limits the useful numerical aperture at readout. Recently, the design of synthetic Bragg holograms with a binary surface relief has been proposed.[4–6] The modulated binary relief function of these elements is interesting because it can be realized in stable substrate materials with a single lithographic step. In addition, the angular selectivity is reduced compared to volume holograms. However, Bragg diffraction behavior and high first-order diffraction efficiency with thin binary phase gratings requires carrier grating periods of the order of the wavelength. As a consequence, electromagnetic diffraction theory must be applied to determine the diffraction efficiency of the grating structure.

Synthetic Bragg DOEs with submicrometer carrier grating periods have been fabricated by using direct electron beam (e-beam) writing[4] and by two-beam holographic recording in photoresist with an optimized object beam.[7] For industrial fabrication, however, photolithography is more convenient. The accurate transfer of submicrometer features (<0.5 μm) requires the use of advanced lithographic equipment, such as deep-UV, x-ray, or phase-shift lithography. In this context, total internal reflection (TIR) holographic lithography represents a very flexible alternative approach that offers the required resolution over a large printing area.[8–10] We have investigated for the first time the potential of this lithographic technology for the fabrication of binary DOEs with submicrometer features in the relief. The main potential problems associated with holographic recording methods arise from coherent noise and intermodulations that degrade the binary surface relief structure. The off-axis fan-out gratings considered are sensitive to fabrication errors. Therefore, the quality of the fabricated off-axis fan-out gratings provides a good criterion for the precision of the TIR holographic printing process.

TIR holographic lithography is a proximity copying technique and therefore requires a $1 \times$ amplitude mask of the final structure. In the following section, we present the encoding of the amplitude mask for high-carrier-frequency fan-out gratings. This high-resolution mask is then fabricated by e-beam writing. The influence of quantization errors on the

* On leave from University of Joensuu, Department of Physics, Väisälä Laboratory, P.O. Box 111, FIN-80101, Joensuu, Finland.

Paper SWI-42 received Jan. 15, 1994; revised manuscript received Jan. 18, 1995; accepted for publication Jan. 26, 1995.

fan-out function is analyzed using rigorous electromagnetic diffraction theory. In the third section, the recording conditions of the intermediate TIR volume hologram for high reconstruction fidelity are discussed. Experimental results of holographically printed fan-out elements are then given in Sec. 4.

2 Encoding of Binary Off-Axis Fan-Out Gratings

The readout geometry of binary off-axis fan-out gratings in transmission is represented in Fig. 1. The grating structure is illuminated from the substrate of refractive index n_s with a TE-polarized, monochromatic plane wave at the Bragg angle $\theta_B = \arcsin(\lambda/2n_s d_c)$, where λ is the free-space wavelength and d_c is the period of the carrier grating. The carrier grating is modulated so that it generates the desired fan-out function in the -1st diffraction order. For off-axis incidence, higher diffraction orders can be made evanescent by the use of a high carrier frequency. From the grating equation, it follows that only the zero and the -1st diffraction orders are propagating in the output medium ($n=1$), if the carrier grating period is in the range $0.5\lambda < d_c < 1.5\lambda$. Rigorous analysis has shown that in this case, high -1st order diffraction efficiencies can be achieved for Bragg angle incidence and for an appropriate choice of the binary grating parameters.[5]

The modulated high-frequency grating structure for off-axis fan-out generation can be efficiently calculated using hybrid encoding schemes,[4–6] which assume a slowly varying modulation signal compared to the carrier frequency. In this case, the off-axis fan-out function can be described by the normalized interference function

$$I(x) = \frac{1}{2} + \frac{1}{2}\cos[2\pi x/d_c - \Phi(x)] \ , \tag{1}$$

where $\Phi(x)$ represents the phase function of an on-axis fan-out element, which can be determined by paraxial scalar diffraction theory. High fan-out efficiency η_F is achieved by calculating an on-axis fan-out element $\Phi(x)$ with a continuous phase function using iterative Fourier optimization.[11] For 2-D

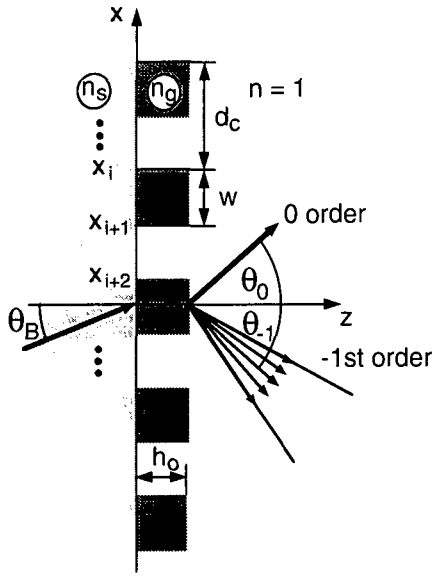

Fig. 1 Readout geometry of high-carrier-frequency off-axis fan-out gratings in transmission.

elements, the strip geometry of Ref. 6 is advantageous for mask encoding.

The binary amplitude transmittance function $T(x)$ of the required mask is obtained from Eq. (1) by hard clipping the interference function $I(x)$ to 0 and 1, which can be written as

$$T(x) = \frac{1}{2} + \frac{1}{2}\,\mathrm{sign}\{\cos[2\pi x/d_c - \Phi(x)]\} \ , \tag{2}$$

where $\mathrm{sign}(x) = 1$ for $x > 0$ and $\mathrm{sign}(x) = -1$ for $x \le 0$. This results in a pulse-frequency-modulated carrier grating with a local filling factor ($f = w/d_c$) equal to $f \cong 0.5$. If the period Λ of the fan-out function $\Phi(x)$ is an integer multiple of d_c, i.e., $\Lambda = Nd_c$, the overall period of $T(x)$ becomes equal to Λ and is completely defined by $2N$ transition points x_i, determined from Eq. (2).

The final phase grating printed in positive photoresist is determined by the binary surface-relief function $h(x)$, which can then be written as

$$h(x) = h_0[1 - T(x)] \ , \tag{3}$$

where h_0 represents the relief depth. Because the carrier grating is locally only weakly perturbed, the efficiency in the -1st order can be optimized using rigorous diffraction theory by considering only the carrier grating.

The overall diffraction efficiency η of the off-axis fan-out element is defined by the combined efficiency of the fan-out signal beams, which can be written as

$$\eta = \sum_{i=1}^{N} \eta_i \ , \tag{4}$$

where η_i are the efficiencies of the N fan-out diffraction orders. We can estimate the value of the diffraction efficiency η in the hybrid encoding approach by calculating the hybrid diffraction efficiency η_H, which is determined by $\eta_H = \eta_{-1}\eta_F$, where η_{-1} represents the -1st order efficiency of the carrier grating and η_F is the efficiency of the paraxial fan-out element. The value of η_F indicates the fraction of the power inside the -1st carrier grating order, which falls in the ideal case into the desired N fan-out orders.

The quality of the encoded off-axis fan-out element is characterized by the uniformity error u, which can be defined by the contrast function

$$u = \frac{\eta_{\max} - \eta_{\min}}{\eta_{\max} + \eta_{\min}} \ , \tag{5}$$

where $\eta_{\max}$ and $\eta_{\min}$ are the maximum and minimum efficiencies of the fan-out diffraction orders η_i. The validity of the hybrid encoding approach and the conditions for high efficiency and low uniformity error are discussed in Ref. 5.

We encoded a 9×1 fan-out element of period $\Lambda = 125.0$ μm with a carrier frequency of 1000 lines/mm. The continuous phase function of the on-axis 9×1 fan-out element was optimized according to Ref. 11. It offers a high fan-out efficiency of $\eta_F = 99.3\%$ and a uniformity error below 0.1%. In this case, the carrier grating period of the amplitude transmittance function $T(x)$ in Eq. (2) varies continuously between 0.96 and 1.04 μm.

Fabrication of the amplitude mask by e-beam writing[12] requires quantization of the exact transition points x_i to the pixel grid of the e-beam writer. For high resolution, typical pixel sizes are in the range of 25 to 100 nm. We used a pixel grid equal to $\Delta = 50$ nm, which corresponds to a scan field of 800×800 μm^2. For larger grating patterns, stitching of several scan fields must be applied, which introduces stitching errors between the fields of the order of 100 nm. The encoded solution was obtained by rounding the exact transition points x_i to the nearest grid position. The rounding of the transition points shifts the centers of the binary grating pulses and introduces detour phase errors in the fan-out phase function $\Phi(x)$ up to $\pi\Delta/d_c = \pi/20$. In addition, rounding introduces fast modulation on the carrier grating period d_c of the order of Δ and also modulates the filling factor. This results in additional amplitude modulation of the emerging wavefront in the -1st diffraction order. Detour phase errors and amplitude modulation will deteriorate the uniformity of the array.

The performance of the encoded amplitude mask was first evaluated using amplitude transmittance theory and scalar wave propagation. In this approximation, ideal transition points would still produce a uniformity error below 1%, whereas the solution with rounded transition points yields a uniformity error $u = 3\%$. This increase is essentially caused by the detour phase errors. Rigorous diffraction theory was applied to analyze the diffraction efficiency and the uniformity of the high-carrier-frequency surface-relief fan-out gratings in photoresist. An efficient implementation for rigorous analysis of dielectric gratings has been obtained by using Knop's model,[13] as described in Refs. 5 and 14. We considered readout with a TE-polarized HeNe laser of wavelength $\lambda = 633$ nm at the Bragg angle, as shown in Fig. 1. Refractive indices of $n_s = 1.515$ for the BK7 glass substrate and $n_g = 1.645$ for the photoresist are assumed. In this geometry, two additional carrier grating diffraction orders, the $+1$st and -2nd orders, are below cutoff in the air region and in the substrate region. The evolution of the diffraction efficiency η in the fan-out orders and the uniformity error u as a function of the relief depth h_0 are shown in Fig. 2. The continuous curve represents the hybrid efficiency $\eta_H = \eta_{-1}\eta_F$, where only the -1st order carrier grating efficiency η_{-1} is rigorously calculated and η_F represents the efficiency of the on-axis fan-out solution. The markers represent rigorously calculated values for the efficiency η (x markers) and the uniformity error u (o markers) of the modulated carrier grating structure of period $\Lambda = 125.0$ μm. The results for the modulated carrier grating with large paraxial periodicity were obtained by considering about 900 orders in the expansions that describe the diffracted electromagnetic fields.[13] This value was limited by the available memory space for the computation. In this case, the diffraction orders up to the first two evanescent orders of the carrier grating on both sides of the propagating orders are retained in the analysis. Convergence of the results were verified for smaller fan-out periods Λ, where more evanescent orders can be included. It is seen that the hybrid efficiency η_H is a good approximation of the rigorously calculated efficiency η, even in the case of a large uniformity error. In the region of maximum efficiency, around $h_0 = 1.2$ μm, however, the hybrid calculation gives slightly too high values for the efficiency. Low uniformity errors, comparable to the 3% predicted by scalar theory, are obtained for small relief depths $h_0 \leq 0.4$ μm. For deeper gratings, the uniformity error increases up to 40% and the hybrid encoded solution fails. It was found that in this region of low efficiency, the -1st order efficiency of the carrier grating depends strongly on the variations of the carrier grating period d_c. Therefore, the fast frequency modulation of the rounded solution introduces considerable amplitude modulation, which becomes more important than the detour phase errors. In the region of interest with high efficiency around $h = 1.2$ μm, again a low uniformity error in the order of $u = 5\%$ is reached. In this region the -1st order efficiency is stable against variation of the carrier grating period and the filling factor, and the uniformity error is essentially determined by the detour phase errors.

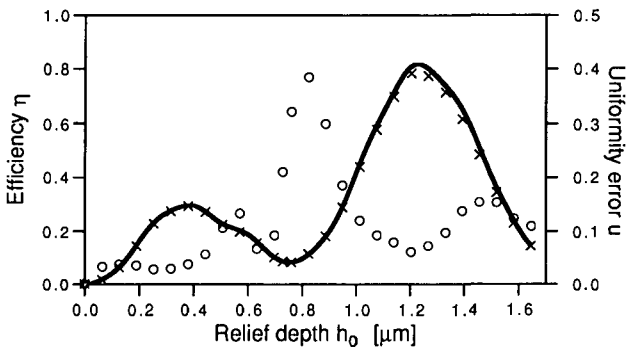

Fig. 2 Performance of the high-carrier-frequency fan-out gratings in photoresist as a function of relief depth h_0: solid line, calculated efficiency η_H in the hybrid approach; x markers, rigorously calculated efficiency η of the modulated carrier grating; and o markers, rigorously calculated uniformity error u of the modulated carrier grating.

3 TIR Holographic Lithography

A commercially available holographic mask aligner (HMA 150) was used to copy the high-resolution fan-out mask into photoresist. A detailed description of this system, which is able to print features down to 0.25 μm over substrates up to 6- × 6-in., is given in Refs. 10 and 15. The principle of this holographic mask aligner is based on TIR near-field holography, which is able to print submicrometer features.[8,9] The recording geometry of the intermediate TIR volume hologram is shown in Fig. 3. The chrome mask is placed near the holographic layer, typically at a distance of $d_g = 100$ μm. The mask is then illuminated with a collimated expanded beam, which is polarized perpendicularly to the plane of incidence (TE). The diffracted field from the mask interferes in the holographic layer with the reference wave at 45-deg incidence, which is fed through a prism and totally internally reflected at the film-air interface. The resulting interference pattern consists of three primary grating structures: a reflection grating from the interference of the object beam with the reference wave, a transmission grating from the interference of the object beam with the TIR wave, and a Lippmann grating from the interference of the reference wave with the TIR wave. In addition, the self-interference of the object beam in the holographic layer produces undesired intermodulation gratings.

At readout, the TIR hologram is illuminated with the conjugate reference beam at the recording angle. Interaction with mainly the transmission grating generates the conjugate of the recorded object beam, which reconstructs the original

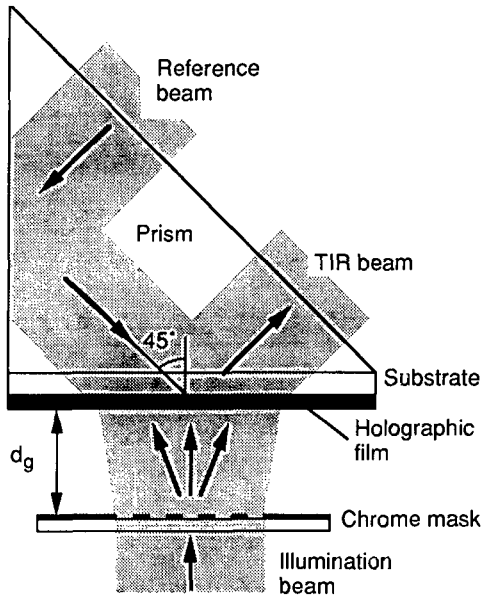

Fig. 3 Recording geometry of the intermediate volume hologram for TIR holographic lithography.

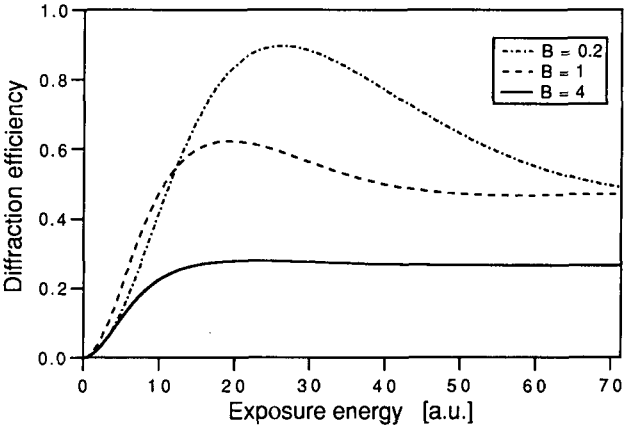

Fig. 4 Diffraction efficiency of the TIR volume hologram versus exposure energy calculated for TE polarization and for different recording reference-to-object beam ratios: $B=0.2$, 1, and 4.

mask pattern at the distance d_g. For lithographic applications, the critical process parameters are high reconstruction fidelity and low coherent noise. This requires that all the recorded primary gratings are optically thick and generate only one diffraction order. For the recording of object beams with high numerical apertures, this condition can be satisfied by increasing either the thickness of the holographic layer or the recording angle of the reference beam. Undiffracted light in the reference beam is backreflected because of the TIR condition and cannot reach the printing area. Intermodulation effects are minimized for a high reference-to-object beam ratio at recording. This produces a strong Lippmann grating that couples light directly from the reference wave to the TIR wave. In a previous publication,[16] we analyzed the diffraction behavior of TIR holograms recorded with plane waves by using a model based on first-order coupled wave theory. We used this model and studied the diffraction efficiency in the object beam as a function of the exposure energy for different reference-to-object beam ratios B. The results are represented in Fig. 4. For the calculation, a linear relation between the index modulation and the exposure energy was assumed. For small beam ratios of $B<1$, high diffraction efficiency in the object beam is possible. If the beam ratio is increased, the diffraction efficiency saturates before high values are reached. The typical sinusoidal diffraction efficiency characteristic of a single thick phase grating in transmission is no longer observed. As a consequence, the high recording beam ratio required for high reconstruction fidelity affects the diffraction efficiency in the TIR geometry.

The Lippmann grating can be eliminated by the use of TM-polarized light at recording, because then the electric field vectors of the reference wave and the TIR wave are orthogonal. However, for TM-polarized light the index modulation of the grating depends on the angle between the two recording beams.[17] This results not only in a smaller contrast compared to TE polarization but also, because of the off-axis incidence of the reference beam, in an asymmetric angular attenuation of the transmission grating index modulation. The consequence is a reduction of the contrast in the image plane at readout, therefore the use of TE polarization is preferable for printing high-resolution features.

The intermediate TIR volume hologram of the fan-out mask was recorded in a 15-μm-thick layer of the photopolymer material (HRS 352 without dye) from Du Pont[18] using an argon laser at $\lambda=363.8$ nm. The final elements are printed into a layer of *g/i*-line resist (O.C.G. HiPR 6512), which is compatible with the UV argon laser wavelength. To ensure uniform illumination of the photoresist layer over the printing area, the TIR volume hologram was scanned at readout. Standard resist processing according to the manufacturer was used for the preparation of the plates and the development.

4 Experimental Results

The off-axis 9×1 fan-out elements were printed by TIR holographic lithography into photoresist on silicon wafers and on glass substrates. The silicon wafers were used for scanning electron microscope (SEM) inspection of the resulting photoresist relief, carried out by first coating the relief with a thin gold layer. Figures 5(a) and 5(b) show cross-sectional and top views of the fabricated modulated grating structure with a carrier grating period of $d_c=1.0$ μm. A binary relief with almost vertical sidewalls and a filling factor of $f=0.5$ can be seen. The small ripples in the sidewalls result from standing wave patterns in the resist layer at recording. These effects are reduced for the gratings recorded on the glass substrate with an absorber on the back side because of the smaller reflectivity of the glass substrates compared to the silicon wafers. The uniform relief depth of about 1.0 μm indicates that, using the recording conditions for the TIR hologram described in the previous section, an accurate transfer of the mask pattern into a deep binary grating structure can be achieved.

The elements on the glass substrates were optically characterized. The relief depth of the grating structure was determined to be $h\cong1.15$ μm by measuring the thickness of the photoresist layer at a large opening in resist near the grating region with a mechanical stylus. We measured the efficiency of the 9×1 fan-out signal in the -1st transmission order

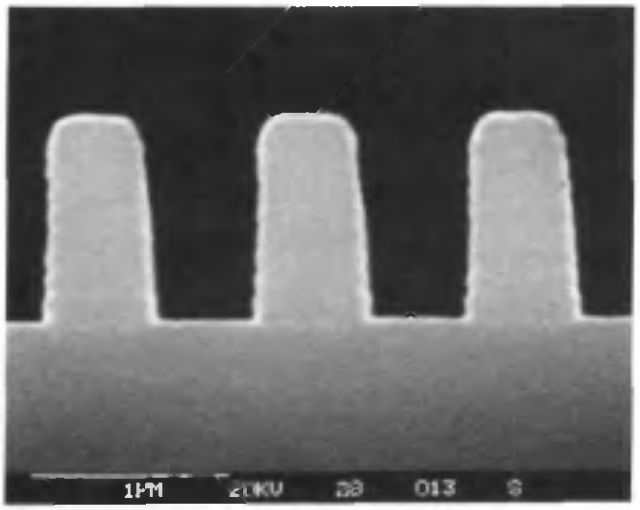

(a)

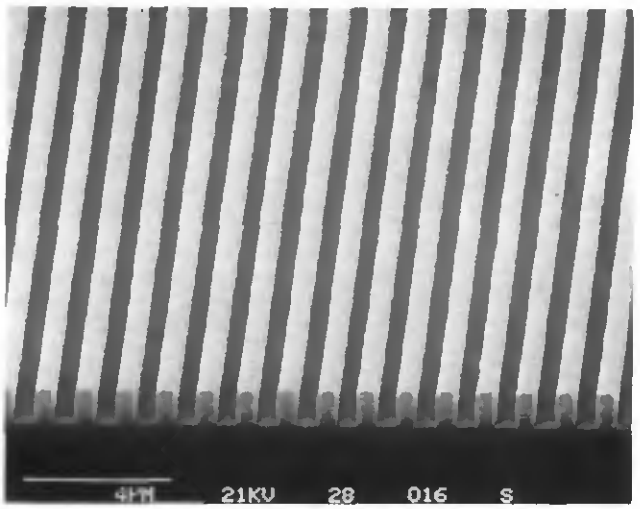

(b)

Fig. 5 SEM pictures of the fabricated modulated high-carrier-frequency surface relief grating in photoresist: (a) cross-section view of the relief profile and (b) top view on a larger scale.

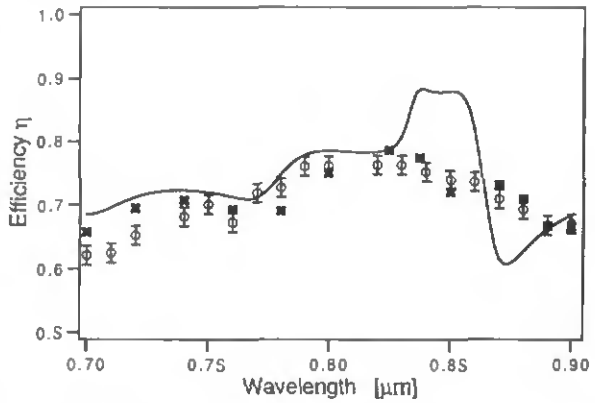

Fig. 6 Fan-out efficiency as a function of the readout wavelength for TE polarization: o markers, measured efficiency values with mean error; x markers, rigorously calculated efficiency η of the modulated carrier grating; and solid line, calculated hybrid efficiency η_H of the carrier grating.

over the near-IR region, where the grating reaches its maximum efficiency. As a light source for the measurement, we used a tunable titanium-sapphire laser. The measurements were made with TE-polarized light for Bragg angle incidence from air to the grating medium. A wedge was index matched at the back side of the substrate, to eliminate fluctuations of the diffraction efficiency resulting from Fabry-Pérot effects in the substrate. Figure 6 represents the measured values (o markers) with error bars. Fresnel reflection losses at the wedge-air interface were compensated. A maximum efficiency of $\eta \approx 77\%$ is obtained for a wavelength of $\lambda = 830$ nm. For comparison, we also plotted the rigorously calculated efficiency η of the modulated grating (x markers) and the hybrid efficiency η_H (solid line), as described in Sec. 2. For the calculation, refractive index dispersion curves for the BK7 glass substrate and for the photoresist are taken from the manufacturers data sheets. Good agreement between the measured efficiency and the rigorously calculated values is obtained. The high diffraction efficiencies near 90% in the region of $\lambda = 860$ nm and the pronounced decrease predicted by the hybrid efficiency calculation are not observed in measurements. The measured behavior, however, is confirmed by the rigorous calculation of the modulated structure and can be explained by the fact that in this region, the -1st order efficiency of the carrier grating is sensitive to frequency modulation. The differences of the measurements compared to theory of the order of 5% are caused by scattering losses, absorption in the photoresist, and deviations from the ideal relief parameters, which are not considered in the theoretical model.

The uniformity of the fan-out elements was characterized using a HeNe laser at $\lambda = 632.8$ nm. The measurements were made by scanning with a detector through the spot array in the back focal plane of a lens for incidence from the substrate to air with TE polarization. Therefore, they can be directly compared to the calculated encoding errors in Sec. 2. At this wavelength, we measured a diffraction efficiency of about 70%, which corresponds to the rigorous value calculated in Fig. 2. To determine the quality of the TIR holographic lithographic process, we analyzed the fan-out function of the original amplitude mask and the copy in photoresist. Minimum uniformity errors are found, when one scan field (800×800 μm^2) of the e-beam writer is illuminated. In this case, about six periods of the fan-out function are illuminated and small random positioning errors inside the scan field are averaged. The amplitude mask produces uniformity errors of the order of 5%, which are only slightly higher than the predicted value of 3% by scalar theory. The binary surface relief grating in photoresist generates larger uniformity errors of about 9%. However, uniformity errors of this size are predicted by the rigorous analysis shown in Fig. 2 for a relief depth of $h = 1.15$ μm. Therefore, they were not introduced during the TIR holographic printing. Figure 7 shows an intensity line scan through the array generated by the off-axis fan-out elements in the photoresist. If more than one scan field is illuminated, the uniformity error of both elements fluctuates strongly, depending on the position of the element. In this case, larger stitching errors between the scan fields degrade the performance. If the whole element (10×10 mm^2) is illuminated, the amplitude mask and the element copied

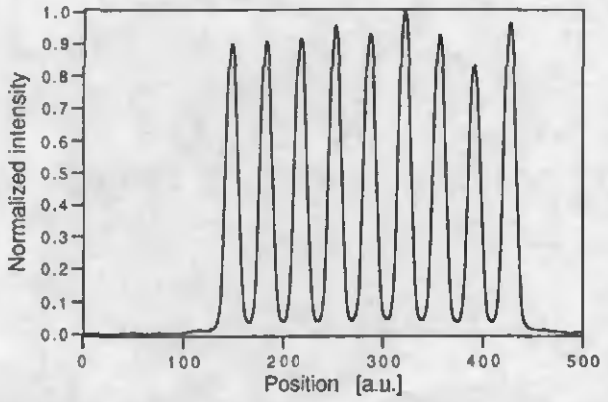

Fig. 7 Measured far-field intensity distribution of the 9×1 fan-out diffraction orders.

in photoresist generate again a fan-out with good uniformity: 6% uniformity error for the mask and 10% for the copy.

5 Conclusions

Off-axis fan-out gratings with a carrier grating frequency equal to 1000 lines/mm were fabricated using an unconventional lithographic approach, based on TIR holography. In a single holographic printing exposure, rectangular grating shapes with deep relief depths up to 1.15 μm were achieved in photoresist, which resulted in fan-out efficiencies close to 80% in transmission for near-IR light. Optical characterization of the fabricated elements showed that the measured efficiency and uniformity is close to the ideal performance of the encoded element over the printed area of 1 cm^2. The fabrication process is not yet limited by the resolution of the photolithographic step, so that the printing of even smaller period grating structures with good optical quality and over much larger areas is realizable. The results demonstrate clearly that TIR holographic lithography is able to provide high-quality, binary DOEs with submicrometer surface relief features. It is therefore an interesting solution for the fabrication of a broad range of high-resolution elements, including grating couplers, off-axis lenses, and Dammann gratings with large diffraction angles.

Acknowledgments

The authors would like to thank J. Turunen for helpful discussions on rigorous diffraction calculations. This work was partially supported by the Swiss Priority Program, Optique, and by the CERS (Commission pour l'Encouragement de la Recherche Scientifique). M. Kuittinen acknowledges the Academy of Finland and the Finnish Academy of Science for financial support.

References

1. N. Streibl, "Beam shaping with optical array generators," *J. Mod. Opt.* **36** 1559–1573 (1990).
2. D. Prongué and H. P. Herzig, "Total internal reflection holography for optical interconnections," *Opt. Eng.* **33**(2), 636–642 (1994).
3. B. Robertson, J. Turunen, H. Ichikawa, J. M. Miller, M. R. Tagizadeh, and A. Vasara, "Hybrid kinoform fanout holograms in dichromated gelatin," *Appl. Opt.* **30**, 3711–3720 (1991).
4. J. Turunen, P. Blair, J. M. Miller, M. R. Tagizadeh, and E. Noponen, "Bragg holograms with binary surface-relief profile," *Opt. Lett.* **18**, 1022–1024 (1993).
5. E. Noponen and J. Turunen, "Binary high-frequency-carrier diffractive optical elements: electromagnetic theory," *J. Opt. Soc. Am. A* **11**, 1097–1109 (1994).
6. E. Tervonen, J. Turunen, and J. Pekola, "Pulse-frequency-modulated high-frequency-carrier diffractive elements for pattern projection," *Opt. Eng.* **33**(8), 2579–2587 (1994).
7. P. Ehbets, H. P. Herzig, P. Nussbaum, P. Blattner, and R. Dändliker, "Interferometric fabrication of modulated submicron gratings in photoresist," *Apl. Opt.* (in press) (1995).
8. R. Dändliker and J. Brook, "Holographic photolithography for submicron VLSI structures," in *Holographic Systems, Components and Applications*, Conference Publication Number **311**, pp. 127–132, Institution of Electrical Engineers, London (1989).
9. R. T. Chen, L. Sadovnik, T. M. Aye, and T. Jannson, "Submicron lithography using lensless high-efficiency holographic systems," *Opt. Lett.* **15**, 868–871 (1990).
10. F. Clube, S. Gray, D. Struchen, J. C. Tisserand, "Holographic mask aligner," *Opt. Eng.* **32**(10), 2403–2409 (1993).
11. H. P. Herzig, D. Prongué, and R. Dändliker, "Optimized kinoform structures for highly efficient fan-out elements," *Jpn. J. Appl. Phys.* **27**, 1307–1309 (1990).
12. M. J. Verheijen, "E-beam lithography for digital holograms," *J. Mod. Opt.* **40**(4), 711–721 (1993).
13. K. Knop, "Rigorous diffraction theory for transmission phase gratings with deep rectangular grooves," *J. Opt. Soc. Am.* **68**, 1206–1210 (1978).
14. E. Noponen, "Electromagnetic theory of diffractive optics," PhD. Thesis, Helsinki Univ. of Technology, Dept. of Technical Physics, 1994.
15. F. S. M. Clube, S. Gray, D. Struchen, J. C. Tisserand, and S. Malfoy, "Holographic microlithography," in this issue.
16. P. Ehbets, H. P. Herzig, and R. Dändliker, "TIR holography analyzed with coupled wave theory," *Opt. Commun.* **89**(1), 5–11 (1992).
17. H. Kogelnik, "Coupled wave theory for thick hologram gratings," *Bell. Syst. Tech. J.* **48**, 2909–2946 (1969).
18. A. M. Weber, W. K. Smothers, T. J. Trout, D. J. Mickish, "Hologram recording in Du Pont's new photopolymer materials," in *Practical Holography IV, Proc. SPIE*, **1212**, 30–39 (1990).

Peter Ehbets received the diploma in physical electronics from the University of Neuchâtel, Switzerland, in 1990 and joined the Applied Optics Group at the Institute of Microtechnology of the University of Neuchâtel as a graduate research assistant. His current research deals with the design and fabrication of diffractive optical elements for beam shaping and optical interconnects.

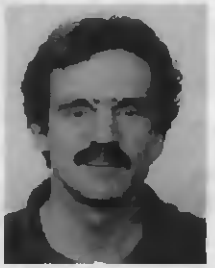

Hans Peter Herzig received the diploma in physics from the Swiss Federal Institute of Technology in Zürich (ETHZ), Switzerland, in 1978. From 1978 to 1982 he was a scientist in the Optics Development Department of the Kern Company in Aarau, Switzerland, where he worked in lens design and optical testing. In 1983, he joined the Applied Optics Group at the Institute of Microtechnology of the University of Neuchâtel, Switzerland, as a graduate research assistant, working in the field of holographic optical elements, especially scanning elements. In 1987, he received the PhD degree in optics from the University of Neuchâtel. Currently, he is lecturing modern optics and is responsible for the research in micro-optics, including diffractive optical elements and microlenses.

Markku Kuittinen received the MS and LicPhil degrees in physics from the University of Kuopio in 1989 and 1992, respectively, and the PhD degree in physics from the University of Joensuu in 1994, where he is a research assistant in the Department of Physics. Currently he is a visiting researcher at the Institute of Microtechnology in Neuchâtel, Switzerland. His research interests are in the area of numerical simulation and design and optimization of diffractive optical elements.

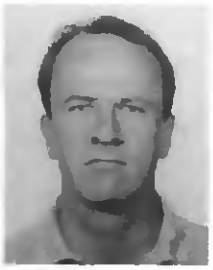

Francis S. M. Clube studied physics at Oxford University, graduating in 1981. He then spent eight years at the GEC-Marconi Research Centre working on a variety of holographic projects, including work on the development of the LANTIRN head-up display (HUD) for the F16 aircraft, the world's first holographic HUD to be put into production. Thereafter he was in charge of the holographic development program for a more advanced HUD, which has since been selected for the new European Fighter Aircraft. Mr. Clube joined Holtronic Technologies in 1989, where he developed the fine alignment system and is now the company's chief scientist. He is the author of several patent applications.

Yves Darbellay obtained his engineering degree in microtechnology from the Swiss Federal Institute of Technology, Lausanne, in 1993. He is now with Holtronic Technologies as an optical engineer in the production of large holographic masks.